STRONTIUM ISOTOPE COMPOSITION: INSIGHTS INTO GEOLOGICAL AND ENVIRONMENTAL INFLUENCES ON THE PROVENANCE STUDIES OF DAIRY PRODUCTS AND TIMBER

Majda Nikezić

Doctoral Dissertation
Jožef Stefan International Postgraduate School
Ljubljana, Slovenia

Supervisor: Assoc. Prof. Dr. Tea Zuliani, Jožef Stefan Institute, Ljubljana, Slovenia

Evaluation Board:
Prof. Dr. Maja Ponikvar-Svet, Chair, Jožef Stefan Institute and Jožef Stefan International Postgraduate School, Ljubljana, Slovenia
Prof. Dr. Sonja Lojen, Member, Jožef Stefan Institute and Jožef Stefan International Postgraduate School, Ljubljana, Slovenia
Dr. Željka Fiket, Member, Ruđer Bošković Institute, Zagreb, Croatia

MEDNARODNA PODIPLOMSKA ŠOLA JOŽEFA STEFANA
JOŽEF STEFAN INTERNATIONAL POSTGRADUATE SCHOOL

Majda Nikezić

STRONTIUM ISOTOPE COMPOSITION: INSIGHTS INTO GEOLOGICAL AND ENVIRONMENTAL INFLUENCES ON THE PROVENANCE STUDIES OF DAIRY PRODUCTS AND TIMBER

Doctoral Dissertation

IZOTOPSKA SESTAVA STRONCIJA: VPOGLED V GEOLOŠKE IN OKOLJSKE VPLIVE NA ŠTUDIJE POREKLA MLEČNIH IZDELKOV IN LESA

Doktorska disertacija

Supervisor: Assoc. Prof. Dr. Tea Zuliani

Ljubljana, Slovenia, October 2024

Acknowledgments

The completion of this dissertation was made possible through the guidance and support of many individuals who contributed to my PhD studies in various ways.

First and foremost, I would like to express my sincere appreciation to my supervisor, Assoc. Prof. Dr. Tea Zuliani, for her helpful insights and thoughtful critiques throughout my research journey. I am immensely grateful for the warm welcome from day one, her generous sharing of knowledge, and the reassurance of her support every step of the way. Her mentorship has fostered my curiosity, resilience, and independence – qualities I will carry forward throughout my career.

I am also thankful to the members of my doctoral dissertation evaluation committee, Prof. Dr. Maja Ponikvar-Svet, Prof. Dr. Sonja Lojen, and Dr. Željka Fiket, for their constructive feedback, which has greatly enriched this work. I would like to thank Dr. David Kocman as well, for dedicating his time to exploring the development of Sr isoscapes with us; without his expertise, this work would not have been possible. Additionally, I am also grateful to the Public Scholarship, Development, Disability and Maintenance Fund of the Republic of Slovenia, whose scholarship made it possible for me to come to Slovenia and pursue my PhD. I would like to extend my heartfelt thanks to Asst. Prof. Dijana Đurović, my former mentor from Montenegro. Her belief in my potential and early career guidance played a significant role in leading me to this opportunity.

My warm thanks go to the entire Research Group for Trace Elements Speciation, especially Radmila, Janez, Janja, Tjaša, Katarina, Stefan, Pia, and Miroslav. I am deeply appreciative of the time and patience you dedicated to teaching me new techniques, guiding me through procedures, and for always being there to lend a hand during instrument troubleshooting. To all my current and former colleagues and visiting researchers at the Department of Environmental Sciences – many of whom have become cherished friends – thank you, for your support and camaraderie. I am incredibly fortunate to have shared this journey with each of you. My gratitude also goes to my friends from home and outside academia, whose presence and kindness have been a constant source of strength throughout my PhD journey.

Finally, I would like to give special thanks to my family for their continuous emotional support and understanding. Their love, encouragement, and faith in me have been invaluable in keeping my spirits and motivation high, especially during challenging times, and for that, I am forever grateful.

Abstract

This dissertation aimed to explore the potential of Sr isotope ratio analysis, combined with multi-elemental profiling, as a tool for geographic discrimination, focusing on two projects: tracing the provenance of cheese/milk from Naxos, Greece (Project 1), and wood in the Eastern Carpathians, Romania (Project 2). The goal was to understand how the Sr isotope ratio and elemental composition are transferred along the chain of soil – water – plant – animal – animal-derived product (milk), the factors influencing this transfer, and the main sources of Sr isotopes in the final products.

The first project highlights the geochemical authentication of PDO Graviera Naxos cheese, a complex dairy matrix where the Sr isotopic and multi-elemental analyses face challenges due to the diverse sources contributing to the final product, including seasonal variations in milk composition and external inputs such as sea salt and rennet. Despite these complexities, this study successfully demonstrated strong correlations between the Sr isotopic signatures of milk and local environmental factors, such as feed and water, showcasing the potential of Sr isotopes in tracing the geographical origin of dairy products. This project not only enhances our understanding of Sr isotopic variation but also contributes to the broader application of creating detailed isoscapes, which are essential for forensic and archaeological investigations. The second project documents the temporal variability in Sr isotopic and multi-elemental signatures of Norway spruce trees across the Rodna, Rarău, and Călimani Mountains over the past 50 years, revealing how environmental factors influence the geochemical profiles of timber. Through the analysis of wood core segments, the research tracks changes in elemental concentrations and Sr isotopic ratios, illustrating fluctuations within these geochemical signatures across time. This segment of the research highlights the transmission of unique geochemical signatures from the environment to the wood, offering promising avenues for timber provenance verification. Both studies emphasize the importance of considering the entire environmental context, from the composition of bedrock, soil, water, and atmospheric deposits, to plants and, in the case of dairy, further to animals, for accurately interpreting the Sr isotopic signature of a material. Instead of attributing the Sr isotopic signature solely to the geological substrate, our findings show that the Sr isotopic composition of the final product (wood, milk) or the derived product (cheese) depends on various factors, such as soil properties, plant uptake capacity, and Sr concentration at each stage. The collected data on elemental and Sr isotopic composition in wood, milk, and cheese, as well as environmental samples, form the basis for further efforts in safeguarding the geographical origin of Carpathian timber and Naxos cheese.

The presented dissertation fills a gap in understanding the contributions of different Sr sources, providing insights into the complexity of linking geological and environmental Sr isotopic and multi-elemental fingerprints with final products. Additionally, the results of this study have improved the quality of Sr isoscapes for Europe, covering both bioavailable Sr in soils and Sr in surface and groundwater.

Povzetek

Namen doktorske disertacije je bil raziskati učinkovitost uporabe izotopske sestave stroncija (Sr) v kombinaciji z večelementno sestavo kot orodja za geografsko diskriminacijo različnih vzorcev naravnega izvora. Osredotočili smo se na dva projekta, in sicer sledenje porekla sira in mleka z otoka Naksos v Grčiji (Projekt 1) in lesa iz vzhodnih Karpatov v Romuniji (Projekt 2). Cilj je bil ugotoviti, kako se izotopsko razmerje Sr in elementna sestava prenašata v verigi zemlja – voda – rastlina – žival – živalski proizvod (mleko), kateri dejavniki vplivajo na njihov prenos ter kateri so glavni viri Sr izotopov v končnih pridelkih ali produktih.

V prvem projektu smo se osredotočili na preverjanje geografskega porekla zaščitenega sira PDO Graviera Naxos. Sir predstavlja zahteven vzorec zaradi svoje kompleksne matrice. Analiza izotopov Sr in večelementna analiza sta tu še posebej zahtevni tako zaradi same priprave vzorcev za natančno določanje elementne in izotopske sestave kot tudi zaradi številnih virov, ki prispevajo h končni elementni in izotopski sestavi izdelka, vključno s sezonskimi spremembami v sestavi mleka ter zunanjimi vnosi, kot je morska sol in sirilo. Kljub naštetim izzivom smo v raziskavi uspeli pokazati močne povezave med izotopsko sestavo Sr v mleku in lokalnimi okoljskimi dejavniki, kot sta krma in voda, kar potrjuje uporabnost izotopov Sr pri sledenju geografskega porekla mlečnih izdelkov. Projekt ne poglablja zgolj razumevanja variacij izotopov Sr, temveč prispeva tudi k širši uporabi teh podatkov pri oblikovanju natančnih izotopskih zemljevidov (isoscapes), ki so bistveni za forenzične in arheološke študije. Drugi projekt dokumentira časovno spremenljivost elementne in izotopske sestave Sr v lesu navadne smreke iz gorovij Rodna, Rarău in Călimani v vzhodnih Karpatih v Romuniji v zadnjih 50 letih ter prikazuje vpliv okoljskih dejavnikov na geokemijske značilnosti lesa. Z analizo posameznih segmentov lesnega jedra smo sledili spremembam koncentracij elementov in izotopskega razmerja Sr. Rezultati so pokazali, da s časom prihaja do sprememb. S to raziskavo smo potrdili prenos edinstvenih geokemijskih značilnosti iz okolja v les, kar odpira nove možnosti za preverjanje porekla lesa. Obe študiji poudarjata pomen upoštevanja celotnega okolja, od sestave geološke podlage, tal, vode in zračnih depozitov, do rastline v primeru lesa in do živali v primeru mleka in sira, za natančno interpretacijo Sr izotopskega odtisa materiala, namesto da bi ga pripisali izključno matični geološki podlagi, kar je redna praksa v literaturi. Naše ugotovitve so pokazale, da je Sr izotopski odtis v končnem pridelku (les, mleko) ali izdelku (sir) odvisen od različnih dejavnikov, kot so fizikalno-kemijske lastnosti tal, sposobnosti rastline za privzem Sr in drugih elementov in ne nazadnje od koncentracije Sr v posamezni fazi. Zbrani podatki o elementni in Sr izotopski sestavi lesa, mleka in sira ter okoljskih vzorcev so podlaga za nadaljnje ukrepe za zaščito geografskega porekla karpatskega lesa in sira z Naksosa.

Predstavljena doktorska disertacija je zapolnila vrzel v razumevanju vpliva prispevkov različnih virov Sr, ki omogočajo vpogled v zapletenost povezovanja geoloških in okoljskih Sr izotopskih in večelementnih odtisov virov s končnimi pridelki in izdelki. Poleg tega so rezultati študije izboljšali kakovost porazdelitvenih map $^{87}Sr/^{86}Sr$ izotopskih razmerij za dele Evrope, tako za biodosegljiv Sr v zemlji kot Sr v površinski in podzemni vodi.

Contents

List of Figures

List of Tables

Abbreviations

CEC	. . . Cation Exchange Capacity
CRM	. . . Certified Reference Material
ESA	. . . Electrostatic Analyzer
FC	. . . Faraday Cups
IAEA	. . . International Atomic Energy Agency
ICP-MS	. . . Inductively Coupled Plasma Mass Spectrometer
IDW	. . . Inverse Distance Weighting
IIF	. . . Instrumental Isotopic Fractionation
KDE	. . . Kernel Density Estimate
LOD	. . . Limit of Detection
MC-ICP-MS	. . . Multi-Collector Inductively Coupled Plasma Mass Spectrometer
MCMC	. . . Markov Chain Monte Carlo
MDF	. . . Mass-dependent Fractionation
MIF	. . . Mass-independent Fractionation
NIST	. . . National Institute of Standards and Technology
PCA	. . . Principal Component Analysis
PDO	. . . Protected Designation of Origin
PTE	. . . Potentially Toxic Element
SD	. . . Standard Deviation
SIMM	. . . Stable Isotope Mixing Model
SRM	. . . Standard Reference Material

Chapter 1

Introduction

1.1 Strontium Isotopes in Environmental Studies

1.1.1 Strontium Isotopes Geochemistry and Evolution on Earth

Strontium (Sr) is a ubiquitous alkaline earth metal, discovered in 1790 in a mine near the Strontian (Scotland), and was first isolated in 1808. It is never found in its metallic form in nature as it rapidly oxidizes to form strontium oxide, which has a yellowish tint. It is the element of the group II of the periodic system and is analogous to calcium (Ca), according to its chemical properties. However, despite these similarities, the two differ in several key properties, such as ionization constants and solubility products (Sillen & Kavanagh, 1982). Sr is found in volcanic, alkali, and pegmatitic rocks. From these and other igneous rocks, as well as from sediments, Sr, along with Ca, is carried by rivers to the sea, partially dissolved and partially in crystalline silt particles. The crystalline fraction quickly settles in marine argillaceous sediments, while the dissolved fraction enriches the ocean's Sr concentration. Organisms incorporate Sr into their carbonate and phosphatic skeletons, removing it from the ocean at roughly the same Sr/Ca ratio as it entered. These Sr-bearing calcareous and argillaceous deposits are later uplifted during orogenesis and eroded, returning Sr and Ca to the sea. Some sedimentary Sr may also be incorporated into magmas, from which it is returned to the continental surfaces as volcanic or plutonic igneous rock, thus partially closing the cycle. These elements behave similarly in the environment – they are both highly plant available and are characterized by similar plant uptake from soil and distribution and accumulation to various organs of plants. Sr cycles through the environment similarly to Ca, but is about 1/500 as concentrated in most phases (Odum, 1951). Sr easily enters the food chain, since it is contained in all plant and animal organisms. The organism of an adult human contains about 0.3 g of Sr, most of which (99 %) is localized in the skeleton, incorporated by exchanging Ca ions in the hydroxyapatite crystal lattice (Gupta & Walther, 2017). Sr has not been proven to be essential for human health, yet there is speculation that osteoporosis might be linked to a degree of Sr deficiency. This hypothesis is supported by the effectiveness of Sr ranelate, which enhances bone Ca and reduces fracture rates in osteoporotic patients (Blake & Fogelman, 2006; Marx et al., 2020). Adults typically absorb up to 80 % of ingested Ca but only 20–40 % of ingested Sr, indicating a preferential absorption of Ca in the digestive tract. Additionally, mammalian kidneys excrete Sr more rapidly than Ca. This selective absorption and excretion pattern is consistent across mammals and influences the distribution of these elements in food chains. For instance, plants exhibit high Sr/Ca ratios, yet herbivores that consume these plants show lower ratios due to digestive discrimination. Carnivores, in turn, consume herbivores and thus have even lower Sr concentrations in

their tissues. This progressive decrease in Sr/Ca ratios along the food chain is used in research to estimate the dietary proportions of meat versus plant-based foods by analyzing these ratios in human and animal skeletons (Pors Nielsen, 2004).

Sr occurs naturally as a mixture of four stable (non-radioactive) isotopes, with approximate abundances of 0.56 % (^{84}Sr), 9.87 % (^{86}Sr), 7.04 % (^{87}Sr), and 82.53 % (^{88}Sr). Sixteen radioactive isotopes of Sr have been synthesized and identified, the most relevant being ^{90}Sr, a betta emitter with a half-life period of 28.8 years. It has been a radiological concern since the dawn of the nuclear industry, associated primarily with the fallout from atmospheric nuclear weapon testing and major nuclear accidents (Joyce, 2017).

However, Sr isotopes are most known for their application as tracers in geological processes and as indicators of provenance in an archaeological context, because naturally occurring rubidium (^{87}Rb), with a half-life of 4.9 x 10^{10} years, undergoes radioactive decay to stable, radiogenic ^{87}Sr. Produced ^{87}Sr is continuously being added to its "initial" amount in a given material. This phenomenon has become the base principle of dating rocks and minerals and establishing a method for the measurement of geologic time. Studies of the isotopic composition of Sr had a great impact on understanding the chemical evolution of Earth (Faure & Powell, 1972). The isotope ratio ^{87}Sr/^{86}Sr is used as an index of the ^{87}Sr enrichment, and the higher it is, the more the rock is aged and initially rich in Rb. The relative abundance of radiogenic ^{87}Sr is very specific to rock type, making it a powerful tracer of source material. Rb and Sr show specific affinities for minerals (Rb is incorporated in potassium (K) minerals, while Sr is incorporated in Ca minerals), which leads to their different partitioning not only at the mineral scale but at the large scale between the mantle and the crust (Plimer & Elliott, 1979).

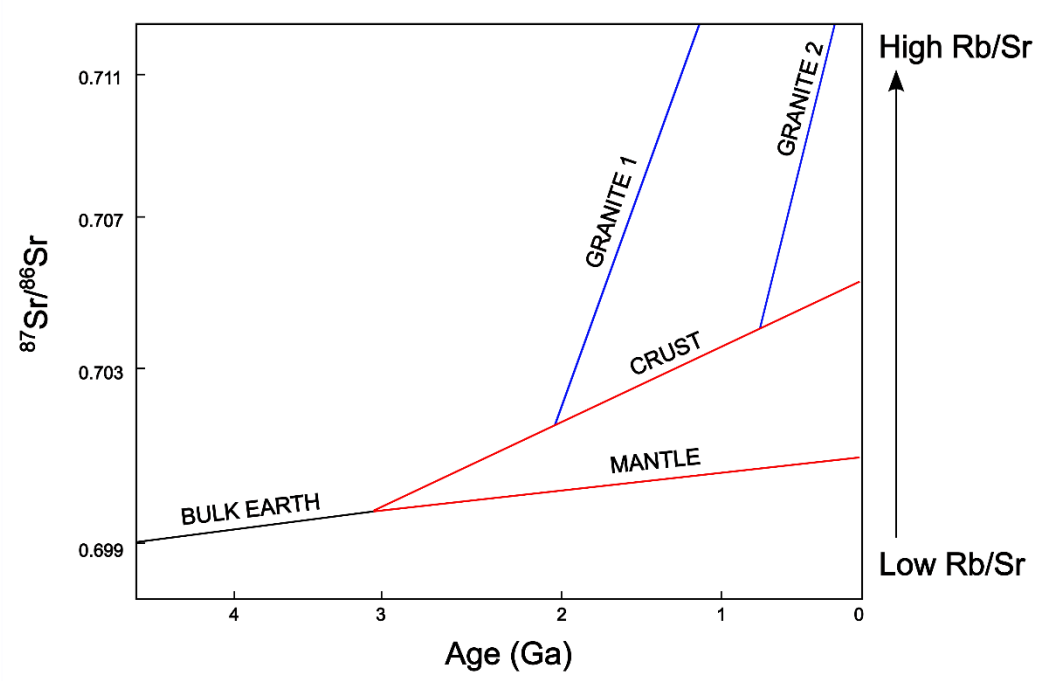

Figure 1.1: Three-stage model for the evolution of ^{87}Sr/^{86}Sr in Earth materials through geological time (Adapted from Bataille & Bowen (2012)).

Bataille & Bowen (2012) proposed a model of the ^{87}Sr/^{86}Sr evolution, which considers each rock's geological history. This three-stage model is based on the concept developed

by Capo et al. (1998) and explains the crustal differentiation as well as distribution of Rb, which, due to its higher affinity to crustal minerals, ended mainly in different crustal layers. Consequently, newly formed rocks inherited initial $^{87}Sr/^{86}Sr$ from their precursors, but different Rb/Sr, which leads to $^{87}Sr/^{86}Sr$ evolution. The range of modern $^{87}Sr/^{86}Sr$ ratios in natural materials is limited by the primordial Sr isotope composition (basaltic achondrite best initial – BABI) and the radiogenic growth of ^{87}Sr from the radioactive decay of ^{87}Rb over time (Figure 1.1) (Papanastassiou & Wasserburg, 1968). When the Earth formed around 4.56 billion years ago, it had an initial Sr isotope composition of approximately 0.69899. Over time, the radiogenic production of ^{87}Sr has caused this primordial isotope composition to shift to higher values. The extent of this radiogenic increase, and the resulting Sr isotope composition in different Earth reservoirs today, is determined by the half-life of ^{87}Rb, as well as the age and Rb/Sr ratios of the individual geochemical reservoirs (e.g., Earth's mantle, continental crust, and seawater) or rock types (such as basalt, granite, or sediments).

1.1.2 Variation of Strontium Isotopes at the Global Scale

1.1.2.1 Fractionation of Strontium Isotopes

Isotopes show a shift in their relative abundances during biogeochemical and biomineralization processes. For most elements, the processes that act in order to separate isotopes from each other depend on differences in mass, so the separation typically scales in proportion to them, which is known as *mass-dependent fractionation (MDF)* (Dauphas & Schauble, 2016).

Heavier elements, like Sr, show less fractionation than the lighter elements (H, C, O, N). Secondly, the fractionation will be the highest for the two isotopes that have the largest mass difference, which is to say that the $^{88}Sr/^{86}Sr$ ratio will fractionate twice as much as the $^{87}Sr/^{86}Sr$ ratio. In natural systems, fractionation of $^{88}Sr/^{86}Sr$ or $^{87}Sr/^{86}Sr$ can occur due to processes like ion exchange, diffusion, or the preferential incorporation of certain isotopes into mineral lattices or biological structures. For example, during the formation of calcium carbonates, slight fractionation of Sr isotopes can occur. However, this fractionation tends to be small compared to other isotopic systems. For most geological and environmental studies involving Sr, mass-dependent fractionation is minimal and plays a much smaller role compared to the effects of radiogenic decay of ^{87}Rb to ^{87}Sr, which primarily drives variations in $^{87}Sr/^{86}Sr$ ratios in nature. The variation in $^{87}Sr/^{86}Sr$ is largely governed by the age of the rocks and Rb content.

In addition, $^{88}Sr/^{86}Sr$ ratio has been considered invariant in nature for a long period of time. Even though that the variation of this isotope ratio has been reported earlier, its application in isotope geochemistry dates back to the last couple of decades (Fietzke & Eisenhauer, 2006). It is expressed as δ – value relative to NIST SRM987 (the international isotopic standard for Sr, with a certified $^{87}Sr/^{86}Sr$ value of 0.71034 ± 0.00026). For the quantification of the mass-dependent fractionation of Sr, the Eq. (1.1) is used (Fietzke & Eisenhauer, 2006). It is the deviation of the $^{88}Sr/^{86}Sr$ value in the sample, with respect to the value of SRM987, and is expressed in ‰ units.

$$\delta^{88/86}Sr = \left[\frac{(^{88}Sr/^{86}Sr)_{sample}}{(^{88}Sr/^{86}Sr)_{SRM987}} - 1\right] \times 10^3 \tag{1.1}$$

Besides, lighter Sr isotopes (^{86}Sr) are more likely to be incorporated into biological systems over heavier isotopes like ^{88}Sr. Such behaviour results in fractionated depletion of

$\delta^{88/86}$Sr values, as Sr cycles through different trophic levels. It is also expected that different biological tissues, formed at different times in a person's life may differ in $\delta^{88/86}$Sr. This may serve as additional information on the source of Sr and could lead to fulfillment of requirements for reliability of Sr isotopes as tracers. Many studies have been conducted in order to obtain data for $^{87}Sr/^{86}Sr$ and $\delta^{88/86}$Sr values in different rocks, soil and water compartments, as well as the atmosphere (Andrews et al., 2016; Oeser & von Blanckenburg, 2020; Pearce et al., 2015). These studies enabled determination of the main contributors to the Sr isotope composition of each of examined compartment. For example, Sr in wet atmospheric deposition is derived from seawater evaporation, while dry deposition has $^{87}Sr/^{86}Sr$ signature similar to the bedrock which it is derived from (soil). The differences are observed in water sources, too. Measured $\delta^{88/86}$Sr ranges from 0.25 ‰ in tap water, 0.36 ‰ in seawater, and 0.40 ‰ in lake water (Knudson et al., 2010).

Although the variation in measured $\delta^{88/86}$Sr is small, recent advances in mass spectrometry and current multi-collector mass spectrometers made it possible to measure them using different correction strategies. The $\delta^{88/86}$Sr values are recently being used in conjunction with the $^{87}Sr/^{86}Sr$ isotope ratio to improve constraints on the sources of Sr in different materials that are studied. As a result, a wide range of new applications of "non-traditional" stable isotopes has occurred. Some of the fields that felt the benefits of this approach are: hydrology, forensics, archeology, ecology, and food traceability and authentication.

Recent studies have revealed that Sr undergoes mass fractionation during terrestrial exogenic cycling, with lighter Sr isotopes being preferentially incorporated into both biogenic and inorganic calcium carbonates. This results in seawater having a relatively heavy stable Sr isotope composition, similar to the behavior observed with Ca isotopes. Sr is nearly unique in its ability to record both its source, via the $^{87}Sr/^{86}Sr$ ratio, and the mass-fractionating processes it has experienced, as captured by $\delta^{88/86}$Sr. The combined use of these isotopic data offers the potential for a highly refined understanding of Sr's exogenic cycle (De Souza et al., 2010; Halicz et al., 2008).

1.1.2.2 Environmental Influences on Strontium Isotope Ratios

The weathering and soil formation processes play a crucial role in shaping the environmental influences on Sr isotopes. Weathering of rocks and minerals, a critical process at the earth's surface, occurs both at the microscopic interface between solids and solutions and at the larger scale where the earth's endogenic and exogenic cycles intersect. Internal forces within the earth dictate the distribution of rocks, minerals, chemical elements, and relief over time and space. Concurrently, the exogenic system transforms these rock-forming minerals and their elements into residual and secondary solids and dissolved products, redistributing them physically, chemically, and biologically (Miller et al., 1993). These interphase interactions between the lithosphere, hydrosphere, atmosphere, and biosphere significantly modify both the earth's surface and the chemistry of its fluid envelopes (Price, 1995). As a consequence of the weathering of rocks, Sr is released and, in that way, becomes available in the soil and ready to be taken up by plants.

Within the *soil-vegetation-atmosphere system*, Sr is derived from parent rock and further supplemented by rainwater and dust deposition. The isotopic composition of Sr in soils can vary due to the heterogeneous mix of Sr-containing minerals in parent rocks, which possess different Rb/Sr ratios. This variability results in distinct $^{87}Sr/^{86}Sr$ values as different minerals weather and release Sr at varying rates. Additionally, temporal fluctuations in the isotopic composition of Sr released from rocks complicate the understanding of Sr cycling. Sr is stored in primary and authigenic minerals, soil solutions, cation exchange sites, and vegetation, including foliage, wood, roots, and decaying material.

It is redistributed throughout the soil-vegetation system via mineral weathering, cation exchange, leaching, root uptake, and bioturbation, creating a distinct Sr isotopic signature in soils. Leaching of Sr from soil, influenced by factors such as soil pH, moisture, and organic matter content, can alter isotopic ratios within different soil horizons. Over time, ongoing weathering, vegetation changes, and climate conditions cause temporal variations in Sr isotopic composition, offering insights into the history of soil development and environmental changes (Åberg et al., 1989; Brass, 1975; Velbel, 1988).

Atmospheric deposition, including rainwater, dust, and sea salt, can contribute additional Sr to the soil-vegetation-atmosphere system, potentially altering the Sr isotopic composition of soils and the broader environment. Studies have shown that the $^{87}Sr/^{86}Sr$ ratios in forest ecosystems are influenced by both local geological conditions and atmospheric deposition, particularly in regions receiving transboundary substances (Urakawa et al., 2023). The Sr isotopic signature thus reflects a combination of parent material weathering and atmospheric inputs, providing valuable insights into the sources and patterns of atmospheric deposition and its effects on soil biogeochemical properties. Over the last few decades, naturally occurring isotopic tracers in the Rb-Sr system have become crucial for understanding the sources and cycling of mineral nutrients in terrestrial ecosystems. Early studies indicated that atmospheric deposition of salts and mineral aerosols (dust) is a major source of Sr and other alkaline earth base cations (Ca, Mg) to forests (Gosz & Moore, 1989; Vitousek et al., 1999). However, it has become clear that all ecosystems derive base cations from various sources, whose importance varies over time and across different landscapes, climate regimes, and geological substrates. Several factors must be considered. Strong temporal variations in the isotopic composition of Sr released from rocks can occur due to their heterogeneous mineral mix. Additionally, the composition of atmospheric inputs from wet and dry deposition varies significantly, influenced by factors such as air parcel trajectory and the addition of various aerosols. Even in regions with relatively simple Sr systematics, such as islands with consistent oceanic Sr sources, understanding Sr isotope variations and their implications for cation dynamics remains complex (Chadwick et al., 2009; Novak et al., 2024).

Anthropogenic activities can also cause local variations in the isotopic composition of Sr. Agricultural practices, industrial processes, and the use of fertilizers, for example, may introduce additional Sr into the environment, potentially altering the natural Sr isotopic signature in certain regions (Aguzzoni et al., 2018; R. C. Hill et al., 2024; Pierson-Wickmann et al., 2009). Sr in fertilizers, often associated with sulfates, phosphates, carbonates, or potassium used in their manufacture, typically exhibits ratios (0.708−0.709), similar to those of late Tertiary and modern seawater and, therefore, with the contemporaneous chemical sediments (sulfates, carbonates, phosphorites) (Otero et al., 2004). One study has shown a similarity between the $^{87}Sr/^{86}Sr$ ratio of phosphate rocks and mineral fertilizers originating from the same geographical region (Sattouf et al., 2007).

Water bodies play a key role in the distribution and variation of Sr isotopes within environmental systems. The isotopic composition of Sr in groundwater does not directly reflect the $^{87}Sr/^{86}Sr$ ratios of the bulk soil or rock it contacts, but rather that of the soluble Sr fraction from minerals. This specific composition remains unaltered by near-surface processes such as mineral precipitation, evaporation, or biogenic metabolism, accurately representing the mixing of Sr from its predominant sources. The strength of Sr isotopes lies in the fact that the isotopic characteristics of the watershed primarily determine the $^{87}Sr/^{86}Sr$ ratio of surface water and groundwater, as natural processes do not cause significant fractionation. This ratio acts as a conservative tracer, remaining unchanged in water until it mixes with other waters containing Sr of different compositions. When natural and anthropogenic sources have distinct Sr isotopic compositions, the $^{87}Sr/^{86}Sr$ ratio in fluvial and groundwater reflects the mixing of different endmembers, providing a

valuable tool even when nitrate or sulfate fertilizer isotopic signatures are indistinct. However, mineral dissolution and cation exchange processes in soils and aquifers must be considered. Variations in the isotopic composition of Sr in seawater, recorded in marine limestones, serve as proxies for the interplay between mantle processes and crustal weathering (Edmond, 1992). The balance between non-radiogenic Sr from deep-sea hydrothermal vents and radiogenic Sr from continental weathering determines the Sr isotopic signature in seawater at any given time. The residence time of Sr in seawater is approximately 2.4 million years, much longer than the ocean mixing time (~1.5 kyr), making the $^{87}Sr/^{86}Sr$ ratio in seawater relatively homogeneous at around 0.709175 (Veizer, 1989). This isotopic composition is influenced by two primary sources: Sr from the weathering of old, Rb-rich continental silicate rocks, which are enriched in ^{87}Sr due to the decay of ^{87}Rb, and Sr with lower $^{87}Sr/^{86}Sr$ ratios derived from the Earth's mantle, entering the ocean through mid-ocean ridges and weathering of mantle-derived rocks. A minor contribution comes from the dissolution and alteration of seafloor sediments. Although riverine $^{87}Sr/^{86}Sr$ ratios are distinct from seawater, ranging from ~0.705 in young volcanic terrains to ~0.735 in older crustal regions, the higher Sr isotope ratio in seawater ensures that even in areas with significant river input, seawater retains its global isotopic signature. Glacial and interglacial weathering cycles have introduced additional complexity to the marine Sr budget, particularly during glacial periods when weathering of continental shelf carbonates contributed significantly to Sr fluxes. Additionally, stable Sr isotopes ($\delta^{88/86}Sr$) reveal that marine carbonates are ~0.2 ‰ lighter than seawater due to the preferential incorporation of lighter isotopes during carbonate precipitation, providing an added dimension to understanding Sr cycling in marine environments (Krabbenhöft et al., 2010). Continental signals from the dissolution of igneous and metamorphic rocks are moderated by carbonate weathering, which retains a "memory" of past isotopic fluctuations. Rivers and streams introduce Sr from the weathering of platform carbonates and evaporites, with minimal contributions from refractory igneous and metamorphic rocks. Groundwater and surface waters further modulate these isotopic ratios as they interact with atmospheric deposition and mineral weathering. Seasonal variations also influence Sr isotopic signatures, with shifts observed in mineral springs during the rainy season due to precipitation-driven mixing and dilution. Consequently, water bodies act as integrators and conveyors of Sr isotopic signals, documenting the complex interactions between the lithosphere, hydrosphere, and atmosphere, and providing insights into both past and present geochemical cycles (Blum et al., 1993; Boral et al., 2021; Colin et al., 2006).

1.2 Determination of Strontium Isotope Ratios

1.2.1 Multi-Collector Inductively Coupled Plasma Mass Spectrometry

The intended use of MC-ICP-MS is the precise and accurate determination of isotope ratios across a wide range of isotopic systems accessible through ICP-MS. The development of MC-ICP-MS about 25 years ago has enabled the precise and accurate analysis of isotopic compositions for a wide range of elements, allowing for the detection of subtle natural variations (Greber & Van Zuilenc, 2022). The components on the front side of the MC-ICP-MS are largely similar to those of other ICP-MS devices. It includes the sample introduction system, the inductively coupled plasma ion source, and a sampling interface.

The sample solution is introduced into the mass spectrometer as an aerosol, which is generated by a nebulizer. This nebulizer can be connected to either a glass spray chamber, which removes larger aerosol droplets, or a desolvator, which dries the sample aerosol before it reaches the plasma. A "dry" plasma (produced by a desolvator) provides higher

ionization efficiency than a "wet" plasma (produced by a spray chamber), resulting in higher signal intensities. The choice of sample introduction system depends on the element being analyzed and its available quantity. Overall, systems with lower yield, such as spray chambers, offer more stable signals and less instrumental isotope fractionation compared to those that provide higher intensities, such as desolvators. For analyzing trace element isotopes with sufficient signal intensity, a desolvation system is often essential. In our case, the sample introduction system was enhanced by integrating the Aridus Desolvating Nebulizer System. This enhancement significantly mitigates issues such as hydride and carbide polyatomic ion interferences, plasma instability, and carbon deposition on the cones. Moreover, by improving analyte transport efficiency, the sensitivity of the system is increased (Thomas, 2023). The schematic diagram of the instrumet used for the scope of this dissertation is shown in Figure 1.2.

The Nu Plasma detector array features sixteen Faraday detectors and five ion-counting multiplier channels strategically interspersed among them. As a hybrid mass spectrometer, the MC-ICP-MS integrates an ICP plasma source with an electrostatic analyzer (ESA), followed by a magnetic sector and multiple collectors for ion measurement. The Nu Plasma II, a double-focusing multi-collector inductively coupled plasma source mass spectrometer, includes a 350 mm radius ESA and a 250 mm radius magnet configured in Forward Nier-Johnson geometry. This instrument delivers high-precision isotope ratio data for elements spanning the mass range from 3 to 300 amu. The ICP source achieves very high ionization efficiency across the mass range, but it also generates an ion population with a significant energy spread. The sample is introduced into an inductively coupled plasma, where electrons are stripped away, creating positively charged ions. The ionization of elements in plasma occurs at temperatures between 6000 and 8000 K. These ions are then accelerated across an electrical potential gradient of up to 10 kV and focused into a beam using a series of slits and electrostatically charged plates. This ion beam passes through an energy filter, ensuring a consistent energy spectrum, and then through a magnetic field where ions are separated based on their mass-to-charge ratio (m/z). The mass-resolved beams are directed into collectors, where the ions are converted into voltage (S. J. Hill, 2006; Holland & Bandura, 2005; Vanhaecke & Degryse, 2012).

The ions exiting the ESA are energy-compensated, meaning that ions of the same mass but different energies enter the flight tube and magnet on different trajectories. As they enter the flight tube and magnet, the ions are separated according to their mass-to-charge ratio by the magnetic field. Each mass exits the magnet along a unique trajectory toward the collector array.

After the separation of ions according to their mass-to-charge ratios, the ions are guided to the detection system. Upon exiting the magnet, the ion beam passes through the Zoom lens assembly, which contains quadrupole lenses used to focus the beam onto the collector-defining slit and optimize beam dispersion. The primary goal of the detection system is to detect each ion of interest and convert and amplify ion signals into a physical signal suitable for further data processing. Faraday cups (FC) are one of the most common detection systems in modern mass spectrometers. They are highly regarded for high-precision isotope ratio measurements due to their stability and linearity. In Faraday cup detection, the ion signal is detected directly by measuring the ion beam intensity as a current, unlike pulse-counting systems that count individual ions. When ions enter the cup, electrons neutralize the incoming positively charged ions. The electron current flows through a high-value resistor, creating a potential difference that is recorded (Balcaen et al., 2005; Barbaste et al., 2002; Becker, 2005).

The Nu Plasma II detector array consists of 16 FC detectors fixed in position. Ion steering into the cups is achieved through a patented variable zoom lens optics system. Additionally, small deflector assemblies located behind the Faraday detector array deflect

ion beams into off-axis secondary electron multipliers. These deflector assemblies allow the multipliers to be independently protected against intense signals by deflecting the ion beam away from the first dynode of the multiplier. Isotope ratios are calculated by comparing voltages from different collectors. The Nu Plasma II offers true high-resolution capabilities, achieved through three sets of independently adjustable slits positioned at various points within the instrument. The first slit encountered by the beam is the source slit, with selectable width settings of 0.3 mm, 0.05 mm, and 0.03 mm. The second slit, known as the alpha slit, is continuously variable from 0 to 7 mm, utilizing "muscle wire" technology, also known as shape memory alloy. The final set of slits consists of adjustable collector slit masks, positioned in front of several specifically chosen collectors (Albarède et al., 2004; L. Yang, 2009).

Despite its many strengths, the system also has some disadvantages. All elements introduced into the plasma are ionized, including doubly charged species, oxides, and argides. Additionally, plasma instability can limit precision. Although the ionization efficiency of the plasma is nearly 100 %, ion transmission is lower compared to Thermal Ionization Spectrometry (TIMS). This reduction in transmission occurs because the plasma-generated ions must be transferred from atmospheric pressure to the high vacuum of the mass spectrometer, resulting in the loss of many ions (Jakubowski et al., 2014).

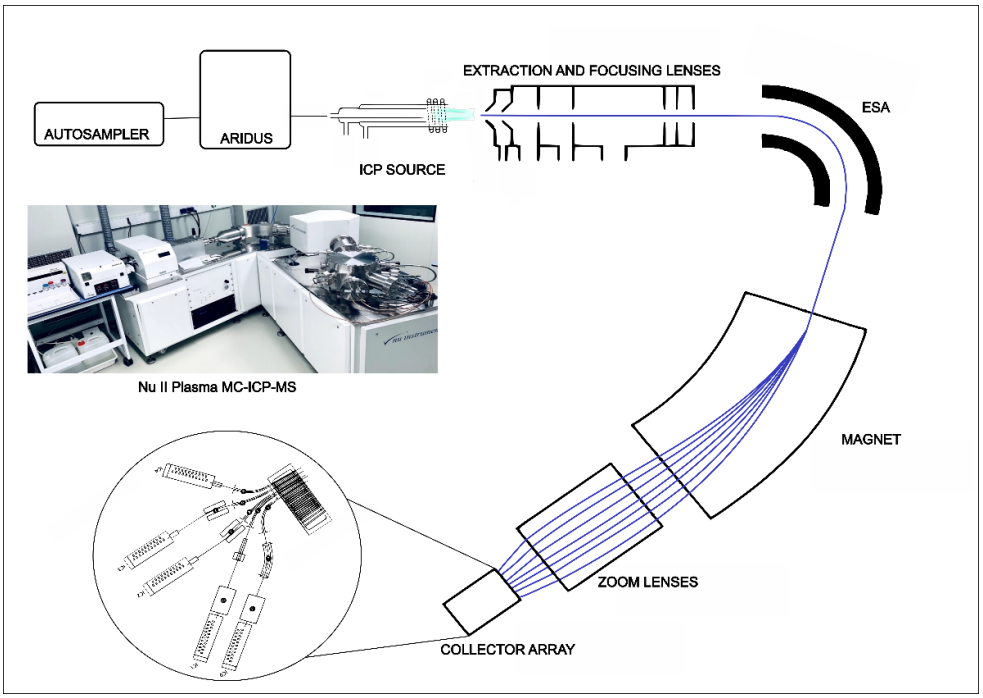

Figure 1.2: Schematic diagram of Nu II Plasma multi-collector-ICP-MS with Forward Nier-Johnson geometry.

1.2.2 Sr Separation from the Matrix: Best Practices for High-precision Measurement

Interferences in ICP-MS are generally categorized into two main types: spectral and nonspectral. Spectral interferences occur when signals are detected at a specific m/z that do not originate from the analyte ion being analyzed (Lum & Sze-Yin Leung, 2016). These

are considered the most significant type of interferences in ICP-MS. They can be caused by various factors, such as the plasma or nebulizer gas, matrix components in the solvent or sample, other elements within the sample, or atmospheric oxygen or nitrogen that gets into the system. These interferences mainly result from three sources: 1) stray ions generating signals at the time of measurement, which are typically removed by applying specific filters, 2) ions with different m/z ratios but varying kinetic energies, which generate signals at a different nominal m/z ratio and can be reduced using a double-focusing mass analyzer for energy focusing, and 3) singly or multiply charged mono- or polyatomic ions with the same nominal m/z ratio, which originate from other sources rather than the analyte ion (Irrgeher et al., 2015). The latter source of interference can be further subdivided, as these can be attributed to isobaric atomic ions, multiply charged ions, and polyatomic ions from various origins.

Isobaric interferences occur when the signals from nuclides of different elements coincide at the same nominal mass. Since most instruments do not possess the mass resolution needed to overcome these interferences, alternative strategies are employed. In most cases, at least one isotope of each element is free from isobaric overlap and can be monitored instead. Isobaric interferences are usually corrected mathematically by considering the natural isotopic abundances of elements. Multiply charged ions typically have a much lower formation rate than singly charged ions, depending on their ionization potential.

For Sr isotope ratio measurements, several types of interferences can arise, including:

1. Isobaric interferences, such as ^{87}Rb overlapping with ^{87}Sr, ^{86}Kr interfering with ^{86}Sr, and ^{84}Kr interfering with ^{84}Sr. The ^{86}Sr interference is especially problematic for $^{87}Sr/^{86}Sr$ ratio measurements because ^{86}Sr is the stable isotope used as a reference for mass fractionation correction.
2. Polyatomic ion interferences, which include Ca-dimer ions ($^{40}Ca^{44}Ca^+$, $^{42}Ca_2^+$, $^{40}Ca^{46}Ca^+$, $^{42}Ca^{44}Ca^+$, $^{43}Ca_2^+$, $^{40}Ca^{48}Ca^+$, $^{42}Ca^{46}Ca^+$, $^{44}Ca_2^+$) and $ArCa^+$ molecular ions ($^{36}Ar^{48}Ca^+$, $^{38}Ar^{46}Ca^+$, $^{40}Ar^{44}Ca^+$, $^{38}Ar^{48}Ca^+$, $^{40}Ar^{46}Ca^+$, $^{40}Ar^{48}Ca^+$), leading to isobaric interferences on Sr signals ($^{84}Sr^+$, $^{86}Sr^+$, and $^{88}Sr^+$).
3. Doubly charged ions, particularly from rare earth elements like ^{172}Yb, ^{174}Yb, and ^{174}Hf, which can interfere with ^{87}Sr.

To address matrix-based spectral and nonspectral interferences, one of the most effective methods is to use proper sample preparation techniques and an appropriate introduction system, which facilitates the separation of the analyte of interest from the matrix. In typical procedures, samples are dissolved and introduced as a solution into the MC-ICP-MS. Solid samples require digestion, and the exact protocol for this depends on the sample material and the element being analyzed. After digestion, the element of interest must be purified from the sample matrix.

When measuring the $^{87}Sr/^{86}Sr$ isotope ratio, the successful removal of Rb is critical. This is because the masses of ^{87}Sr (86.908882) and the isobaric ^{87}Rb (86.909186) are so close that a mass resolution of 2.9 x 10^5 is required to distinguish them, which most modern mass spectrometers cannot achieve (Baffi & Trincherini, 2016). To maintain total uncertainty below 0.05%, the Rb concentration after separation must be less than 0.15%, requiring a removal efficiency of 99.85%. This is difficult to achieve, especially when the Rb/Sr ratio in the original sample can be as high as 10:1. Even small amounts of Rb can interfere due to its high ionization efficiency, making it necessary to ensure efficient removal.

Ion-exchange chromatography is the most common method used to purify Sr from the sample matrix. This method involves dissolving the sample in a mobile phase and introducing it into a column containing a stationary phase (resin). Different sample components interact with the mobile and stationary phases based on their partition

coefficients, with some components remaining in the mobile phase and others being retained by the stationary resin (Greber & Van Zuilenc, 2022). The AG50W-X8 ion exchange resin, commonly used in 2 mol L^{-1} HCl medium, is highly effective at retaining Sr (Nie et al., 2021). In theory, all Rb elutes from the column before the Sr fraction is collected. However, in practice, and especially in samples with high Rb concentrations, achieving a complete separation of Rb from Sr can be challenging. Automated chromatographic systems have also been developed, some of which can be coupled directly to (MC-)ICP-MS for Sr isotope analysis, though not all methods guarantee quantitative Sr recovery.

The Eichrom® Sr-specific resin (100–150 µm particle size) is frequently used for Sr isotope analysis. This resin uses a crown-ether extractant diluted in octanol, with a capacity of 8 mg Sr per mL of resin. The fundamental principle of the protocol using Sr specific resin is illustrated in Figure 1.3.

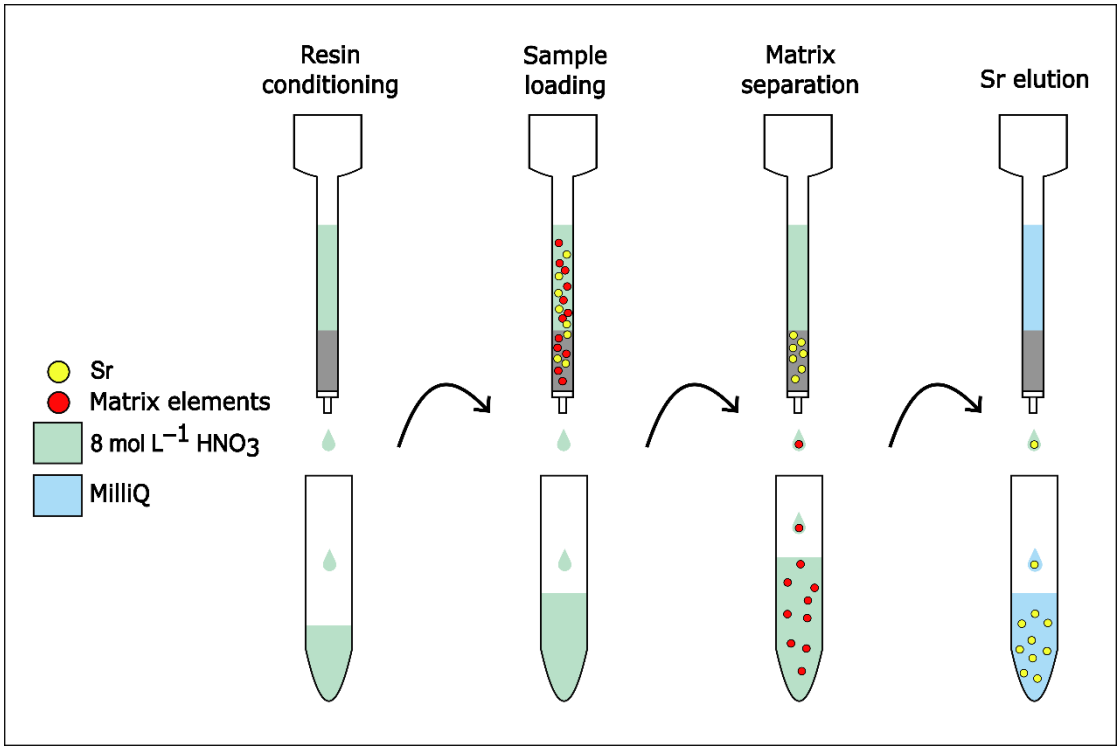

Figure 1.3: Simplified illustration of the Sr separation protocol on Sr specific resin.

The resin's affinity for Sr increases with the concentration of HNO_3, peaking between 3 and 8 mol L^{-1}. However, when the sample contains more than 8 mg Sr (per 2 mL resin), the recovery efficiency decreases, making it crucial to balance the Sr carrier amount and the sample's Sr content. Variability in the application of this resin is evident across different studies, with differences in resin bed volume (ranging from 50 µL to 2 mL) and HNO_3 concentration (2 to 8 mol L^{-1}) affecting Sr retention and recovery. While miniaturized methods work for simple matrices, they may fail with more complex matrices, such as those found in bone or dental tissue samples. Additionally, inconsistent Sr recovery is reported in the literature, with some studies not quantifying recovery and others showing varying results based on the Sr and matrix load. For accurate Sr isotope ratios, quantitative recovery is preferable to avoid isotopic fractionation during isolation. If quantitative recovery cannot be achieved, it is essential to verify that on-column Sr isotopic fractionation does not occur (De Muynck et al., 2009).

1.2.3 Correction of Measured Strontium Isotope Abundance Ratios for Mass Discrimination

In mass spectrometry, the term *instrumental isotopic fractionation (IIF)* refers to the collective effects within a mass spectrometer that occur during processes such as sample introduction, ion formation, extraction, transmission, separation, and detection. These effects result in a difference between the measured and true isotope ratios in a sample. The term IIF encompasses both mass-dependent and mass-independent effects and includes all discriminatory influences. The latter remains less studied and understood to date. Factors such as diffusion repulsion, space-charge effects, absolute isotope mass, ion density, and ionization efficiency are just a few of the potential sources contributing to IIF. It is also commonly referred to in the literature as *instrumental mass bias*, *instrumental mass discrimination*, or *instrumental mass fractionation*.

IIF is typically more pronounced during sample introduction (e.g., evaporation, diffusion, and transport efficiency) and ionization, and it is influenced by the sample's matrix. This makes it a significant source of systematic error in isotope ratio mass spectrometry. As a result, a process known as *mass bias correction* is essential for achieving accurate isotope ratio measurements, particularly when determining absolute isotope ratios. When using δ-values, all factors contributing to the deviation between the measured and true ratios are accounted for, regardless of their origin (e.g., instrumental fractionation or dead time), as long as the sample and standard exhibit identical behavior.

The extent of IIF can be expressed as *mass bias per mass unit (MB)*, in accordance with Eqs. (1.2) and (1.3), and varies significantly across different mass spectrometric techniques. For instance, IIF is more pronounced in ICP-MS compared to TIMS. In ICP-MS, mass bias per mass unit typically ranges from 0.5–1.5% for heavier isotopes like Pb and U, and can reach up to 25% for lighter isotopes. In contrast, TIMS exhibits IIF that is about an order of magnitude lower, largely due to a preference for the evaporation and ionization of lighter ions over heavier ones in the thermal ionization source (Aggarwal et al., 2004; Vance & Thirlwall, 2002). However, the factors driving IIF are still not fully understood. IIF can potentially occur in all parts of an ICP-MS instrument. The sample introduction system, ionization source, and the interface are considered key contributors to IIF. Varying operating conditions, such as sampling depth, carrier gas flow, and ion lens settings, all influence isotopic fractionation. After the ion-beam is formed, the interface is believed to have the most significant impact on IIF in ICP-MS, with the region between the sampler and skimmer cones being the primary site where mass bias occurs.

$$f = \frac{R_{true}}{R_{measured}} \tag{1.2}$$

$$IIF\ (\%) = \frac{(f-1) \times 100}{\Delta m} \tag{1.3}$$

f: mass bias factor
R_{true}: true isotope ratio
$R_{measured}$: measured isotope ratio
Δm: difference in the mass of the heavier and lighter isotope of one element

Historically, the measurement of Sr isotope ratios has relied on a method called *normalization*, which corrects the measured isotopic ratios of $^{87}Sr/^{86}Sr$ and $^{84}Sr/^{86}Sr$ based on the known value of the $^{88}Sr/^{86}Sr$ ratio. This known value was first measured by Alfred Otto Carl Nier in 1938, using a magnetic sector-field mass spectrometer, with a reported ratio of 8.375209 (Nier, 1938). Nier's measurement is still used as a global reference in Sr isotope analysis. Normalization is widely used because it compensates for instrumental mass fractionation, making it possible to compare isotopic data across different samples. However, the procedure is highly dependent on the assumed "true" $^{88}Sr/^{86}Sr$ ratio. If Nier's value is incorrect or outdated, the normalized $^{87}Sr/^{86}Sr$ and $^{84}Sr/^{86}Sr$ values may be precise but inaccurate, as the entire process hinges on the assumption that Nier's ratio is correct. In recent years, an alternative approach called the *double-spike technique* has been introduced for Sr isotope measurements. While initially developed for Pb isotopes, this technique attempts to overcome some of the limitations of normalization. However, the accuracy of the double-spike method is also uncertain because the isotopic composition of the double spike itself is calibrated using the same NIST SRM 987 reference material, which relies on Nier's $^{88}Sr/^{86}Sr$ ratio. Additionally, researchers have explored the *total evaporation method* (*TEM-TIMS*) to determine the true isotopic ratios of Sr. This technique involves TIMS, but its accuracy is limited by isotopic fractionation during the filament heating process, which causes shifts in the measured $^{88}Sr/^{86}Sr$ and $^{87}Sr/^{86}Sr$ ratios to higher values and the $^{84}Sr/^{86}Sr$ ratio to lower values. In conclusion, while normalization and newer techniques like double-spiking are commonly used for Sr isotope ratio measurements, both approaches are limited by uncertainties in the reference values, particularly Nier's $^{88}Sr/^{86}Sr$ ratio, which underpins much of the current methodology (Cavazzini et al., 2022).

1.2.3.1 Internal Calibration of Isotope Abundance Ratios

Different correction strategies for IIF have been applied when using MC-ICP-MS. In order to correct for IIF, an invariant isotope ratio of the same element (intraelemental) or a dopant element (interelemental) should be used. In interelemental internal IIF correction, the calibrant element can be part of the sample already or can be added to the sample before measurement. For MC-ICP-MS, isotope pairs of an element close in mass are usually used. Intraelemental internal IIF correction for Sr isotope ratio measurements relies on calculating the fractionation factor based on $^{88}Sr/^{86}Sr$ isotope ratio in the sample, and correcting the $^{87}Sr/^{86}Sr$ isotope ratio with the same fractionation factor (Fortunato et al., 2004). Any small amount of fractionation in $^{87}Sr/^{86}Sr$ is "normalized away", where samples are routinely corrected to the constant value $^{86}Sr/^{88}Sr = 0.1194$ (Steiger & Jäger, 1977). In that way, the radioactive decay of ^{87}Rb is the only cause for variation of $^{87}Sr/^{86}Sr$ ratios, measured in different materials. Since $^{88}Sr/^{86}Sr$ ratio underlies natural fractionation, it is not stable and consequently, not a great choice for internal mass bias correction of natural samples. Sr isotope ratios can be corrected for mass bias by adding zirconium and using some of the next ratios: $^{92}Zr/^{91}Zr$, $^{92}Zr/^{90}Zr$, $^{91}Zr/^{90}Zr$, but, the mass difference between Sr and Zr is likely to influence the degree of mass bias (Gerritzen et al., 2024; Quemet et al., 2015; Waight et al., 2002; L. Yang et al., 2008).

1.2.3.2 External Calibration of Isotope Abundance Ratios

External IIF correction strategy is based on using a solution containing an isotopic standard of the target element with a known isotopic composition, which is then measured following a bracketing procedure (*sample-standard bracketing*), with the sample and the isotopic standard in a consecutive sequence. The bias between the measured value and the true value of the isotope ratio of interest is observed, which enables the calculation of the correction factor to subsequently be applied to the sample measured in between (Abbyad

et al., 2001). This approach has a great advantage that lies in its simplicity. However, the accuracy may be poor in comparison to double-spike strategy. For Sr isotope ratio measurements, external calibration is done by using NIST SRM 987. Since Sr is isolated from the matrix in the sample pretreatment procedure, there is no matrix influence on the extent of mass discrimination.

1.2.3.3 Double-spike Technique

Double-spike calibration is a well-established technique of correction for instrumental mass discrimination. It applies to Sr, and any other element that has four or more isotopes. Double-spike is added to the sample, where its isotopic composition as well as concentration must be known. Factors that are of great significance are the choice of isotopic composition to be added and also the proportion in which double spike is mixed with the sample. As double-spike for $^{87}Sr/^{86}Sr$ ratio measurement, $^{84}Sr/^{86}Sr$ is used (Irrgeher et al., 2015; Ma et al., 2013; Shalev et al., 2013).

The fundamental principles of the double spike technique were introduced in the 1960s, yet initially, its application remained limited to measurements of certain isotopes like Pb and Ca. Despite its clear advantages, there has been some reluctance to adopt double-spike measurement protocols, potentially due to the perceived complexity of its practical implementation. Although software and tools for data reduction have since been developed to simplify the process, the design, creation, and calibration of a double spike may still present significant challenges for broader adoption (Klaver & Coath, 2019).

In comparison to other methods like sample-standard bracketing, only the double spike technique can correct for all sources of fractionation after the sample is equilibrated with the double spike, including those that occur during chemical separation and measurement. The key advantage of double spiking lies in its ability to accurately correct for isotopic fractionation, provided the double spike is properly calibrated. Unlike the bracketing method, it does not require the assumption that the sample and reference material exhibit identical isotopic fractionation behavior. Given that matrix effects can significantly influence mass fractionation, it is crucial to closely match the sample's matrix to that of the elementally pure reference material, which usually involves extensive elimination of the sample matrix. An optimal double spike is one that minimizes any negative impact on measurement precision, and a selection of double spikes offering the highest theoretical precision has been identified (Rudge et al., 2009).

1.2.3.4 Mass Bias Corrections Based On Fractionation Laws

Throughout the development of isotope ratio mass spectrometry, various correction models for mass bias or mass discrimination have been introduced. Most of these models were initially developed for TIMS and later adapted for MC-ICP-MS, despite the significant differences in the extent and nature of mass discrimination observed between the two techniques. Both TIMS and MC-ICP-MS are notable for their ability to simultaneously detect multiple ion beams, as they are typically equipped with arrays of several detectors. Unlike TIMS, where mass bias can vary over the course of a single measurement, isotope ratios measured by MC-ICP-MS generally exhibit consistent mass bias during individual measurements. However, MC-ICP-MS is subject to greater bias over extended time periods and is heavily influenced by the nuclide mass of the isotopes being measured.

This paragraph provides an overview of commonly used correction models. The advantages and limitations of these models have been widely discussed in the literature. Three main calibration models frequently used for TIMS and MC-ICP-MS are the linear law (Eqs. (1.4) and (1.5)), the power or exponential law (Eqs. (1.6), (1.7), (1.8), and (1.9)), and Russell's equation (Eqs. (1.10) and (1.11)) (Dauphas & Schauble, 2016; Nadia

Marechal et al., 1999; Russell et al., 1978). The choice of model depends on the specific measurement question and the assumptions made about the underlying mass discrimination function. It is important to note that in the literature, the power and exponential laws are often treated as two distinct models, even though they are based on the same mathematical principles. Other fractionation laws take different approaches, such as the equilibrium fractionation law or the Rayleigh fractionation law, which apply different approximations (Cavazzini, 2009). In the Rayleigh law, for example, mass-dependent fractionation is related to the square root of the masses involved. There is ongoing debate about which correction method yields the most accurate results. It is clear that different instruments, particularly with respect to ion sources, require distinct correction models. This issue has gained increasing importance due to the continual improvements in isotope ratio precision. While all these models correct for mass-dependent mass bias, they do not account for mass-independent fractionation. The variety of coexisting mass bias correction approaches highlights the lack of consensus in the field and the challenge of selecting the most accurate model for a given analytical scenario.

$$R_{standard,certified}/R_{standard,measured} = (1 + \ \varepsilon_{linear} \times \Delta m) \tag{1.4}$$

$$R_{sample,corrected} = R_{sample,measured} \times (1 + \ \varepsilon_{linear} \times \Delta m) \tag{1.5}$$

$$R_{standard,certified}/R_{standard,measured} = (1 + \ \varepsilon_{power})^{\Delta m} \tag{1.6}$$

$$R_{sample,corrected} = R_{sample,measured} \times (1 + \ \varepsilon_{power})^{\Delta m} \tag{1.7}$$

$$R_{standard,certified}/R_{standard,measured} = e^{\varepsilon \Delta m} \tag{1.8}$$

$$R_{sample,corrected} = R_{sample,measured} \times e^{\varepsilon \Delta m} \tag{1.9}$$

$$R_{standard,certified}/R_{standard,measured} = (m_1/m_2)^{\beta} \tag{1.10}$$

$$R_{sample,corrected} = R_{sample,measured} \times (m_1/m_2)^{\beta} \quad (1.11)$$

R: measured/certified isotope ratio of standard/sample
Δm: mass difference
$m_{1,2}$: mass of isotope 1 and 2
ε, β: correction factors for IIF

1.3 Overview of $^{87}Sr/^{86}Sr$ Isotope Ratio Applications

Using the substantial heterogeneity present in rock systems and the alignment of isotopic fingerprints among biosphere components, $^{87}Sr/^{86}Sr$ ratios serve as a valuable tracer and recorder of geological, archaeological, and biological processes. These distinctive properties have led to the widespread use of Sr isotopes in provenance studies of various materials, particularly excelling in providing detailed information at local scales (Choi et al., 2023). This is attributed to their minimal dependence on climatic factors. In contrast, light element isotopes (e.g., H, O) are better suited for large-scale studies, as their isotopic ratios are significantly influenced by ambient environmental characteristics such as topography, climate, soil, and hydrologic cycles (Beeckman et al., 2020). First applications of Sr isotopes involved investigation of the Earth surface, weathering and erosion processes, as well as solute and sediment transport (Gosz et al., 1983). Furthermore, studies of prehistoric human ecology, human and animal diets and migrations were conducted (Ericson, 1985; Koch et al., 1995). Over time, the applications of Sr isotopes have expanded and now encompass fields such as hydrology, forensics, archaeology, ecology, and food traceability and authentication (Land et al., 2000; Stevenson et al., 2016; Voerkelius et al., 2010; Willmes et al., 2018).

The effectiveness of discriminating provenance is enhanced in ecosystems that involve isotopically distinct Sr sources. Research has shown that local variations within a single lithological unit can surpass the overall variation observed at the regional scale (English et al., 2001). Consequently, such local nuances must be considered to ensure accurate predictions of provenance based on Sr isotopic data. However, many studies using Sr isotope ratios for provenancing purposes often focus on directly linking the geology of a region to, for example, the final agricultural product, neglecting an examination of the environment (Bontempo et al., 2011; Rossmann et al., 2000). Therefore, this need to assess background and source apportionment within a specific geological and environmental context represents the central problem addressed by this doctoral dissertation. Namely, the overarching issue tackled by the two research projects within this doctoral dissertation lies in the precise determination and investigation of the geographical origin of dairy products, specifically Graviera Naxos PDO cheese and Norway spruce trees from different specific regions in Romania.

1.3.1 Strontium Isotope Analysis in Dairy Provenance Determination: Focus on Graviera Naxos Cheese

Food authenticity refers to the assurance that food products are genuine and adhere to the claims made about their origin, composition, and quality (Schieber, 2018). Historically, concerns about food authenticity have roots in issues such as adulteration and

misrepresentation for economic gain (Giannakas & Yiannaka, 2023; H. Montgomery et al., 2020).

As supply chains have become more complex and globalized, the heightened risk of intentional fraud, unintentional contamination, and product mislabeling presents significant challenges with serious implications for public health, consumer trust, and the economic interests of various stakeholders (Dimara & Skuras, 2005). In addition, ensuring food authenticity is vital for preserving the quality and integrity of food items, as many of them often embody unique characteristics tied to specific regions, reflecting long-standing traditions and distinct production methods (G. P. Danezis, Tsagkaris, Brusic, et al., 2016; G. P. Danezis, Tsagkaris, Camin, et al., 2016; Dimitrakopoulou & Vantarakis, 2023). To safeguard traditional and regionally distinctive foodstuffs, the EU has established quality schemes within the geographical indications system, among which the Protected Designation of Origin (PDO) holds a preeminent position (Martínez-Salvador et al., 2021). Stringent PDO specifications mandate that every aspect of production, processing, and preparation take place exclusively in the designated region. In the dairy industry, marked by a broad spectrum of diverse offerings, this designation assumes a crucial role. The pursuit of authentic food represents a collective objective, engaging entities including law enforcement, food producers, traders, and consumers. Importantly, the scientific community holds a pivotal function through the development of advanced analytical techniques (Kwasi Bannor et al., 2023). The techniques used for this purpose have primarily centered around light stable isotope fingerprinting in conjunction with trace elemental analysis (Bontempo et al., 2012; Griboff et al., 2019; Potočnik et al., 2020) Furthermore, a limited number of studies have explored the application of Sr isotope ratios in elucidating the authenticity of these products. A study by Rossmann et al. (2000) applied $^{87}Sr/^{86}Sr$ isotope ratio analysis to bulk butter to determine its regional provenance. Similarly, Pillonel et al. (2003) analyzed 20 Emmental cheeses from six European regions, using Sr isotope ratios, among other methods, to verify their authenticity. Fortunato et al. (2004) demonstrated that the $^{87}Sr/^{86}Sr$ ratios in cheeses from various regions (Alpine and Pre-Alpine areas, Bretagne, Finland, Canada, and Australia) corresponded well with the local geological characteristics. Additionally, Sr isotope ratio analysis was applied in a study aimed at determining the geographic origin of milk from six dairying regions in Australasia (Crittenden et al., 2007). The $^{87}Sr/^{86}Sr$ ratios in the milk samples showed significant variation, suggesting that Sr isotopes could be a valuable tool for assessing geographic origin within Australasia. However, the study found that the $^{87}Sr/^{86}Sr$ ratios did not consistently correlate with expected values based on the age and composition of the local bedrock. Furthermore, Bontempo et al. (2011) investigated the elemental and isotopic profiles of traditional Italian Alpine cheeses. While Sr isotope ratios helped distinguish cheeses from certain regions, they did not prove to be a significant parameter in the discriminant analysis. Although these studies recognized the potential of Sr isotope ratio analysis in determining food authenticity, they overlooked the contributions from the surrounding environment. Sr isotope signatures of various materials are influenced by local geology rather than climate; however, it is important to recognize that a direct correlation with dairy products may not always be straightforward. Instead, the focus should shift toward the soil-plant system, which plays a more significant role in influencing Sr isotope ratios in food products.

When investigating the chemical signatures in food products, it's crucial to consider a variety of scenarios that might influence the results. Initially, one common scenario involves the direct transfer of the $^{87}Sr/^{86}Sr$ isotope ratio from soil to plants and subsequently to animals feeding on these plants. Notably, during this transfer, the $^{87}Sr/^{86}Sr$ ratio typically remains unaltered (Cellier et al., 2021; Horacek et al., 2023; Swoboda et al., 2008). Secondly, human activities such as irrigation and the use of fertilizers can significantly

alter the Sr isotopic composition of the soil, which subsequently impacts the signature of the plants grown in that soil. Lastly, the isotopic signature of a product can also be affected by various processing and preservation methods, such as salting, which may further alter its original isotopic composition (Epova et al., 2018; Techer et al., 2017). Understanding these scenarios is essential for accurately tracing the provenance and authenticity of food products, as each factor can significantly influence the interpretative accuracy of isotope-based analyses (Tchaikovsky et al., 2019).

By integrating isotope measurements within a geographic framework, complex ecological, geological, and environmental questions can be addressed with unprecedented precision through the use of isoscapes. This approach not only enhances our ability to trace the origin of natural and man-made materials but also increases the accuracy of models used to verify the authenticity and provenance of various products in ecological studies.

There are a few significant studies concerning the geographic distribution of Sr isotopes in Greece, that used various proxies, and they provide a valuable baseline for all provenance research. The Aegean region displays a comparatively low variation in Sr isotope ratios. This uniformity could be attributed to a general similarity in the underlying geology of the surveyed regions, primarily composed of limestone and marine sediments. Naxos, however, stands out due to the inclusion of older granites, which are expected to exhibit higher $^{87}Sr/^{86}Sr$ values (Georgia et al., 1995; Van Breemen et al., 1975; J. H. Yang et al., 2004).

In the study by Andriessen et al. (1979), the geochronological framework for the Alpine events of metamorphism and granitic magmatism in Naxos, Greece, was established through isotopic dating investigations. A schist sample from the southeastern tip displayed $^{87}Sr/^{86}Sr = 0.70930$, while whole-rock granite samples from the north ranged from 0.71418 to 0.72282. Granodiorite samples from the western part exhibited a range between 0.71056 and 0.71724. Importantly, these studies typically measure total rock Sr isotope ratios, which differs from bioavailable Sr, that specifically pertains to the Sr that can be absorbed by organisms through soil and water. Voerkelius et al. (2010) performed a large-scale investigation of Sr isotope ratios of European natural mineral waters, aiming to enhance spatial prediction. While they analyzed 13 samples from Greece which define a $^{87}Sr/^{86}Sr$ value span ranging from 0.70782 to 0.70946, none of these samples originated from the South Aegean, or more specifically, Naxos. Nafplioti (2011) employed isotope geochemistry to investigate population mobility in the Aegean, establishing the first bioavailable $^{87}Sr/^{86}Sr$ baseline for the region. In this study, pig and cow enamel samples, archaeological human bones, as well as modern snail shell samples from Chora (Western island) and Tsikniades (Central island) were examined. The overall range was estimated at $^{87}Sr/^{86}Sr = 0.70903$–0.71002, with a total of 8 samples measured. The study conducted by Prevedorou et al. (2015) contained 6 modern hare (*Lepus europseus*) mandible samples from Naxos, that exhibited higher variation compared to other study areas, with values ranging from $^{87}Sr/^{86}Sr = 0.70881$ (Southern island) to 0.71068 (Central island). As expected, the highest Sr isotope ratio values (0.71056 and 0.71068) were observed in samples derived from the central, more mountainous part of the island, which might be less affected by seaspray, while other values were below 0.70953. The study by Hoogewerff et al. (2019) investigated the distribution of Sr isotope ratios across Europe, by analyzing 1,200 grazing and agricultural soil samples. The spatial model predicted $^{87}Sr/^{86}Sr$ values in the South Aegean region to fall within the range of 0.705–0.710. Frank et al. (2021) defined the first extensive bioavailable Sr isotope baselines for the different geographical regions and surface lithologies of Greece. The $^{87}Sr/^{86}Sr$ data from the South Aegean, as reported by Frank et al. (2021), define rather narrow Sr bioavailable baseline ranges of 0.70889 ± 0.00083 ($\bar{x} \pm 2\sigma$; n=28). However, this range was calculated based on previous research, since no additional samples have been collected from this part of Greece.

The present dissertation focused on the examination of both milk and cheese samples, specifically the Graviera Naxos PDO variety originating from the island of Naxos, Greece. Graviera, a Gruyère-type hard table cheese, is renowned for its semi-sweet, salty, and piquant flavor, firm texture with small eyes, and light-yellow color. Originating from Greece, the first Graviera was crafted with ovine and caprine milk instead of bovine milk, distinguishing it from its Swiss counterpart. Today, the production of Graviera involves a mix of cow, sheep, and goat milk, resulting in a variety of flavors closely tied to local climates, livestock breeds, and traditional cheese-making practices. The EU's PDO scheme ensures the authenticity and premium quality of Graviera, linking its unique characteristics to its geographical origin. Among the various types, Graviera of Crete, Naxos, and Agrafa have achieved PDO status, with Graviera Naxos being registered as a PDO product since 1996. This guarantees that their production, processing, and treatment occur exclusively in specified regions ((EC) No 510/2006). Graviera Naxos's production adheres to traditional methods, focusing on the natural diet of the local livestock, which includes Mediterranean vegetation influenced by the island's unique environmental conditions. Annually, approximately 1,250 tons of Graviera Naxos are produced, highlighting its significance in both domestic and international markets.

Previous research on Graviera's geographical authentication is sparse, with notable studies including Bozoudi et al. (2016) exploring the microbiological and physicochemical properties of Naxos and Crete Gravieras, Danezis et al. (2019) analyzing elemental profiles, and Vatavali et al. (2020) combining fatty acids and minerals to differentiate geographical origins and milk types. These studies underline the complexity and specificity of Graviera production, highlighting its cultural and economic significance within the Greek cheese industry.

PDO Graviera Naxos cheese is primarily manufactured in the southwestern region of Naxos, where the prevalent geological formations consist of granodiorite and marble schist. The production of Graviera Naxos cheese occurs at the facilities of the Union of Agricultural Cooperatives of Naxos, utilizing milk sourced from various farms on the island. This hard cheese is crafted from a minimum of 80 % cow's milk and a maximum of 20 % sheep's and/or goat's milk (Kizos & Vakoufaris, 2011). The production process adheres strictly to traditional cheese-making practices, incorporating rennet following established guidelines. According to Regulation (EC) No 1107/96 (European Commission, 1996) and the Greek national law (Joint Ministerial Decision, 1994), the milk used for the production of Graviera Naxos must come from cows, goats, and sheep traditionally fed and adapted to the delimited area of production.

1.3.2 Strontium Isotope Analysis in Provenance Determination of the Norway Spruce Tree from the Eastern Carpathians, Romania

A wide range of applications of dendro-provenancing include the identification of the origin of wood used for constructing monuments, musical instruments, ships, and historical buildings, as well as understanding wood harvesting and mobility in the past, and subsequently tracking illegal timber logging and exports. Illegal logging and trade of illegally harvested timber products are a global issue with negative environmental, economic, and social impacts including deforestation and biodiversity loss (Deklerck, 2023; Watkinson et al., 2022).

For wood geographic provenance and species identification, numerous anatomical, genetic, and chemical techniques were developed. Since they require different conditions for optimal performance, and therefore have different limitations (e.g., high costs and time consumption) and strengths (e.g., level of resolution), it is often advisable to use a combination of methods (Beeckman et al., 2020). Dendrochronology, which is the most

commonly used method in historical wood provenance studies, typically does not consider multiple variables that influence tree-ring patterns (Visser, 2021). Furthermore, anatomical and genetic analyses that enable comparison with the existing reference data, are used for identifying the provenance of wood (Gapare et al., 2012; Martín et al., 2010). Additionally, some studies involving light stable isotopes in wood have been conducted (Boeschoten et al., 2023; Vlam et al., 2018). The ambient environmental characteristics such as topography, climate, soil, and hydrologic cycles influence the isotopic ratios of H, O, and C, leading to the formation of a specific isotopic signature of wood, that reflects the exact conditions a tree was experiencing at the time of growth (Paredes-Villanueva et al., 2022). This feature makes biogenic stable isotopes suitable for eliciting wood origin on a large-scale (Gori et al., 2015; Horacek et al., 2009). However, it is important to recognize that at local scales, isotope ratios of elements such as Sr, S, and N could be more informative, since they show less dependence on climate. Sr isotope ratio analysis has become a widely used tool in various disciplines and has shown great potential in evaluating wood provenance (D'Andrea et al., 2023; Erban Kochergina et al., 2021; Hajj et al., 2017; Rich et al., 2016).

The analysis of Sr isotopes in wood offers an interesting opportunity to discriminate wood sources according to geological parameters: the assumption is that the tree inherits a Sr isotope signature that reflects the geological history of the region where it grew (Pinta et al., 2021). In general, soils and their substrates share similar $^{87}Sr/^{86}Sr$ values. However, even within the same geologic zone, soil displays a considerable variation, since minerals within the rock weather at different rates, and hence contribute unevenly to bioavailable Sr in soil (Bullen et al., 1997). Other major sources of variability in bioavailable Sr in soil are ground and stream waters, wind-transported dust deposits, as well as sea spray in coastal zones, and rainfall (Alonzi et al., 2020). Therefore, for predicting the isotopic composition of trees growing in a specific location, it is necessary to analyze the topsoil and groundwater responsible for most of the Sr uptake. Kennedy et al. (2002) and Reynolds et al. (2005) showed that sites with shallow soil layers – where trees could access shallow groundwater, are atmospherically dominated, making Sr isotope ratio approach suitable for mountaintops, rather than low topographic areas.

Recent studies have explored the potential of multi-element analysis for tracing timber, identifying elements like Mo, Zn, and Mn as crucial for distinguishing different sites (Boeschoten et al., 2022; Hietz et al., 2015). A significant study involving 929 timber reference samples from four genera across 11 Eastern European countries combined trace element and stable isotope ratio analysis to develop a probabilistic framework for verifying and determining timber harvest locations, aiming to support the enforcement of sanctions and timber regulations (Mortier et al., 2024). While wood chemical composition is influenced by soil chemistry, elemental profiles can overlap among species, reflecting site variations across multiple species. Challenges in this method include the complexity of wood formation, influenced by long-term environmental and ontogenetic changes, and the necessity for distinct elemental variations between origins. The success of this approach relies heavily on strong spatial variation in soil chemistry, which significantly impacts wood elemental composition (Boeschoten et al., 2023). Understanding the mobility and distribution of chemical elements in wood is essential for applying dendrochemistry effectively.

Romania preserves approximately 60 % of Europe's remaining primeval forests, which are home to unique flora and fauna, representing an irreplaceable natural heritage. According to Global Forest Watch, between 2001 and 2023, Romania experienced a loss of 433,000 hectares of tree cover, mainly due to wind damage and bark beetle infestations. Suceava County was the most affected, contributing to 65,000 hectares of the total loss. After Romania joined the EU in 2007, large-scale logging in the Romanian Carpathians

increased significantly. National and EU institutions have raised concerns that this trend is accompanied by a rise in illegal logging. The issue of illegal logging and the mixing of illegally sourced wood with legal supplies has become a prominent topic in public debates in Romania (Bratu et al., 2022). Eliminating illegal logging and timber trade is challenging due to global imbalances in laws and law enforcement, and rising demand for timber and agricultural products. Effective control requires coordination among forestry, agriculture, fisheries, and wildlife sectors to track illegal activities. Engaging major producer and importer countries is crucial, as legal and illegal wood markets are interconnected, complicating monitoring and resolution efforts (Gan et al., 2016; Low et al., 2022). Significant efforts have been made by countries to address the issue of illegal logging, including the development and implementation of legislation aimed at reducing the trade in illegally harvested timber and timber products. The EU has implemented policies to curb the trade of illegal timber through the Forest Law Enforcement, Governance, and Trade Action Plan (FLEGT), adopted in 2003, which aims to enhance the legal trade in sustainably produced forest products (FOREST EUROPE, 2020). Additionally, the EU Timber Regulation, will be repealed by the end of 2024 (European Parliament, 2010). It will be replaced by the Regulation on deforestation-free products, which will impose stricter obligations on operators and traders. Furthermore, countries have begun developing various national timber tracking systems to monitor the flow of timber from producers to final consumers. Romania implemented a digital monitoring system, SUMAL, to increase transparency in wood harvesting activities (Dogaru, 2024). However, shortcomings in this system have been identified, particularly its inability to verify the authenticity of submitted haul photographs, emphasizing the need for more accurate tracing systems.

Norway spruce is a softwood, refractory species with an extensive natural range throughout Europe and ability to reach an age of 200–300 years (Čabalová et al., 2021; Tjoelker et al., 2007). Although its timber is employed in the construction of joists, flooring, and furniture, it is most well-known for its usage in the manufacture of stringed instruments, namely violins (Bernabei & Bontadi, 2011). Alongside these applications, the Norway spruce holds a prevalent role as a Christmas tree, owing to its distinctive appearance. The Norway spruce is native to the Carpathian Mountains, and in Romania it represents 77 % of the coniferous forests' surface and 23.2 % of the entire forest surface of the country (Apostol & Budeanu, 2019).

To date, Sr isotope ratio analysis of wood from Romania has not been thoroughly investigated. Moreover, very few studies have applied this method to other matrices within the country. One notable study by Voerkelius et al. (2010) on natural mineral waters included only a single sampling point in Romania, located in the Eastern Carpathians. Based on geological features and spatial predictions, this location was assigned an Sr isotope ratio range of 0.70701–0.70900. More recently, a study by Török et al. (2023) examined the Sr isotope and elemental signatures of karst groundwaters, focusing on 24 springs in the Southern Carpathians and Apuseni Mountains. The geological formations in these areas include limestone, sandstone, dolomite, conglomerate, crystalline schist, and dolostone. Groundwater samples were collected seasonally – winter and spring – over two consecutive years to observe fluctuations in elemental concentrations and Sr isotope ratios. The study reported a range of Sr isotope ratios, from 0.7038 to 0.7158.

In addition to groundwater, Sr isotope ratios have also been analyzed in Romanian wines for geographical traceability. Geană et al. (2017) examined the elemental composition and Sr isotope ratios of 21 red wines from three southeastern Romanian winemaking regions, with isotope ratios ranging from 0.71015 to 0.72311. Similarly, Bora et al. (2018) studied white and red wines produced in micro-vineyards across three Romanian regions, reporting Sr isotope ratios between 0.7023 and 0.7681, with the highest values found in wines from Ștefănești-Argeș. These wide ranges of Sr isotope ratios suggest that Romania

holds significant potential for using Sr isotope analysis as a tool for local-scale discrimination. However, the need for more comprehensive data and the development of a reference database of Sr isotope values across various regions of Romania is essential to enhance the accuracy and reliability of Sr isotope ratio applications in different provenance studies.

1.4 Bioavailable Strontium Isotope Baseline Maps

Since isotopes were discovered and precise instruments capable of detecting minute variations in isotope abundances were developed, there has been a growing interest in measuring and interpreting the spatial and temporal variations in isotope ratios within natural systems (West et al., 2010). Provenancing biological materials using Sr isotope ratios requires a map of bioavailable Sr, commonly known as an *isoscape* (isotope landscape), to compare results with. This technique is valuable in archaeology, forensics, ecology, and agricultural studies. Sr isotopes are not fractionated by biological processes, making them particularly useful for direct application in isoscape maps for archaeological studies and animal migration tracking without needing fractionation correction. Additionally, because Sr isotope ratios can vary significantly over short distances due to local geological influences, they enable high-resolution provenance assignments.

The challenge of reliably establishing a baseline that reflects the local bioavailable Sr isotope signature, against which a material under examination can be compared to determine its provenance, is increasingly becoming a topic of debate. The choice of proxies depends on the material under investigation and the availability of sampling material (R. Frei et al., 2022). Proxies used for constructing isoscapes include plants, surface and ground waters, soils and soil leachates, and faunal remains, each presenting unique benefits and challenges (Holt et al., 2021). For example, plants are easy to collect, ubiquitous, and form the base of the food chain, making them good indicators of local bioavailable Sr isotope ratios. They directly reflect the Sr in the soil where they grow. However, single plant samples can show point-bias due to localized geological and environmental variations. This can be mitigated by homogenized sampling, combining multiple plants from a collection area to create a single sample. Subsequently, although soils are considered direct indicators of the Sr content available to plants and animals, various factors such as human activity, weather conditions, and geological changes can cause differences between the Sr isotope ratios in soils and plants from the same location (Adams et al., 2019). Surface waters, such as river waters, generally provide an accurate reflection of bioavailable Sr isotope ratios across a region by offering a comprehensive view influenced by the landscapes they traverse. However, these waters can also be contaminated by human activities, such as soil treatments, which may alter their Sr isotope ratios. Water sources derive their $^{87}Sr/^{86}Sr$ ratios predominantly from the weathering of local rocks. The specific contributions of different minerals and rock units to the dissolved Sr pool can vary considerably, depending on their weathering rates and Sr content, often resulting in noticeable differences in $^{87}Sr/^{86}Sr$ ratios between the hydrosphere and the underlying geosphere. Both groundwater and surface water absorb Sr from their respective aquifers and catchment areas, offering averaged regional compositions that mirror the geological characteristics of upstream and surrounding regions. However, groundwater might reflect the compositions of deeper lithological formations rather than surface deposits, which could diminish its relevance for determining the bioavailable Sr for terrestrial animals, except in cases where well water is regularly consumed (K. M. Frei & R. Frei, 2011; Maurer et al., 2012).

Plants and surface waters are often preferred due to their direct link to bioavailable Sr in an area. Most studies have focused on Europe, where intensive agricultural practices

may influence results. The suitability of different proxies might vary globally, necessitating region-specific studies. Effective isoscapes require careful selection of sampling proxies, considering their strengths and potential biases. Plants and surface waters are generally reliable proxies, but regional practices and environmental factors must be considered to ensure accurate provenance analysis. Furthermore, although many studies show a consistent correlation in Sr isotope signatures between major surface water bodies and well drinking waters, there are reports of poor correlation between spring water and other proxies, including surface waters. This inconsistency suggests that spring water may not be an appropriate substitute for surface waters in isotope studies (Frank et al., 2021).

Numerous studies have used soil and water Sr isotope ratio data to develop isoscapes. The most comprehensive studies to date include the research by Voerkelius et al. (2010), which examined natural mineral waters with a dataset of 650 samples from across Europe, and the study by Hoogewerff et al. (2019), that analyzed Sr isotope ratios in 1187 grazing and agricultural soils throughout Europe, establishing a valuable baseline for continental-scale provenance studies. Additionally, there has been a growing trend in conducting studies that focus on building baseline maps for specific countries or regions (Brennan et al., 2016; James et al., 2022; Käßner et al., 2023; Lugli et al., 2022; Snoeck et al., 2020; Willmes et al., 2018).

Regarding Naxos, it's crucial to consider the sea spray effect, which can influence local soil chemistry based on proximity to the coast and wind patterns. To mitigate the impact of sea spray, some mapping studies that use plant archives have deliberately chosen sites that are at least 50 meters away from coastlines. Nonetheless, sampling strategies should aim to identify and elucidate the effects of sea spray, rather than simply avoiding them based on a metric assumption that may not hold true for the area in question. The study of Cyprus by Ladegaard-Pedersen et al. (2020) is particularly relevant given its island geography, similar to Naxos, which is characterized by diverse geology and non-local Sr contamination from aerosols such as sea spray and wind-transported sand or dust particles. This study assessed the use of multiple proxies (81 samples in total) to build a Sr isotope baseline for Cyprus. It found that, overall, the Sr isotope ratios of groundwater correlated with those of leaf samples and soil leachates, although these were generally higher than the concurrent groundwater values. The study also highlighted that differences between proxies are site-specific, emphasizing that a comprehensive bioavailable Sr isotope baseline cannot be adequately established without employing a multi-proxy approach.

Existing European Sr isoscapes lack sufficient data points for Romania, leaving a critical gap in accurately representing the region's unique geological and environmental variability. This highlights the urgent need to generate a dedicated isoscape for Romania to facilitate more precise provenance and mobility studies, as well as to enhance environmental and archaeological research across the country. Without a regional isoscape, we face challenges when attempting to use Sr isotopes for the provenance and mobility studies, as we lack a reliable reference map to interpret isotope ratios. Romania's diverse geology, especially in its mountainous regions like the Carpathians, leads to distinct Sr isotopic signatures in soils, water, and biological materials. Developing an isoscape would help in understanding these local variations and provide a reference for comparing Sr isotope data across different regions of the country.

Building bioavailable $^{87}Sr/^{86}Sr$ isoscapes typically involves analyzing a series of environmental/biological samples that represent the bioavailable Sr pools within a specific area. This method relies on the premise that closer points in space tend to show similar characteristics, a concept known as spatial autocorrelation. The data from these samples are often processed using geostatistical algorithms which interpolate the $^{87}Sr/^{86}Sr$ ratios to create continuous isoscapes. However, these maps may suffer from ambiguities and inaccuracies due to the challenges in handling non-normal and skewed distributions of data.

Another common method averages the $^{87}Sr/^{86}Sr$ data across regions with similar geological features, but this can result in overlaps and imprecise maps, reducing their utility for detailed provenance analysis. To address these limitations, a more nuanced approach incorporates the use of mechanistic models that predict changes in $^{87}Sr/^{86}Sr$ based on geochemical principles and radiogenic decay equations. Although this method holds promise for enhancing the accuracy of isoscapes, it requires complex modeling of various geochemical processes and is hindered by the current lack of detailed global geological maps. An emerging alternative that seeks to bridge the gaps between geostatistical and mechanistic methods is the application of multivariate random forest regression (Bataille et al., 2020). This machine-learning technique combines empirical data with a range of geo-environmental variables like bedrock and terrane age, soil properties, and climatic conditions to refine the modeling of $^{87}Sr/^{86}Sr$ distributions. While the development of global $^{87}Sr/^{86}Sr$ isoscapes remains a work in progress, leveraging such advanced data integration methods promises significant progress in the field of large-scale provenance studies. This innovative approach is paving the way for more precise and reliable applications of Sr isotopes in tracing the origins of biological materials.

1.5 Aims and Hypotheses

The dissertation aimed to explore the potential of Sr isotope ratio analysis as a tool for geographic discrimination, focusing on two projects: the geographical origin of milk/cheese from Naxos, Greece (Project 1), and wood in the Eastern Carpathians, Romania (Project 2). By integrating multi-elemental and Sr isotopic ratio analysis, the research sought to establish a distinctive multivariate fingerprint for these products. While light element isotopes have traditionally dominated provenance studies, the recognition of Sr isotope ratios as a powerful method is relatively recent. Its usefulness is particularly evident in discriminating between sources in small geographic areas, where variations in bedrock geology are pronounced. However, limitations persist, prompting the need for a comprehensive investigation.

The two projects within this dissertation focused on specific, relatively small geographical locations, where Sr isotope ratios could offer discerning discrimination compared to light isotopes. The distinct objectives of the two projects – investigating the geographical origin of food (milk/cheese) and wood – highlight the versatility of Sr isotope analysis. In situations where multiple potential sources contributed to the analyzed material, such as food products, interpreting Sr isotope ratios becomes more complex. The examination of different potential sources in each project, such as water, soil, feed, milk, salt, and rennet, provided an opportunity to assess the applicability of Sr isotope ratios. This dissertation aimed to link cheese and milk to their environmental sources – feed, soil, and water – through $^{87}Sr/^{86}Sr$ isotope ratios and multi-element analysis. Over three years, we tracked seasonal variations in Sr isotopes, established a geochemical database for Graviera Naxos cheese, and assessed the potential of these methods to authenticate dairy product origin.

In Project 2, where wood was the material of interest and only soil and water served as possible sources, the study aimed to understand how the Sr isotopic composition was influenced by a limited number of sources. This study focused on documenting the Sr isotopic and multi-element signatures of Norway spruce (*Picea abies* (L.) Karst.) trees growing in the Eastern Carpathians, Romania, an area of intensive forest logging. The specific aims were as follows: i) Contribute to the development of a geochemical wood provenancing tool with applicability in wood traceability systems. By providing essential data for the geochemical profiling of wood provenance, we aimed to enrich the incomplete

map of $^{87}Sr/^{86}Sr$ values across European soils and waters, filling critical data gaps and addressing the lack of data on bioavailable $^{87}Sr/^{86}Sr$ ratios in Romanian soils and waters; ii) Assess temporal variability by analyzing tree rings corresponding to the last 50 years (1970-2020) from three trees at each site. This helps us understand how wood elemental composition and Sr isotopic ratios vary over time and determine the stability of these signatures. Recognizing that a single tree cannot be a true representative of a site, we collected samples from three trees at each site, focusing on tree rings from the same period (1970-2020). These samples were pooled into a compound sample to obtain an average for each specific site, ensuring a more accurate representation; iii) Investigate environment-wood relationships. Given the significant influence of soil chemistry on wood elemental composition, this study sought to link the elemental and Sr isotopic compositions of wood to those of local soil and water; iv) Develop a species- and site-specific origin fingerprint. While previous studies have examined various species and their connections to soil chemistry, our focus was on the Norway spruce, a species with significant use in the timber industry. We sought to explore its unique origin fingerprint using Sr isotope ratio and multi-element analysis.

One of the overarching objectives was to compare these two projects, recognizing that Project 1 involved a broader array of sources than Project 2, contributing to a comprehensive understanding of Sr isotope ratio behavior in diverse provenance scenarios. Additionally, Project 1 explored the correlation between milk and feed, investigating how the feeding practices of animals influenced the Sr isotopic ratio of milk. Specifically, the study assessed whether imported feed, originating from a different location than the study site (Naxos), posed a challenge to the Sr isotopic fingerprint of milk. This examination contributed valuable insights into the reliability and robustness of Sr isotope ratios in tracing the geographical origin of dairy products. Furthermore, the outcomes of this study contribute to the enhancement of current Sr isoscapes for Europe. These spatial representations of Sr isotopic ratios within a geographic region play a crucial role in investigations related to both food sourcing and the determination of the origin of archaeological artifacts. The georeferenced data collected in this research facilitates the identification of patterns and variations across the landscape. While existing isoscapes for Europe often relied on modeled values due to a scarcity of actual sampling points in the areas investigated, this research aimed to verify these models by providing real data from the specific sampling locations.

Having laid out all the aims and goals of the research within this dissertation, the following hypotheses were defined:

1. Multivariate fingerprint for geographic discrimination: A combination of multi-elemental and Sr isotopic ratio analysis would yield a distinctive and reliable multivariate fingerprint, facilitating the differentiation of Naxos milk/cheese and Eastern Carpathian wood from diverse provenances.
2. Environmental samples and cheese/wood – strong positive correlation: The bioavailable fraction of soil and water, characterized by their unique Sr isotope ratio, would exhibit a robust positive correlation with the Sr isotopic composition of milk and cheese in Project 1, and wood in Project 2.
3. Identification of dominant Sr source in milk/wood Sr isotopic composition: Through rigorous analysis and employing mixing models, it would be possible to identify and quantify the relative contributions of different Sr sources to the isotopic composition of milk from Naxos, Greece, and wood from the Eastern Carpathians, Romania.
4. Spatial distribution of Sr isotope ratios across Romania and preliminary isoscape for Naxos island: Groundwater is a suitable proxy for establishing relevant Sr isotope baselines used in provenance and mobility studies. Combining Sr isotopic

data from water and bioavailable soil fraction samples will amalgamate crucial information and enhance the isoscape.

Chapter 2

Materials and Methods

2.1 Reagents and Materials

For the preparation of samples and reagents, ultrapure water with a resistivity of 18.2 MΩ cm, dispensed from a Direct-Q 5 purification system (Millipore, Watertown, MA, USA) was used (MilliQ). Nitric acid (67–69 % (*w/w*) HNO_3, Suprapur) was obtained from Carlo Erba Reagents Srl (Milan, Italy), while hydrogen peroxide (30 % (*w/w*) H_2O_2, Suprapur), hydrofluoric acid (40 % (*w/w*) HF, Suprapur), and ammonium nitrate ($\geq$ 99.0 %, NH_4NO_3) were purchased from Merck Ltd (Darmstadt, Germany). Boric acid (99.8+ % H_3BO_3, Ultrapure) was obtained from Chem-Lab NV (Zedelgem, Belgium). For filtration of water and bioavailable fraction of soil samples, 0.45 µm Minisart cellulose nitrate membrane filters (Sartorius, Goettingen, Germany) were used. Standard solution Multi VI (ICP Standard Certipur, Merck, Darmstadt, Germany) was used in preparation of external calibration for multi-element analysis, while accuracy was checked using a certified reference material for trace elements in surface water SPS-SW1 (Spectrapure standards, Oslo, Norway). The following CRMs were digested and measured together with the samples during multi-elemental analysis: IAEA 153 (Milk powder, International Atomic Energy Agency, Vienna, Austria), NIST SRM1573a (Tomato leaves, National Institute of Standards and Technology, Maryland, USA), ERM-CC141 (Loam soil (elements), Joint Research Center, Geel, Belgium). During Sr isotope analysis, NIST SRM 987 standard (Sr carbonate, Gaithersburg, National Institute of Standards and Technology, Maryland, USA) was used for calibration.

2.2 Study Area and Sample Collection

A study examining the origin of milk and cheese used samples from Naxos Island in the South Aegean, Greece, while the timber provenance study involved samples from the Eastern Carpathians in Romania. Detailed information is provided in the following paragraphs.

2.2.1 Naxos, Greece

Naxos is the largest island of the Cyclades (429.79 km^2), located in the center of the Aegean Sea. The island of Naxos exhibits an elliptical shape, with a primary orientation of N15 °E, and consists of metamorphic and igneous rocks of various ages and deformations, allochthonous molasse sediments of the Miocene, and pyroclastic rocks and newer, primarily terrestrial, sediments of the Pliocene-Pleistocene. The greater part of Naxos, especially the eastern and southern section, is occupied by a series of platform metamorphic sediments of Mesozoic age, which were involved in the Alpine orogeny in a lithospheric

plate convergence environment. These metamorphic rocks are primarily marbles, interspersed with schists and dolomites, which have a zonal distribution in roughly a NE-SW direction, coinciding with that of the island's main mountain range (Mount Zeus). The western part of the island is characterized by the appearance of Cycladic I-type granitoids, whose contact with the metamorphic complex is directed N-S, including clays, sandstones, diabases, gabbros, and ultrabasic rocks. Considering the above geographical distribution of geological formations, three main units can be identified on the island: the upper non-metamorphosed unit, the Cycladic Blueschist Unit, and the granodiorite unit (Brichau, 2004; Cao et al., 2013; Georgia et al., 1995; Partsinevelou et al., 2011).

The climate of the study area, although classified as a Mediterranean climate type according to the Thornthwaite climate classification, is dry, and more specifically, xerothermic, with a strong influence of the sea in shaping its thermal character. However, the Aegean Sea, due to its geographical position, numerous islands and peninsulas, bays, and many mountain ranges, as well as other physical and geographical factors, exhibits special meteorological and climatological conditions to such an extent that a specific type of climate has been established for the Aegean Sea with the term Aegean climate (temperate to maritime) (Leonidopolou et al., 2008). The annual isotherms range from 18 °C to 19 °C, with a low level of annual rainfall of about 366.80 mm (Theocharatos, 1978). From a meteorological and climatological perspective, the year is divided into two seasons, the cold and the warm period. The cold period lasts from October to March, while the warm period lasts from April to September. The temperatures prevailing in Naxos in the summer are lower than those in other Greek areas (HNMS 1955–1977). This is due to the influence of the sea, but also to the winds with high frequency and intensity, resulting in a reduction in temperature. The prevailing direction of the winds throughout the year is from north to south, and the average annual humidity is about 72 %.

Water, soil, feed, milk, and cheese samples were collected from sampling stations on Naxos Island, Greece, as shown in Figure 2.1. Soil and water were sampled once, in August 2020 and January 2021, respectively. The sampling campaign in August 2020 aimed to study the distribution of Sr isotope ratio values across the entire island, with soil, feed, and milk samples collected from stations #1 to #43. However, the primary focus was on the subsequent campaigns conducted in January 2021 and June 2021, during which both milk and feed samples were collected from identical stations (#51 to #63), allowing for more direct comparisons. Additionally, milk samples were obtained from stations #64 to #66, corresponding to the milk collecting tanks of the cheese-making factory. Furthermore, milk samples were collected in July 2021 and January 2022, all originating from different milk tanks of the cheese-making factory. The summary of the number of samples collected and the sampling campaigns is presented in Table 3.1.

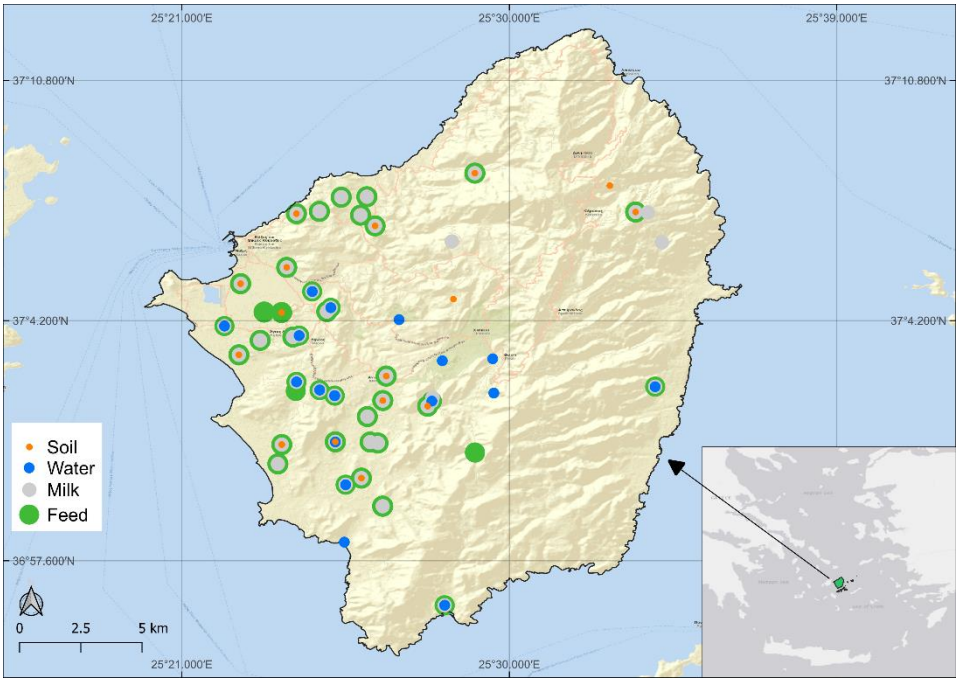

Figure 2.1: Sampling sites and samples collected in Naxos, Greece.

2.2.2 Eastern Carpathians, Romania

Sampling sites are distributed across three geologically different regions: Rodna, Rarău and Călimani, at altitudes ranging from 713 to 1735 m, as shown in Table 2.1. The distribution of the sampling locations within these regions, along with the sample types that were collected at each site, are shown in Figure 2.2.

Table 2.1: Geographic coordinates and altitudes of sampling locations in the Eastern Carpathians.

Rodna Mts	**Latitude**	**Longitude**	**Altitude (m)**
Rodna 1	47°32'19.90"N	24°57'5.60"E	1735
Rodna 2	47°32'44.50"N	24°58'29.90"E	1548
Rodna 3	47°32'40.40"N	24°58'42.80"E	1454
Rodna 6	47°32'45.30"N	25° 0'36.50"E	1258
Rodna 7	47°32'46.90"N	25° 0'47.30"E	1239
Rodna 8	47°33'38.10"N	25° 3'1.10"E	983
Rarău Mts	**Latitude**	**Longitude**	**Altitude (m)**
Rarău 1	47°28'41.20"N	25°29'50.90"E	906
Rarău 2	47°27'37.70"N	25°29'50.90"E	1217
Rarău 3	47°27'0.30"N	25°33'47.80"E	1519
Rarău 4	47°26'58.60"N	25°33'28.20"E	1475
Rarău 5	47°26'58.60"N	25°33'28.20"E	971
Chiril	47°24'14.50"N	25°34'23.50"E	758

Pietr	47°24'23.50"N	25°31'6.40"E	767
Rusca	47°23'34.30"N	25°29'4.70"E	713
Călimani Mts	**Latitude**	**Longitude**	**Altitude (m)**
Călimani 1	47° 6'23.60"N	25°14'17.20"E	1640
Călimani 2	47° 7'56.30"N	25°15'8.30"E	1269
Călimani 3	47°10'11.60"N	25°14'38.40"E	1210

These regions stretch across several counties, including a portion in Suceava. The geological composition of the Rodna Mountains is primarily characterized by a core of crystalline schists (with mica schists, paragneiss with amphibolites and sericitous schists), which includes several epi- and meso-metamorphic series. These formations are overthrusted and extensively faulted in both the northern and southern parts of the mountains (Munteanu & Tatu, 2003). Rarău Mountains, positioned in the northern segment of the crystalline axis of the Eastern Carpathians, showcase a diverse range of genetically distinct landforms, particularly in limestone and dolomites (Oprea & Buta, 2014). Samples were collected from an area covered by Cretaceous sedimentary limestones grading into late-Cretaceous sandstones. The Călimani Mountains represent the largest and most complex volcanic structure in the northern part of the Călimani-Gurghiu-Harghita range in Romania. Being remnants of a large Neogene stratovolcano, these mountains are composed predominantly of andesites and dacites, and feature a prominent central caldera approximately 10 km in diameter, formed by explosive volcanic activity (Erzsébet & Weiszburg, 2010; Sandulescu & Dimitrescu, 2004). For all three mountains, no lithological changes were observed between the sampling sites from the same region.

A total of 17 sampling sites were chosen across the three regions during the summer of 2021, yielding the following samples: at 11 of these locations, Norway spruce wood samples were collected from three closely situated trees at each site; 17 water samples, including 13 from groundwater and 4 from rivers; and 18 soil samples.

Besides the samples from the Eastern Carpathians, another 187 water samples were collected from January to October 2021, from various regions of Romania, primarily mountainous areas (Apuseni Mts., Banat, Cluj- Neamț, NW Romania, Târnavele, and Southern Carpathians). The purpose of these sampling campaigns was to collect water samples for Sr isotope ratio analysis and to investigate the spatial distribution of Sr isotope ratios across Romania.

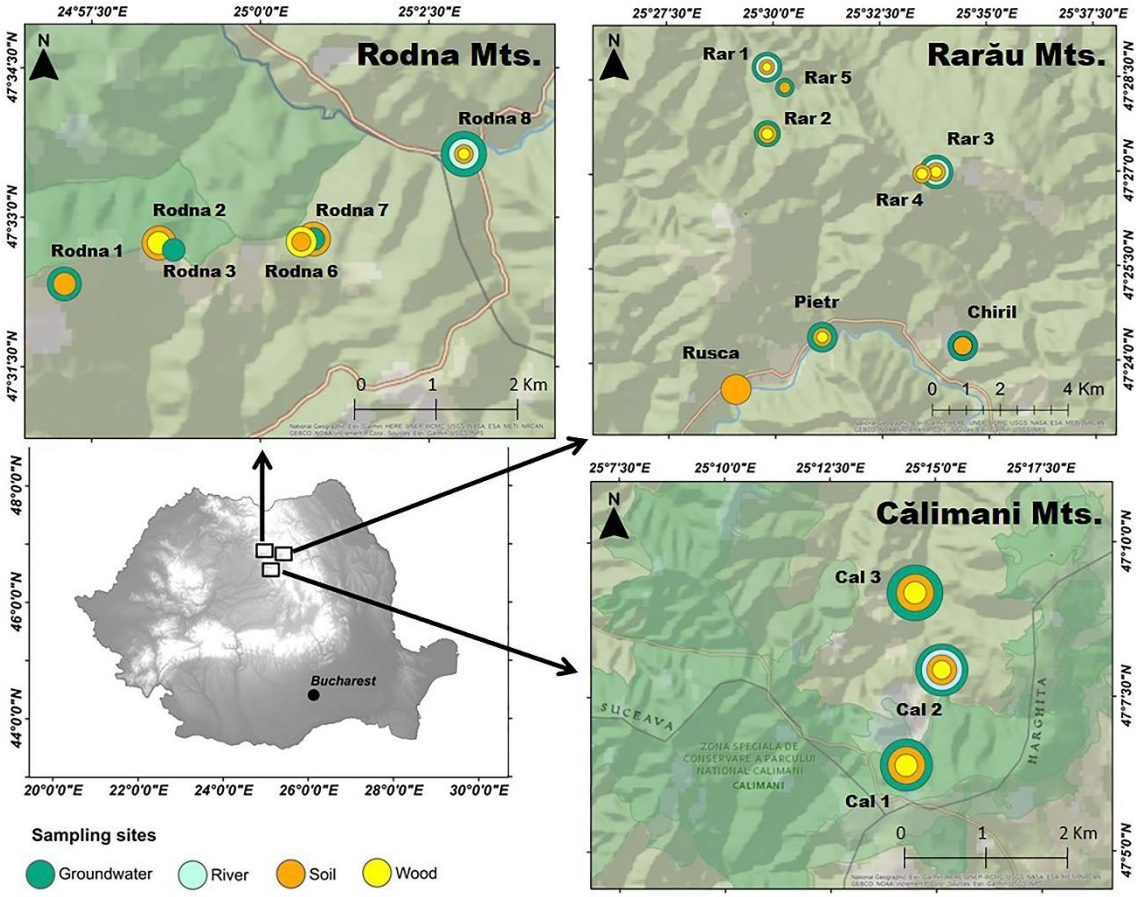

Figure 2.2: Sampling sites and samples collected in the Eastern Carpathians, Romania.

2.3 Sample Preparation

2.3.1 Preparation of Water Samples

Water samples from both studies were acidified on site with suprapure HNO_3, and stored at –20 °C until analysis. Acidified water samples were filtered through a 0.45 µm filter before analysis.

2.3.2 Preparation of Soil Samples

Soil samples were air-dried and ground using an agate mortar and pestle. They were subsequently put through a stainless-steel sieve with a mesh size of 63 µm (US Standard 230) to remove larger grains and obtain fine powder particles. Both bioavailable fractions and bulk samples were analyzed. For the assessment of bioavailable elements in the soil sample fractions, 1 mol L^{-1} NH_4NO_3 was used as an extraction solvent. This extraction process is a common method used in environmental chemistry, and is particularly effective because it mimics the ion-exchange processes that occur naturally in the soil-root interface (Gryschko et al., 2005). Approximately 2 g of the sample was weighed into a 30 mL test tube, and 5 mL of 1 mol L^{-1} NH_4NO_3 was added. The tubes were placed on an orbital shaker used to assist the single extraction process, for 2 h at 300 rpm. Afterward, the samples were centrifuged at 8000 rpm for 15 min. The supernatant material was separated

from the precipitate solution using a 0.45 µm filter. All samples were prepared in replicates and analyzed on the day of preparation to avoid jeopardizing sample integrity.

Additionally, bulk soil samples were subjected to a two-cycle acid digestion in the closed vessel microwave digestion system MARS 6 (CEM corporation, NC, USA). Approximately, 0.25 g of the sample was weighed into PFA digestion vessel, to which a mixture of HNO_3, HCl, and HF was added in the amounts of 4 mL, 1 mL, and 2 mL, respectively. The second cycle was conducted following the addition of 12.5 mL of H_3BO_3 (4 % (*w*/*w*)). The resulting clear solution was quantitatively transferred to 30 mL PP graduated conical tubes and filled to the mark with MilliQ water.

2.3.3 Preparation of Biological Samples

2.3.3.1 Feed Samples

Feed samples were freeze-dried inside the ice condenser (single-chamber method, Gamma 2–16 LSCplus, Martin Christ Gefriertrocknungsanlagen GmbH, Osterode am Harz, Germany) upon reception at the laboratory. They were subsequently digested in a MARS 6 microwave to prepare them for multi-elemental analysis. For this procedure, 0.30 g of the sample was weighed with the addition of 4 mL of HNO_3, 1 mL of H_2O_2, and 0.1 mL of HF. Afterward, obtained sample solutions were quantitatively transferred into PP graduated conical tubes and adjusted to a volume of 20 mL with MilliQ water.

Figure 2.3: Example of a feed mixture sample before and after freeze-drying and homogenization.

2.3.3.2 Dairy Samples

Milk samples were transported frozen to the laboratory and stored at –80 °C until freeze-drying. For multi-elemental analysis, samples were prepared through a one-cycle microwave digestion, using a MARS 6 digestion system. Approximately 0.30 g of freeze-dried milk was introduced in PFA digestion vessels and added with 6 mL HNO_3 and 1 mL of H_2O_2. The resulting solution was quantitatively transferred into PP graduated conical tubes and filled to 20 mL with MilliQ water.

Cheese samples were processed and prepared using the same methodology as employed for the milk samples. Rennet was digested in a similar way as milk and cheese samples. The same procedure (acids only) was applied to the blank samples. A 4 % sea salt solution

was prepared by dissolving 2 g of the salt in 50 mL of MilliQ water. All samples were diluted 5 to 10-fold before further analysis.

2.3.3.3 Wood Samples

Wood samples were subjected to acid digestion in the closed vessel accelerated reaction microwave digestion system MARS 5 (CEM corporation, NC, USA). Each sample (weighing approximately 0.25 g), without prior grinding, was introduced in PFA digestion vessels, along with 5 mL of HNO_3 and 2 mL of H_2O_2. The mixture was allowed to react overnight. Before sealing the vessels, 0.1 mL of HF was added. After the microwave digestion program, the clear solution was quantitatively transferred into PP graduated conical test tubes and filled to 20 mL with MilliQ water.

2.4 Determination of Total Concentrations of Elements in Analyzed Samples

Multi-elemental analysis (Ag, Al, As, B, Ba, Ca, Cd, Co, Cr, Cu, Fe, K, Li, Mg, Mn, Mo, Na, Ni, Pb, Rb, Sb, Se, Sr, Tl, U, V, and Zn) was performed by ICP-MS (7700x series, Agilent Technologies, Tokyo, Japan), with daily optimization of parameters for maximum sensitivity. Typical operating parameters are presented in Table 2.3.

2.5 Isolation of Sr from the Matrix and Sr Isotope Ratio Analysis

For Sr isotope ratio analysis, Sr was initially isolated from the matrix through a column procedure using Sr-specific resin Eichrom® (particle size (100–150) μm, SR-B200-A, TrisKem International, Brittany, France), following the method outlined in Table 2.2, adapted from previos research (Zuliani et al., 2020). An aliquot of the sample was evaporated to dryness on a sand bath at $\leq$ 90 °C, then redissolved in 1 mL of 8 mol L^{-1} HNO_3 and subjected to ultrasonication for 30 minutes. Subsequently, the solution was loaded onto a column containing 150 mg of the resin. The separation protocol is shown in Table 2.2.

To assess the efficiency of Rb removal and Sr recovery after separation, the total Sr and Rb concentrations were measured by ICP-MS. Rb concentration was below the limit of detection, and Sr concentration ranged from 15 to 25 ng mL^{-1} in all samples, with a recovery rate exceeding 95 %.

The $^{87}Sr/^{86}Sr$ isotope ratio was determined using Nu II Plasma MC-ICP-MS (Ametek, Wrexham, United Kingdom) equipped with the Aridus II Desolvating Nebulizer System (Teledyne Cetac, Omaha, Nebraska, USA) with a PFA nebulizer (100 μL min^{-1}). Instrumental mass discrimination was corrected by internal normalization using the ratio $^{86}Sr/^{88}Sr = 0.1194$, and interferences from Rb and Kr were corrected mathematically using the $^{87}Rb/^{85}Rb$ and $^{86}Kr/^{83}Kr$ ratios of 0.38567 and 1.50566, respectively.

All measurements followed the bracketing method (standard-sample-standard sequence) with a sample-matched concentration of the isotope standard reference material NIST SRM 987 ($^{87}Sr/^{86}Sr = 0.71034 \pm 0.00026$). The instrument underwent daily optimization for maximum sensitivity and signal stability (Table 2.3).

Table 2.2: Sr separation protocol using Sr specific resin.

Procedure	Volume	Description
Resin washing	3 x 1 mL MilliQ H_2O	discard
	1 mL 6 mol L^{-1} HCl	
	10 x 1 mL MilliQ H_2O	
Resin conditioning	3 x 1 mL 8 mol L^{-1} HNO_3	discard
	10 x 1 mL MilliQ H_2O	
Sample loading	1 mL (8 mol L^{-1} HNO_3)	discard
Matrix separation	5 x 1 mL 8 mol L^{-1} HNO_3	discard
Sr elution	10 x 1 mL MilliQ H_2O	collect

Table 2.3: Operating conditions for the 7700x ICP-MS and Nu II MC-ICP-MS.

ICP-MS		
Nebulizer	MiraMist	
Spray chamber	Scott double-pass	
RF power	1550 W	
Plasma gas flow	15 L min^{-1}	
Carrier gas	1.05 L min^{-1}	
Dilution gas	0.15 L min^{-1}	
Sampling depth	7.5 mm	
Sample uptake rate	0.3 mL min^{-1}	
Sampler and skimmer cones	Ni	
Isotopes of internal standards	^{45}Sc, ^{72}Ge, ^{89}Y, ^{103}Rh, ^{115}In, ^{193}Ir	
MC-ICP-MS		
Desolvator temperature	160 °C	
Ar sweep gas rate	~ 4 L min^{-1} (optimized daily)	
RF power	1300 W	
Plasma gas flow	13 L min^{-1}	
Auxiliary gas flow	0.80 L min^{-1}	
Nebulizer gas pressure	38 Psi	
Sampling cone	Ni, aperture diameter 0.9 mm	
Skimmer cone	Ni, aperture diameter 0.7 mm	
Integration time	10 s	
Number of cycles	30	
Number of blocks	2	
Mass assignment to Faraday cup detectors	H5	88
	H3	87.5
	H1	87
	L1	86.5

	L3	86
	L5	85.5

2.6 Data Analyses and Statistical Evaluation

Approximately 20 % of all samples were digested in replicates as a quality control measure. For soil samples, the bioavailable fractions of all samples were extracted in replicates to ensure better precision. The data, including Sr isotope ratios and concentrations of a few selected elements, are presented as the average ± standard deviation in Appendix A. Furthermore, results obtained for CRMs are presented in Appendix A. The results for Sr isotope ratios in these CRMs, though not certified, were in agreement with data previously reported in the literature.

For samples from Naxos, Greece, appropriate tests were performed on Sr isotope ratio analysis data. The Shapiro-Wilk test showed no significant departure from normality ($p > 0.05$). This finding was further supported by visual inspection of Q-Q plots. However, Levene's test revealed significantly different variances across groups. Given this violation of homogeneity of variances, the Kruskal-Wallis test was used for comparing means across matrices and within specific matrices, where multiple sampling campaigns occurred. It indicated overall group differences ($p < 0.05$). Dunn's test was applied for post-hoc pairwise comparisons. For comparisons involving paired milk and feed samples from January 2021 and June 2021 campaigns, the Wilcoxon signed-rank test with continuity correction was used. Dixon's test was used for detecting outliers in the datasets. Statistical tests and data visualizations were conducted in R Statistical Software (v4.3.2, R Core Team 2021), using packages such as simmr, ggplot2, ggbeeswarm, among others. The package simmr was specifically used for running the mixing model.

Additionally, preliminary $^{87}Sr/^{86}Sr$ isoscapes of Naxos were built using the open-source QGIS (v3.34.3, QGIS Association). For this purpose, the IDW interpolation technique was applied.

For samples from the Eastern Carpathians, Romania appropriate statistical tests, for which the significance level was set at 0.05, as well as linear regression analysis with the calculation of adjusted R-squared, were performed in OriginPro software (v2020b, OriginLab Corporation, Northampton, MA, USA). Given the non-normal distribution of data, the Kruskal-Wallis test was applied to compare elemental mass fractions and Sr isotope ratio values in wood samples across three regions. Significant differences identified by this test led to subsequent pairwise comparisons using Dunn's post hoc test with Bonferroni correction. Principal Component Analysis (PCA) was conducted using the packages MASS, factoextra, and ggplot2 in R Statistical Software (v4.3.2, R Core Team 2021).

Chapter 3

Results and Discussion

3.1 Integrated Strontium Isotope and Multi-Elemental Approach to PDO Graviera Naxos: Evaluating Source Complexity

The findings discussed in this sub-chapter were originally published by Nikezić et al. (2024) in *Foods*.

3.1.1 Elemental Composition of Environmental Samples

The content of selected elements is shown in Appendix A. For the feed samples, the presence of As, Cd, and Pb was observed in the majority of cases; however, the detected mass fractions remained under the threshold limits established by Directive 2002/32/EC. Expectedly, the contents of these elements were higher in pasture samples than in feed mixture samples. For example, while the average mass fraction of Pb in feed mixture samples was 0.143 mg kg^{-1}, in one pasture sample the Pb mass fraction was measured at 2.14 mg kg^{-1}. In terms of water samples, all tested instances showed Cd levels below the LOD, while the measured levels of As and Pb did not surpass the threshold values outlined in the Guidelines for Drinking Water Quality, which are 10 µg L^{-1} and 9 µg L^{-1}, respectively (World Health Organization, 2022). Furthermore, water samples were in accordance with the requirements from the Drinking Water Directive (98/83/EC) regarding As, B, Cd, Cr, Ni, Pb, Sb, and Se concentrations.

3.1.2 Elemental Composition of Milk and Graviera Naxos Cheese Samples

The content of selected elements is presented in Appendix A. Mass fractions of Ag, Co, Li, Sb, Tl, U, and V were below the LOD in most of the milk and Graviera Naxos cheese samples. On average, macroelements in cow and goat milk were found in the following sequence from lowest to highest mass fractions: Mg < Na < Ca < K, ranging from 739 mg kg^{-1} to 10311 mg kg^{-1}, while in Graviera Naxos cheese samples as well as sheep milk samples mass fractions of Ca were the highest. The content of the microelements in the goat and sheep milk was as follows: Zn > Fe > Cu > Mn > Se > Mo > Cr. However, cow milk samples showed a different pattern, with higher average mass fractions of Mo, rearranging the sequence to: Zn > Fe > Cu > Mo > Mn > Se > Cr. In Graviera Naxos cheese samples, the order of microelement content was found to be Zn > Fe > Cu > Mn > Mo > Se > Cr. The comparative analysis of elemental composition indicated that the pasteurization process does not significantly alter the mineral composition of milk, aligning with the

conclusions of earlier studies (Khan et al., 2017). Additionally, the data revealed less than 25 % seasonal fluctuations in the content of most elements (Figure 3.1). Comparative assessments further suggest that goat and sheep milk exhibit marginally higher levels of most elements, compared to cow milk (Nečemer et al., 2016). Similarly, Graviera Naxos cheese demonstrates a modestly enriched elemental profile when compared to its milk precursor (Figure 3.1). However, this enrichment does not extend to Mg and K, aligning with previous findings (Bontempo et al., 2019). Given that cheese production involves the mixing of three types of milk, a variance in mineral composition in the cheese is anticipated. Moreover, the creation of dairy matrices during this process leads to unique structures and distributions of essential minerals, distinguishing cheese from its milk source (Teixeira et al., 2022). In the case of milk, As and Cd mass fractions were found to be below LOD, and Pb was detected only in a minority of the samples without exceeding the maximum levels permitted by the Regulation (EU) No 2023/915. Mass fractions of these elements were below the LOD in all Graviera Naxos cheese samples.

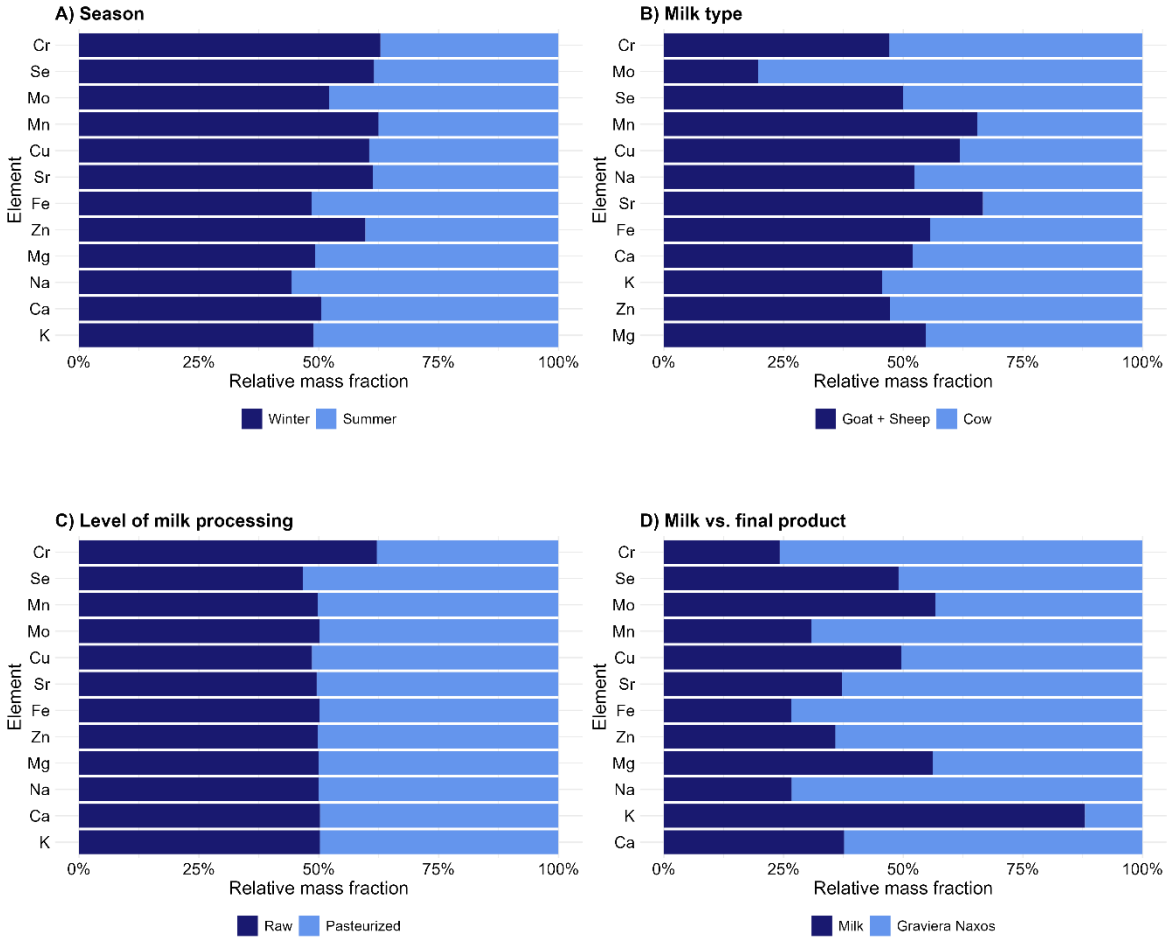

Figure 3.1: Variations of Sr and essential elements' levels across a) sampling seasons (January 2021 and June 2021), b) milk types, c) pasteurized and raw milk, and d) milk from milk tanks and Graviera Naxos cheese. The relative mass fraction is normalized to 100 % for all elements. Elements are displayed based on their total mass fraction, from lowest to highest.

3.1.3 Distribution of $^{87}Sr/^{86}Sr$ Values and Statistical Analysis

$^{87}Sr/^{86}Sr$ isotope ratio was determined in soil, water, feed, milk, and cheese samples. Sr isotopic ratio values ranged from 0.70781 to 0.72276 in all analyzed matrices (Table 3.1).

Table 3.1: Overview of the samples and their $^{87}Sr/^{86}Sr$ values.

Matrix	Sampling campaign	N° of samples	$^{87}Sr/^{86}Sr$				
			Mean	Median	Min.	Max.	SD
Bulk soil	August 2020	16	0.71303	0.71182	0.70865	0.72276	0.00373
Bioavailable soil fraction	August 2020	16	0.70967	0.70956	0.70859	0.71150	0.00067
Water	January 2021	18	0.70996	0.70978	0.70831	0.71209	0.00100
Feed	August 2020, January 2021, June 2021	67	0.70963	0.70935	0.70855	0.71613	0.00109
Milk	August 2020, January 2021, June 2021, July 2021, January 2022	96	0.70940	0.70926	0.70781	0.71225	0.00058
Graviera Naxos cheese	August 2020, January 2021, June 2021, January 2022	7	0.70928	0.70938	0.70891	0.70952	0.00021

$^{87}Sr/^{86}Sr$ isotope ratio values observed for bulk soil were expectedly high (0.72276), as this is a result of total Sr that is present in all the minerals and organic phases present in the soil. The ranges for the rest of the matrices are characterized by the maximum value of 0.71613, observed in a feed sample. Similarly, it is evident from Table 3.1 that matrices, except bulk soil, share similar $^{87}Sr/^{86}Sr$ isotope ratio means (Water > Bioavailable soil fraction > Feed > Milk > Cheese).

Figure 3.2 displays the $^{87}Sr/^{86}Sr$ values across matrices: bioavailable soil fraction, water, feed, milk, and cheese, with each data point representing a distinct sample. This presentation enables the observation of sample density, their respective Sr isotope ratio ranges, and the frequency of sampling during winter and/or summer seasons. Notably, feed and milk samples, collected during summer sampling campaigns, display some of the highest Sr isotope ratio values observed. On the right side of the figure, a Kernel density estimation (KDE) plot is presented, depicting the estimated probability density function of the underlying distribution of $^{87}Sr/^{86}Sr$ values across the examined matrices.

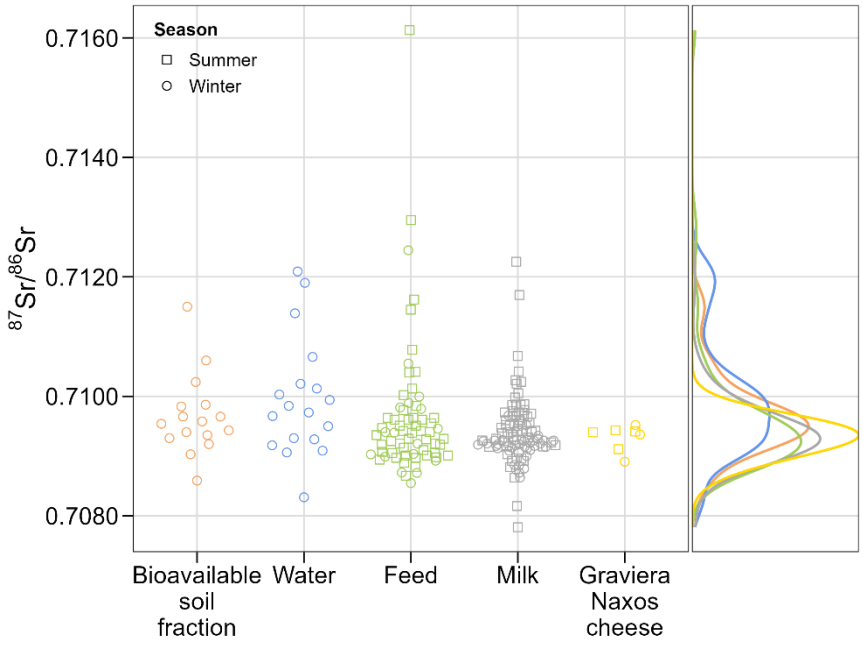

Figure 3.2: Ranges and distribution of $^{87}Sr/^{86}Sr$ values across matrices.

The bandwidth was determined following Scott's rule of thumb. This data smoothing technique facilitates a closer examination of the local range of bioavailable Sr. Prior to initiating mixing models, this KDE analysis provides a foundational framework. By visually assessing the positions of the generated peaks, we can infer whether specific sources are likely contributors to the mixture. The primary mode encompasses $^{87}Sr/^{86}Sr$ values ranging between 0.7085 and 0.7105, aligning with the bioavailable baseline range for the South Aegean as established by Frank et al. (2021). Nonetheless, the range observed in this study marginally exceeds those previously established boundaries. The cheese matrix peak shows the highest density, indicating the central density of the distribution, as well as the prevalence of these values within the dataset. This is likely due to the smaller number of samples collected and analyzed for cheese compared to feed and milk. Additionally, because cheese is a processed product, its isotopic composition is expected to show less variation compared to milk and environmental samples. The peaks corresponding to cheese, milk, and feed matrices align closely, with each peak falling slightly below the next. Conversely, peaks representing the bioavailable soil fraction and water matrices exhibit a slight upward shift (higher values). Bimodal distribution is observed for water matrix, suggesting the underlying heterogeneity in the data, probably arising from the presence of multiple distinct sources. Furthermore, no skewness is observed in the distribution, revealing a relatively balanced representation of data around the central mode.

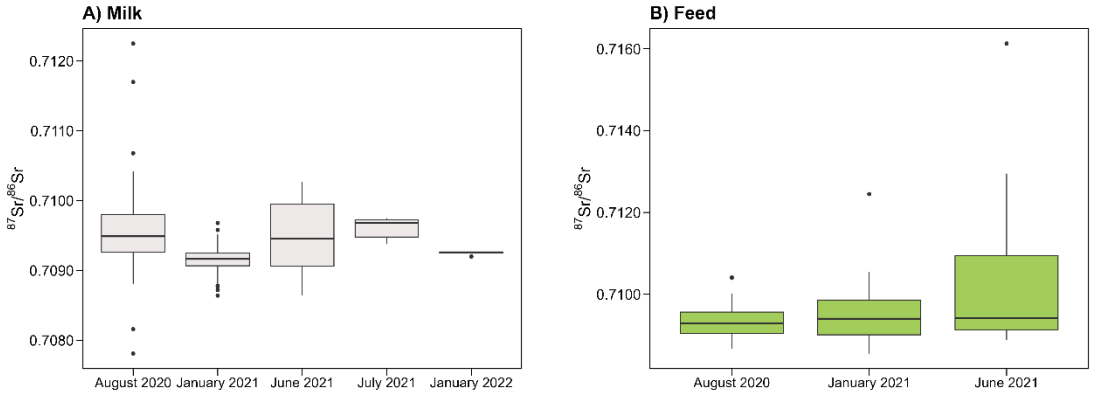

Figure 3.3: Boxplots representing ranges of $^{87}Sr/^{86}Sr$ values for a) milk and b) feed across different sampling campaigns, the median of the data is the line, points outside whiskers are points beyond 1.5 times the IQR from the quartiles.

The outcomes of Dunn's test, considering adjusted p-values below 0.05, elucidated notable distinctions in median values among the groups, except between water and bioavailable soil fraction, feed and milk, feed and cheese, and between milk and cheese, where no significant differences were observed. Focusing on the milk matrix, the results, validated by Dunn's test with Bonferroni correction, revealed significant differences in medians between following campaigns: August 2020 and January 2021, January 2021 and July 2021, as well as July 2021 and January 2022. Wilcoxon signed-rank test resulted in p-value of 0.008, indicating a significant shift in the median between January 2021 and June 2021 milk samples. The graphical representation of these findings, as depicted in the boxplots from Figure 3.3a), best illustrates the observed results. Clearly, the differences were consistently observed between campaigns conducted in the summer and winter seasons. Conversely, comparisons between summer-to-summer or winter-to-winter campaigns did not yield significant differences. Additionally, analogous tests were conducted to compare pasteurized and non-pasteurized milk, as well as various milk types, including cow, goat, and sheep. The results did not show significant differences in the medians of Sr isotope ratio values among these categories. This insight proves particularly valuable given that Graviera Naxos cheese is crafted from a blend of various milks. However, statistical tests performed on feed samples did not provide sufficient evidence to conclude that there is a significant difference in the median values among sampling campaigns (Figure 3.3b)). While it is reasonable to anticipate a significant difference in the medians of Sr isotope ratio values of the samples collected in summer and winter campaigns, due to seasonal variations in animal diet, namely more pasture grass in summer and limited grazing time in winter, we need to stress out that the analyzed feed samples were mostly cereal mixtures – same in both summer and winter. This uniformity in feed composition across seasons could likely explain the inability to detect significant differences in medians of Sr isotope ratios within the feed samples. In contrast, variations observed in milk samples, probably influenced by the changing diet of animals, could account for the detection of differences in medians of Sr isotope ratios between the two seasons. Despite the presence of points outside the whiskers in Figure 3.3, which likely represent outliers, the Dixon's test identified only one outlier: feed sample with a $^{87}Sr/^{86}Sr$ value of 0.71613. However, this value was retained for further analysis as it is believed to reflect a genuine measurement rather than an error.

3.1.4 Contributions to Strontium Isotopic Composition of Milk

Soil, water, and feed samples were investigated as environmental factors likely to influence the Sr isotopic composition of milk. There was no correlation between milk and bioavailable soil fraction samples. Milk samples from August 2020 were used for this comparison, since they originate from the same stations as soil samples. Moreover, the Sr isotope ratio in vegetation primarily reflects the bioavailable Sr fraction of the soil in which it grows (Aguzzoni et al., 2019; Choi et al., 2023). Consequently, we investigated the correlation between soil and feed samples. The absence of a correlation between bioavailable soil fraction and feed samples (August 2020), suggests that the feed mixtures were likely not sourced locally from the farms but instead imported to the island.

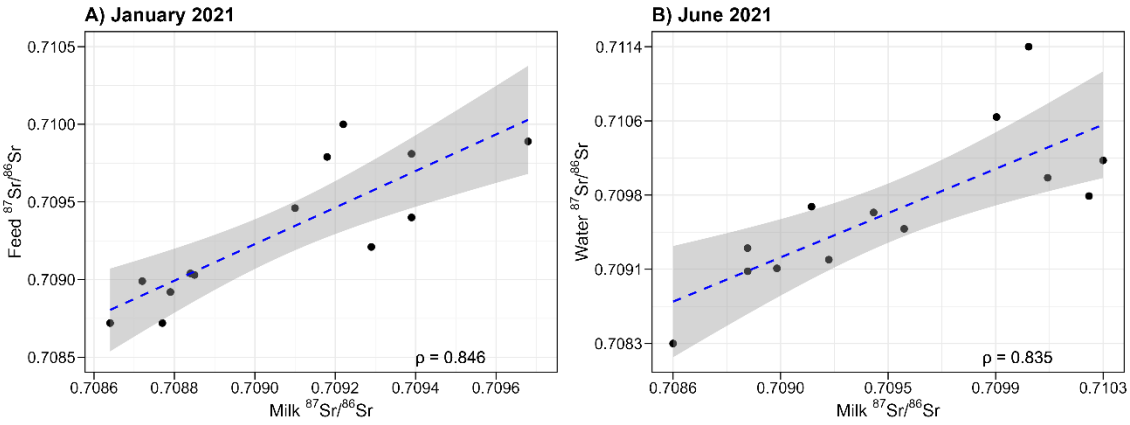

Figure 3.4: Correlation between $^{87}Sr/^{86}Sr$ values of a) milk and feed samples from January 2021 and b) milk (June 2021) and water samples. Line of best fit is represented by a dashed blue line, the shaded area surrounding the line depicts the 95% confidence region.

For the correlation between milk and feed samples, we focused on campaigns conducted in August 2020, January 2021, and June 2021. Despite no significant difference in the medians of $^{87}Sr/^{86}Sr$ values of feed samples from August 2020, January 2021, and June 2021, a moderate to strong positive correlation emerged between the $^{87}Sr/^{86}Sr$ values of milk and feed sampled in January 2021 (Figure 3.4a)). This correlation was quantified by a Spearman correlation coefficient of $\rho = 0.85$. Interestingly, no obvious correlation was noted for samples from either August 2020 or June 2021. As previously noted, all feed samples, regardless of season, consist of mixtures of various cereals. This suggests that the absence of correlation between milk and feed in August 2020 and June 2021 may be attributed to increased grazing time during this period, leading to a higher proportion of pasture in the animals' diets. Conversely, during winter, the feed mixtures analyzed constitute a substantial portion of the animals' diet, resulting in a stronger correlation between milk and feed.

These statements can be confirmed with further analysis. Namely, relationship in $^{87}Sr/^{86}Sr$ values between milk and water samples were also examined. Values for water and milk from corresponding farms were compared, from both January 2021 and June 2021. No correlation between milk and water $^{87}Sr/^{86}Sr$ values from January 2021 was found. However, a moderate to strong positive correlation was observed for the samples from the June 2021 campaign, as shown in Figure 3.4b). This is in agreement with another study (Gregorčič et al., 2021), which also found a correlation between milk and corresponding river samples. Animals' drinking behavior and water intake are influenced by various factors, including climatic conditions and individual characteristics such as lactation stage.

Despite these influences, the average daily free water intake remains relatively high at 83.6 ± 17.1 liters per day (Cardot et al., 2008). However, water is unlikely to be a major contributor to the Sr isotopic composition of milk due to low Sr concentrations in water samples (from 0.103 mg L^{-1} to 2.48 mg L^{-1}). Instead, pasture grown on the island, which contains more moisture compared to the dry mixtures provided in winter, may have a similar Sr isotope ratio as water samples from the island. This suggests that during summer, pasture is likely shaping the Sr composition of milk. The Sr isotopic signature of milk is influenced by the diet, significantly altering the $^{87}Sr/^{86}Sr$ ratio in milk between seasons, likely masking local Sr isotope ratio levels (water, soil). This finding complicates using the $^{87}Sr/^{86}Sr$ ratio as a method for verifying the geographical origin of dairy products. In Naxos's case, where the area for growing feed is limited and there's a necessity to import feed from the mainland, this is particularly challenging.

3.1.5 Mixing Model for Estimating Contributions to Cheese Strontium Isotopic Composition

Mixing model calculations were applied in order to determine the contributions of existing sources to Sr isotopic composition of Graviera Naxos cheese. For this purpose, milk, sea salt, and rennet were defined as possible Sr sources. For fitting stable isotope mixing model (SIMM) via Markov Chain Monte Carlo (MCMC) algorithm, R package simmr was used (Govan et al., 2023). Mixing models have proven critical for detailed investigations. Namely, in the archaeological domain, they are indispensable for delineating local bioavailable Sr isotope ranges, facilitating the reconstruction of ancient population migration patterns and geographical origins (Lengfelder et al., 2019; J. Montgomery et al., 2007; Toncala et al., 2020).

In the present model, 2 tracers were used: $^{87}Sr/^{86}Sr$ isotope ratio value and Sr mass fraction. Milk samples obtained from stations 64–66 in January 2021, along with samples collected during the July 2021 and January 2022 campaigns were used, as these samples were sourced from the milk tanks at the cheese manufacturing facility directly. Additionally, the $^{87}Sr/^{86}Sr$ isotope ratio of the analyzed sea salt sample was 0.70928 ± 0.00001. This value aligns with the reported modern seawater $^{87}Sr/^{86}Sr$ ratio of 0.7091 (Spooner, 1976). The $^{87}Sr/^{86}Sr$ isotope ratio for rennet was determined to be 0.70821 ± 0.00002. To the best of our knowledge, there are no existing reports of $^{87}Sr/^{86}Sr$ isotope ratio values specifically for rennet used in cheese production.

The isospace plot (Figure 3.5) illustrates the positioning of the mixtures relative to potential sources. Observations indicate that the mixtures fall within the polygon formed by connecting the sources with straight lines, suggesting that likely no sources have been overlooked. After checking the convergence, the model provides the summary that includes the mean and standard deviation estimates for the proportion of each source. Additionally, the three cheese samples from August 2020 are noticeably clustered closely together on the isospace plot. Yet, there is no discernible pattern relating to the season or year of cheese production in their distribution on the plot. Furthermore, it is evident that cheese samples are positioned significantly closer to sea salt and milk sources than to rennet, which is distinctly separate on the plot. Moreover, the larger SD associated with the milk source, in comparison to the other two sources, indicates potential uncertainties in determining source contributions.

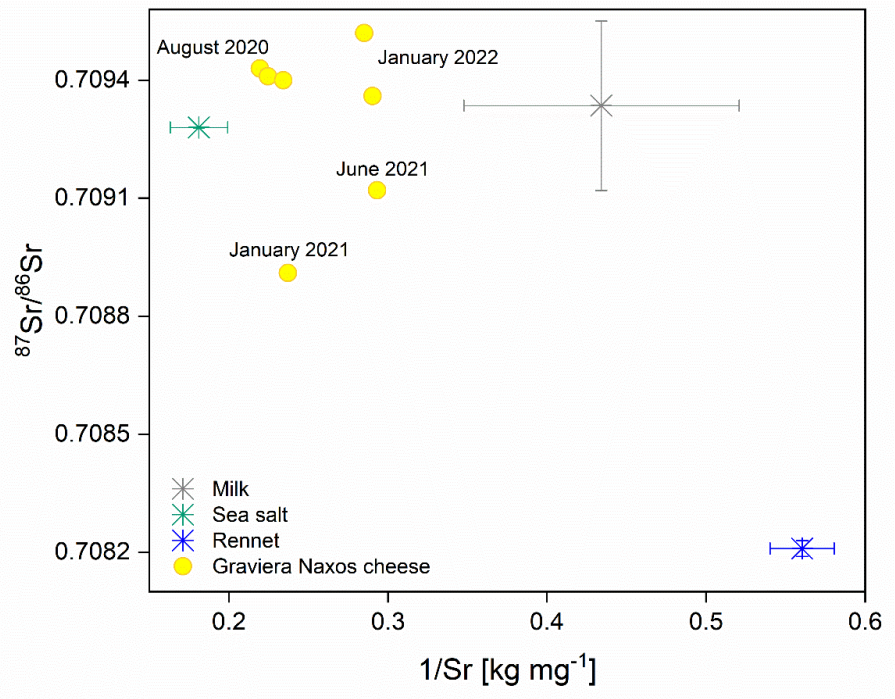

Figure 3.5: Isospace plot, $^{87}Sr/^{86}Sr$ ratios of sources (milk, sea salt, rennet) and Graviera Naxos cheese samples plotted against their respective inverse Sr mass fractions.

All SIMMs use informative prior distributions as a default. The shape and spread of the prior distribution indicate lower degree of certainty (Figure 3.6a)). In the case of sea salt, the posterior distribution differs notably from the prior: the peak has moved closer to the likelihood and become narrower, signifying increased confidence. It means that on average, sea salt contributes approximately 73.1 %, constituting the predominant source influencing the overall Sr isotopic composition of the Graviera Naxos cheese. The estimates for milk and rennet are 15.3 % and 11.7 %, respectively (Figure 3.6b)).

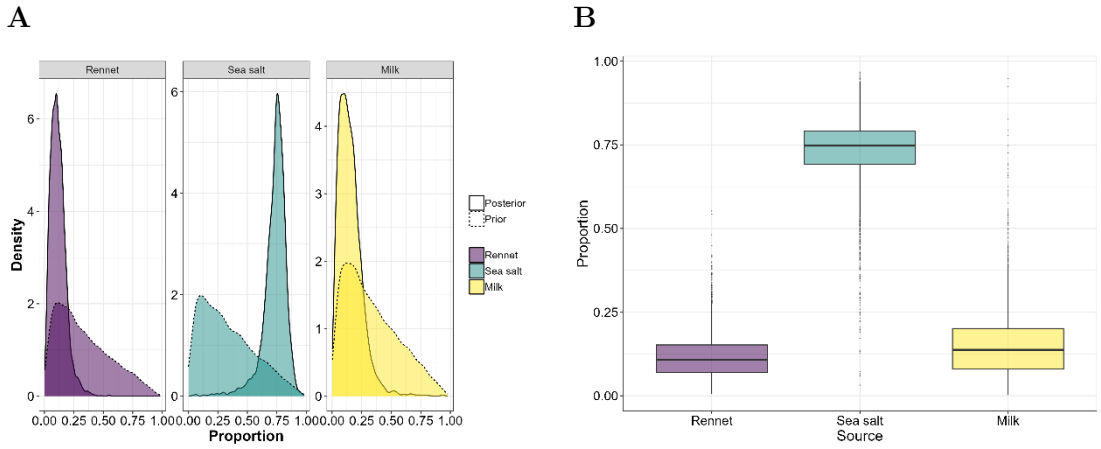

Figure 3.6: a) Prior and posterior distributions and b) comparison of source proportions.

Figure 3.7 shows the source histograms, contour plots of the relationship between the sources, and the correlation between the sources. It can be deduced that there is no observable correlation between rennet and sea salt, and rennet and milk. However, a moderate to strong negative correlation exists between sea salt and milk. This suggests that the model struggles to differentiate between the two sources, likely due to their proximity in the isospace (Figure 3.5) along the y-axis. The provided probability table (Table 3.2) indicated the probabilities of different mixing scenarios based on the model results.

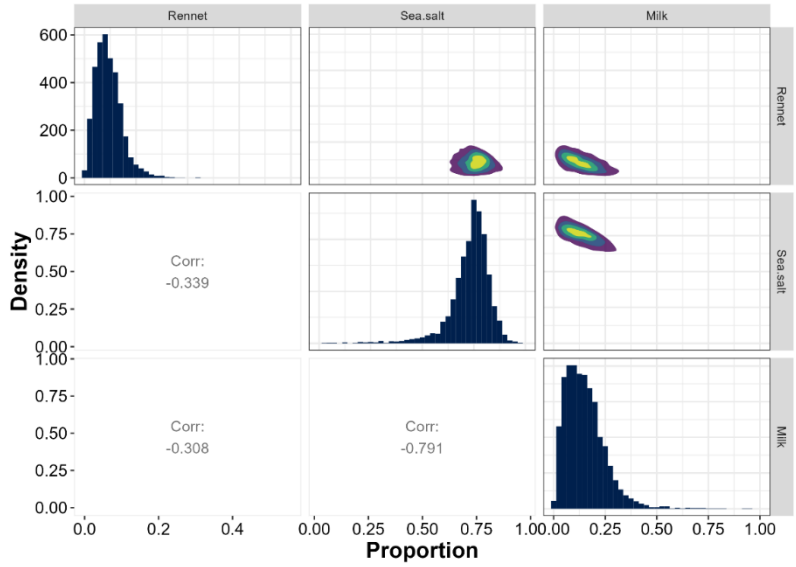

Figure 3.7: Correlation matrix showing relationships among sources: milk, sea salt, and rennet.

Table 3.2: Most probable orderings of contributions according to the mixing model.

Ordering	**Probability**
Sea Salt > Milk > Rennet	0.5683
Sea Salt > Rennet > Milk	0.4156
Milk > Sea Salt > Rennet	0.0117
Milk > Rennet > Sea Salt	0.0025
Rennet > Sea Salt > Milk	0.0011
Rennet > Milk > Sea Salt	0.0008

The model strongly supports the hypothesis that sea salt is a major contributor to the Sr isotopic composition of the analyzed cheese samples. The significant influence of salt used in cheese production on its Sr isotopic fingerprint is plausible, especially considering that it typically contains 2.4 g of salt per 100 g of the final product, and the concentration of Sr in the seawater lies between 7.2 mg L^{-1} and 7.8 mg L^{-1} (Angino et al., 1966). Some researchers studied the influence of salt on the Sr isotope ratio in the cured ham, and their findings indicated that the $^{87}Sr/^{86}Sr$ isotope ratio in cured Bayonne ham was strongly influenced by the Sr isotope composition in the salt form the local salt-mine (Epova et al., 2018). However, arriving at a definitive conclusion is challenging due to the close Sr isotope

ratio values between sea salt and milk. This suggests that sea spray could significantly affect the entire island's environment, dispersing onto pastures and consequently impacting the Sr isotope ratio in milk (Alonzi et al., 2020). As demonstrated in Figure 3.4b), there is a notable correlation between milk and water during the summer, indicating this influence. The mixing model provides a structured approach to understanding the complex mixing scenarios that can occur during cheese production, aiding in the identification of the origins of specific isotopic signatures. However, in cases where sources exhibit similar isotopic ratios, such as sea salt and milk in this instance, the model's effectiveness may be limited. The proximity of isotopic values between these sources poses challenges in accurately distinguishing their contributions, highlighting the need for additional complementary techniques or refined modelling approaches to overcome such complexities. Moreover, the potential influence of salt on the cheese's Sr isotopic fingerprint suggests the need for further investigation.

3.1.6 Spatial Distribution of $^{87}Sr/^{86}Sr$ Ratio Values Across Naxos Island

Figure 3.8 illustrates the distribution of sampling sites for soil and water, along with the values for $^{87}Sr/^{86}Sr$ isotope ratio across Naxos Island. The primary objective of this dissertation was to trace the provenance of Graviera Naxos cheese; hence, sampling locations were strategically concentrated in the southwestern part of the island where most cheese production occurs. Consequently, this area was sampled more densely compared to other regions of the island. To date, this study boasts the most comprehensive sample collection from Naxos Island and is among the few studies focusing on such a localized area. In contrast, previous research typically covered a much larger area, averaging one sampling site per approximately 600 km^2 (Snoeck et al., 2020; Willmes et al., 2018).

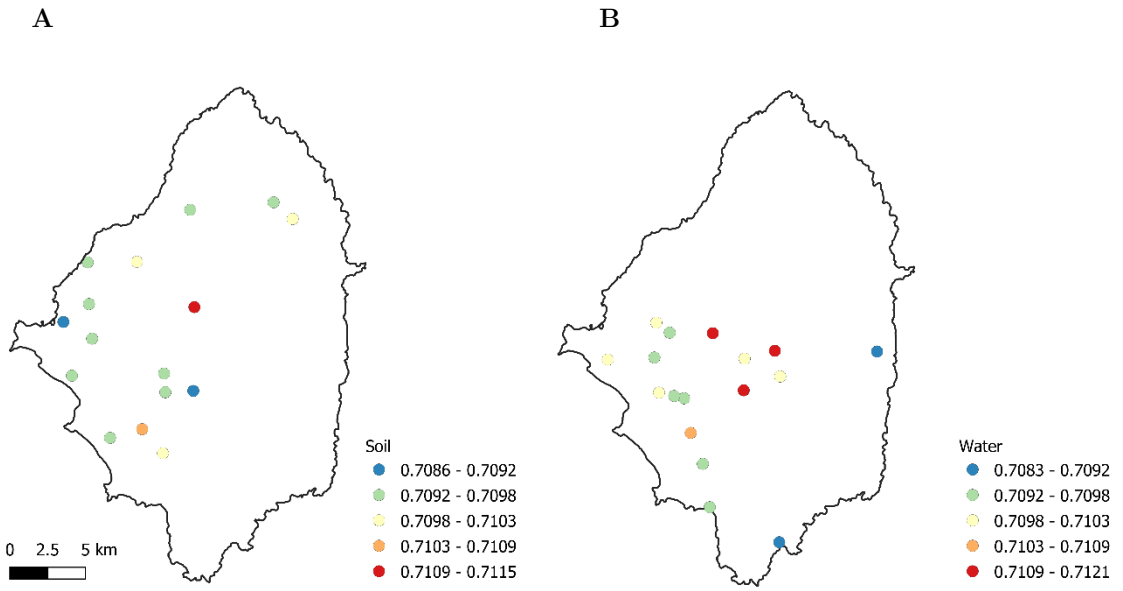

Figure 3.8: Spatial distribution of $^{87}Sr/^{86}Sr$ values in a) bioavailable soil fraction and b) water samples.

To facilitate trend analysis, the same color scales were applied to the maps of both the bioavailable soil fraction and water samples. The efficacy of using groundwater as a proxy

for constructing baseline maps of $^{87}Sr/^{86}Sr$ on islands is ambiguous. On one hand, groundwater offers a more averaged baseline, integrating signals over extensive spatial and temporal scales. On the other hand, its ability to capture the sea spray effect, which significantly influences marine Sr signatures in coastal areas, is uncertain. Groundwater in coastal zones may be subject to saltwater intrusion, particularly in karst or fractured rock environments, complicating its representation of terrestrial Sr sources. Furthermore, the Sr isotope composition in groundwater varies with depth due to geological factors and mineral interactions, potentially misrepresenting the bioavailable Sr accessible to local flora and fauna (Käßner et al., 2023). Notably, despite Naxos island's area of 429.8 km^2 and a coastline spanning 150 km, it features an elevation range from –3 to 985 m, primarily in the central and northern regions. This elevation variation is significant as the sea spray effect – which markedly influences the $^{87}Sr/^{86}Sr$ isotopic signature – is more pronounced at lower elevations.

Although some studies suggest that no single material fully captures Sr variability as effectively as a combination of different archives, others indicate that inter-site variation generally surpasses intra-site variation. Thus, using a single material could still optimally represent spatial variability. In our study, since soil and water samples were not collected from identical sites, we opted to construct individual isoscapes for each material initially, to compare trends. Subsequently, we assessed whether combining these materials would result in information loss or, conversely, optimize the isoscape map by enhancing the resolution and accuracy.

To establish the local $^{87}Sr/^{86}Sr$ baseline for sites on Naxos, additional measurements would ideally be needed. However, given the constraints, simplified isoscapes were constructed using lithology as explanatory data, depicted in Figure 3.9. For these isoscapes, Inverse Distance Weighting (IDW) interpolation was applied separately to the bioavailable soil fraction and water sample datasets. IDW is a deterministic spatial interpolation method where interpolated variables are predicted using a weighted average of nearby sample values. The weights assigned to each sample decrease with increasing distance from the prediction location, according to a power function. This method is advantageous due to its simplicity and minimal data requirements. It does not necessitate complex statistical models or extensive auxiliary datasets, making it particularly suitable for scenarios where only primary data and basic geographical information are available. The process of IDW interpolation inherently involves data smoothing, which can obscure finer isotopic variations, rendering smaller areas of diversity less visible in the final isoscape. However, incorporating lithology as an explanatory variable helps to mitigate this effect by providing additional context that reduces over-smoothing. IDW operates under the assumption that spatial entities that are closer together are more similar than those farther apart. It uses the values from surrounding measured points to predict values at unmeasured locations, assigning greater influence to points nearer to the prediction site. This influence diminishes with distance. While this method can lead to localized *bull's eye patterns* – where predicted values strongly reflect nearby measurements, particularly in sparsely sampled regions – it does not model spatial data structures like spatial autocorrelation or incorporate prediction uncertainties, unlike more sophisticated methods such as Empirical Bayesian Kriging (EBK).

Despite these limitations, IDW remains a viable initial approach for constructing Sr isoscapes on Naxos due to its straightforward application and effectiveness in scenarios with limited data. It provides a general overview of the spatial distribution of Sr isotopes, offering a foundational layer from which more detailed and comprehensive analyses could potentially be developed in the future. Emery et al. (2018) applied same interpolation method for generating first $^{87}Sr/^{86}Sr$ isoscape for Italy, using archaeological human and

faunal data, modern wine, beef, cheese, sediment, natural spring water, fossil, and tomato sauce data.

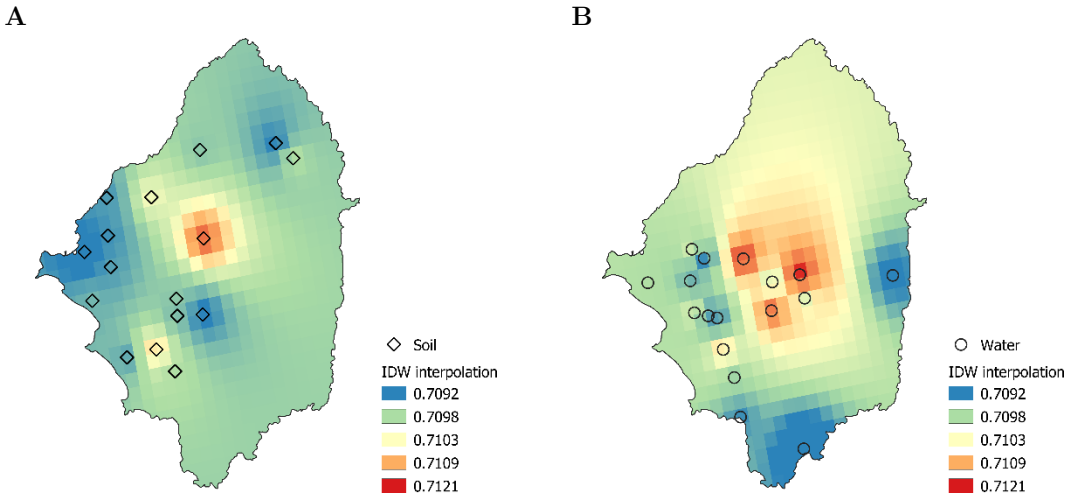

Figure 3.9: IDW interpolation a) bioavailable soil fraction and b) water samples.

In the comparison of isoscapes generated from soil and water data for Naxos, distinct trends emerge. The central part of the island displays the highest $^{87}Sr/^{86}Sr$ ratios on both maps, indicated by yellow to red hues, while the coastal areas show blue tones, aligning with the modern seawater $^{87}Sr/^{86}Sr$ ratio of 0.7091. Notably, discrepancies between the two maps are apparent in regions lacking data points. For instance, in Figure 3.9a), the absence of samples in the south and southeastern parts of the island results in these areas being shaded green. A similar pattern is observed in Figure 3.9b) for the northern regions where no water samples were collected. This suggests that, where no soil samples exist in the south, water samples from these areas approximate seawater $^{87}Sr/^{86}Sr$ values. Given these observations, it seems that integrating both maps would yield the most comprehensive and accurate representation of Sr isotopes across the island. Prior to merging these maps, it was essential to examine the $^{87}Sr/^{86}Sr$ ratios across different lithological units on the island (Figure 3.10).

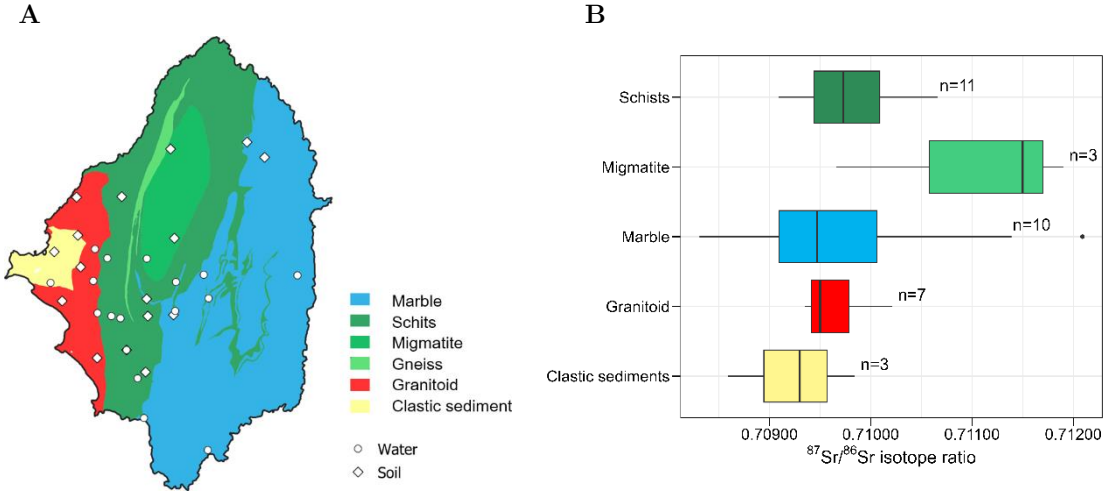

Figure 3.10: a) Naxos Island lithology and b) $^{87}Sr/^{86}Sr$ isotope ratio values of bioavailable soil fraction and water samples classified by lithological units.

To this end, data from both bioavailable soil fractions and water samples were combined to maximize the coverage of information. Although some lithological units are underrepresented with as few as three samples, the insights obtained are useful. For example, areas characterized by clastic sediments exhibited the lowest $^{87}Sr/^{86}Sr$ ratios, while areas with migmatite displayed the highest. Marble units showed the greatest variability in $^{87}Sr/^{86}Sr$ ratios, highlighting the diverse geochemical landscapes of Naxos.

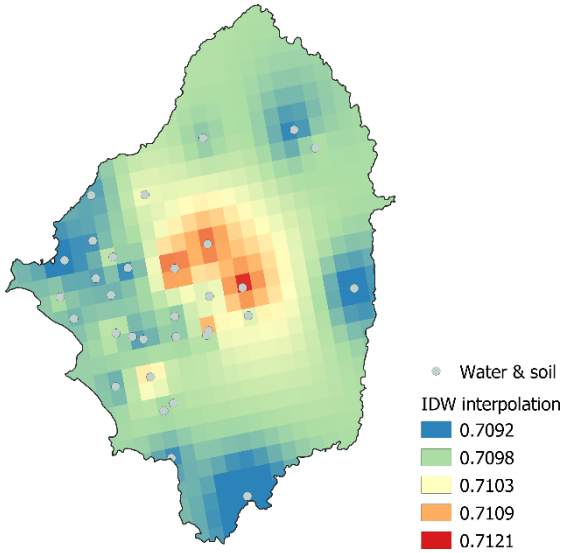

Figure 3.11: IDW interpolated bioavailable Sr baseline map of Naxos, incorporating both bioavailable soil fractions and water samples.

Merging the two maps has effectively consolidated the most crucial information (Figure 3.11). The central region of the area, characterized by migmatites, is distinguished by the highest Sr isotope ratio values, whereas the coastal areas predominantly reflect seawater values. However, it is evident that some parts of the island lack sampling sites, and thus, predictions of Sr isotope ratios in these areas should be approached with caution. Additional sampling is necessary to enhance the map's reliability as a reference dataset. Nevertheless, the established map represents a preliminary bioavailable Sr isoscape of Naxos. Thus, this preliminary assessment of $^{87}Sr/^{86}Sr$ variation across Naxos is an initial step in developing a comprehensive baseline map of the island that includes only bioavailable $^{87}Sr/^{86}Sr$ values. With more bioavailable $^{87}Sr/^{86}Sr$ data and improved spatial algorithms, we anticipate achieving more accurate geo-provenancing of isotope values for forensic and archaeological applications.

3.2 Geochemical Fingerprinting of Norway Spruce From the Eastern Carpathians: Sr Isotopic and Multi-elemental Signatures

The findings discussed in this sub-chapter were originally published by Nikezić et al. (2024) in *Science of The Total Environment*.

3.2.1 Multi-elemental Composition of Wood, Water, and Soil Samples

Soil bioavailable nutrient composition is reflected in the vegetation of a particular location. Bioavailability is influenced by various factors including soil pH, humidity, porosity, and the presence of clay and humic complexes, which is why the elemental composition is important for geographical origin assessment studies (Drivelos & Georgiou, 2012). However, soil chemical composition might not always reflect that of the underlying lithology (Kelly et al., 2005).

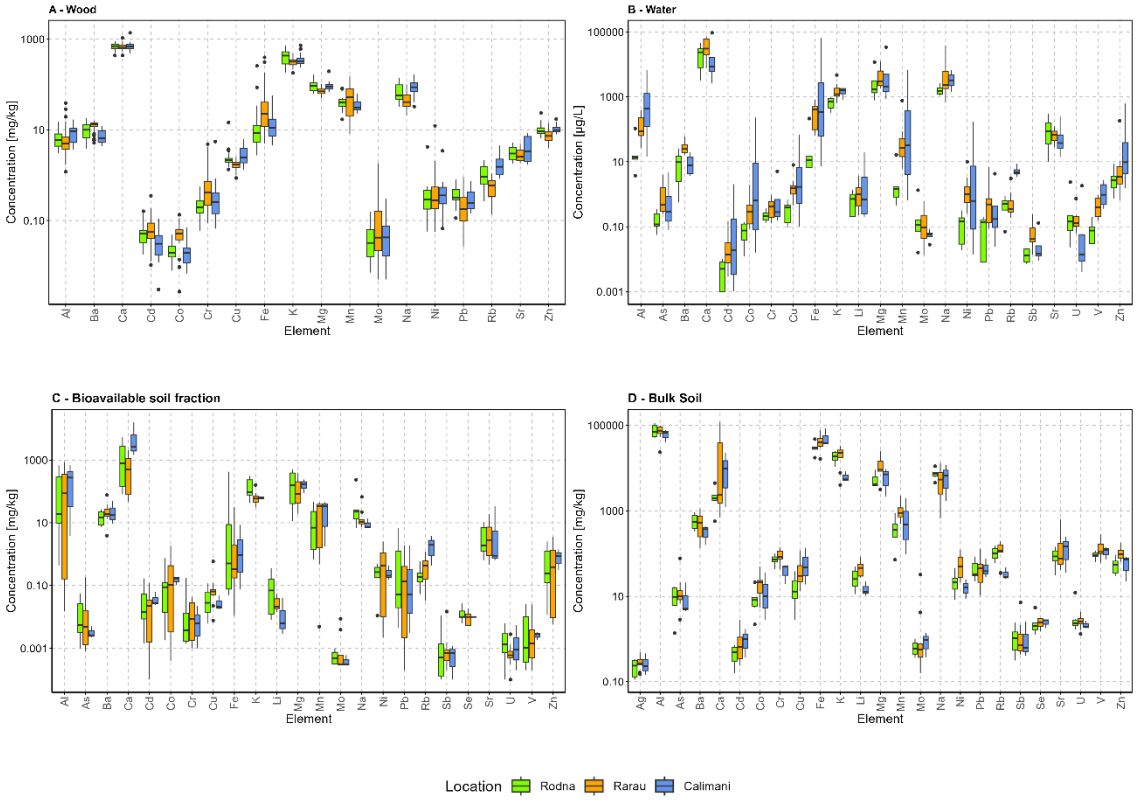

Figure 3.12: Boxplots with the median line representing elements mass fractions/concentrations in a) wood, b) water, c) bioavailable soil fraction and d) bulk soil samples from the three regions.

The content of selected elements is presented in Appendix A. Figure 3.12 presents the levels of major, trace, and potentially toxic elements that were measured above the established LODs in the analyzed samples, including wood, water, bioavailable soil fraction, and bulk soil. Boxplots for each region visually demonstrate differences in elemental compositions across water, bioavailable soil fractions, and bulk soil samples, where almost all elements' medians vary by region. In the analysis of water samples, the ranges and medians of elemental concentrations, specifically Al, Ba, Ca, Ni, Pb, Sb, U, and V, exhibit significant variability across the three regions studied. For bioavailable soil fraction samples, it is evident that the Rarău region demonstrates the most extensive ranges of mass fractions for the majority of measured elements, including Al, As, Ca, Cd, Co, Cr, Mn, Ni, Pb, and Zn. This observation confirms that the Rarău region, which had the highest number of collected samples, is characterized by distinct soil composition and texture. These factors influence the soil's capacity to retain and release nutrients.

Additionally, elevation and slope can affect drainage patterns and erosion, leading to differences in nutrient accumulation and loss (Zheng, 2006).

The elemental composition of the soil is also affected by the underlying geological material from which the soil is derived. For bulk soil samples, the trend of significant variations in concentrations is particularly pronounced for Ca. However, this pattern was not observed for wood samples. The results show significant differences ($p < 0.05$) in Rb, Na, and Ba concentrations in trees across all three regions. In Călimani, Rb and Na were found at the highest levels, with concentrations of 4.49 mg kg^{-1} and 168.7 mg kg^{-1}, respectively. Meanwhile, Ba reached its highest concentration in Rodna, at 18.3 mg kg^{-1}. For Mg, Cr, Fe, Co, Cu, and Zn, significant differences exist between Rarău and Călimani, as well as between Rodna and Rarău, but not between Rodna and Călimani. Differences in K and Pb were observed exclusively between Rodna and Rarău, with Rodna showing the highest concentrations for both elements (732.4 mg kg^{-1} and 0.933 mg kg^{-1}, respectively). Similarly, differences in Al and Cd were noted only between Rarău and Călimani, with Rarău having the highest concentrations for both elements (38.9 mg kg^{-1} and 0.351 mg kg^{-1}, respectively).

The Sr concentrations of the river and groundwater samples are quite low and range from 10 µg L^{-1} to 300 µg L^{-1}. The levels of Sr in the bioavailable soil fraction range from 0.4 mg kg^{-1} to 33.5 mg kg^{-1} relative to the weighed amounts. The highest level of Sr is found in the bioavailable fraction of the soil sample from Călimani 3. Consistently, the wood from the same location shows the highest Sr level among all wood samples, at 8.41 mg kg^{-1}. The lowest Sr level in the analyzed wood samples is 1.71 mg kg^{-1}.

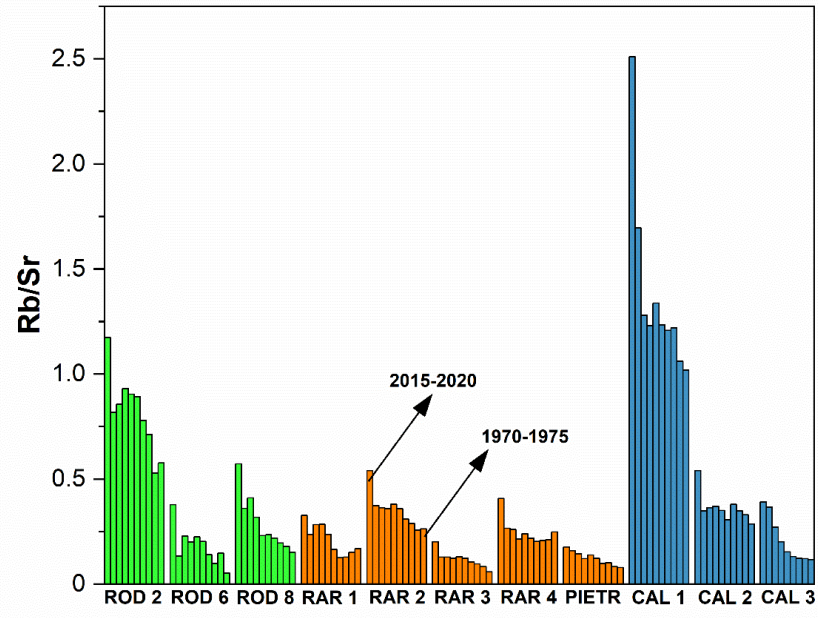

Figure 3.13: Rb/Sr ratio across wood samples (10 core segments per each site). Samples are numbered from 1 to 10, with segment 1 corresponding to the period 2015–2020, and segment 10 to the period 1970–1975.

Typically, an increase in macro-minerals across the sapwood is observed, due to their partial remobilization from older annual rings to the younger and more active parts of the wood (Levy et al., 1996). Our study confirms this in the case of K, but also Fe, Co, and Cr, which appear to be most concentrated in core segment 1 (2015-2020) and gradually decrease across the segments, reaching their lowest in core segment 10, at all study sites.

Rb levels followed the same trend as observed for K, reflecting their analogous chemical behavior. Any environmental change that enhances the availability of K, similarly, elevates the levels of Rb. Therefore, the presence and increase in concentrations of these elements in recent tree core samples reflect their shared uptake pathways and environmental influences. This trend was not consistent for Ca, Mg, and Na. Although observed at some sites, it was not a universal pattern.

Examining temporal variability is vital to determine whether results can be effectively applied in discriminant analysis, or if the variability in elemental content across core segments might pose challenges for such applications. It is crucial to consider these factors in any discriminant analysis to ensure that comparisons are not made between fundamentally different conditions. The accumulation and distribution of elements within tree rings, including whether they are more prevalent in earlywood or latewood, sapwood or heartwood, or various tree cell types, are influenced by multiple factors. These include climate and season conditions, ionic solubility and charge, pH, tree species and their uptake capacity, but also soil nutrient availability (Andrews et al., 2016; Meerts, 2002). This complexity is further highlighted by the limited data on the accumulation of elements such as Cd, Pb, and Zn in the earlywood of *Tipuana tipu* (Locosselli et al., 2018), and spatial distributions of Ba, Cu, Fe, Mn, Ni, and Pb on the wood surface, which reveal that they are neither homogeneously nor randomly distributed within tree rings (Amais et al., 2021).

Figure 3.13 shows that the first core segments (corresponding to the 2015-2020 period) of all sampled trees have the highest Rb/Sr ratio. There is a general trend of declining Rb/Sr ratio in wood cores 1 through 10, which suggests that the Sr isotope ratio should be measured in all 10 core segments from each site to assess possible variability over a 50-year period. Measuring the Sr isotope ratio in multiple segments provides a more comprehensive understanding of temporal changes and ensures the reliability of the wood's geochemical fingerprint over time.

Furthermore, the Rb/Sr ratio varies across sampling sites, influenced most probably by the underlying bedrock composition and not due to the distribution between sapwood or heartwood, as the trees in all areas were of the same species and age. Rb/Sr ratio in sediments has been suggested as an indicator of physical and chemical weathering intensity, showing that greater precipitation usually corresponds to a higher Rb/Sr ratio on decadal scales (Xu et al., 2010). This might be true in the case of the Călimani region, considering the fact that the Rb/Sr ratio is much higher in trees from site Călimani 1 (located at the altitude of 1640 m), compared to trees from sites Călimani 2 and 3 (at altitudes 1269 m and 1210 m, respectively).

Further, the site Călimani 1 is located close to the top of the mountain, directly facing the prevalent westerly winds, the main sources of moisture in the area, while Călimani 2 and 3 are sheltered on the eastern slopes of the mountains, thus providing further evidence for increased weathering at the higher altitude site (Călimani 1). Tree cover density was lowest at the high-altitude site and increased with decreasing altitude, supporting this hypothesis. The natural timberline in Călimani Mts. (~1700 m asl) remains well-preserved on steep, north-facing slopes where human activities such as grazing and wood cutting are minimal (Kern & Popa, 2008). Air temperature differences between the sites were minimal, averaging less than 0.8 °C between the lowest and highest altitudes. No significant difference in forest cover was observed between the Rarău and Rodna sites. In Rarău, however, soil thickness varied considerably between sites, being greatest at low altitudes and patchy at mid-altitudes, where limestone was exposed at the surface.

3.2.2 Strontium Isotope Ratio of Wood Core Segments

Table 3.3 shows an overview of $^{87}Sr/^{86}Sr$ ranges of wood samples in the studied regions. The $^{87}Sr/^{86}Sr$ values span a wide range from 0.70842 to 0.72667, with the minimum and maximum values observed for samples from Călimani and Rarău, respectively.

Table 3.3: $^{87}Sr/^{86}Sr$ isotope ratio of wood samples including statistical measures for each region: mean, median, minimum, maximum, and standard deviation.

Location	$^{87}Sr/^{86}Sr$				
	Mean	Median	Min.	Max.	SD
Rodna	0.71303	0.71182	0.70865	0.72276	0.00373
Rarău	0.70967	0.70956	0.70859	0.71150	0.00067
Călimani	0.70996	0.70978	0.70831	0.71209	0.00100

The results from the performed statistical tests suggest that the median ranks for each group are significantly different. Călimani tends to have lower Sr isotope ratio values compared to both Rarău and Rodna, and Rarău tends to have higher values compared to Rodna.

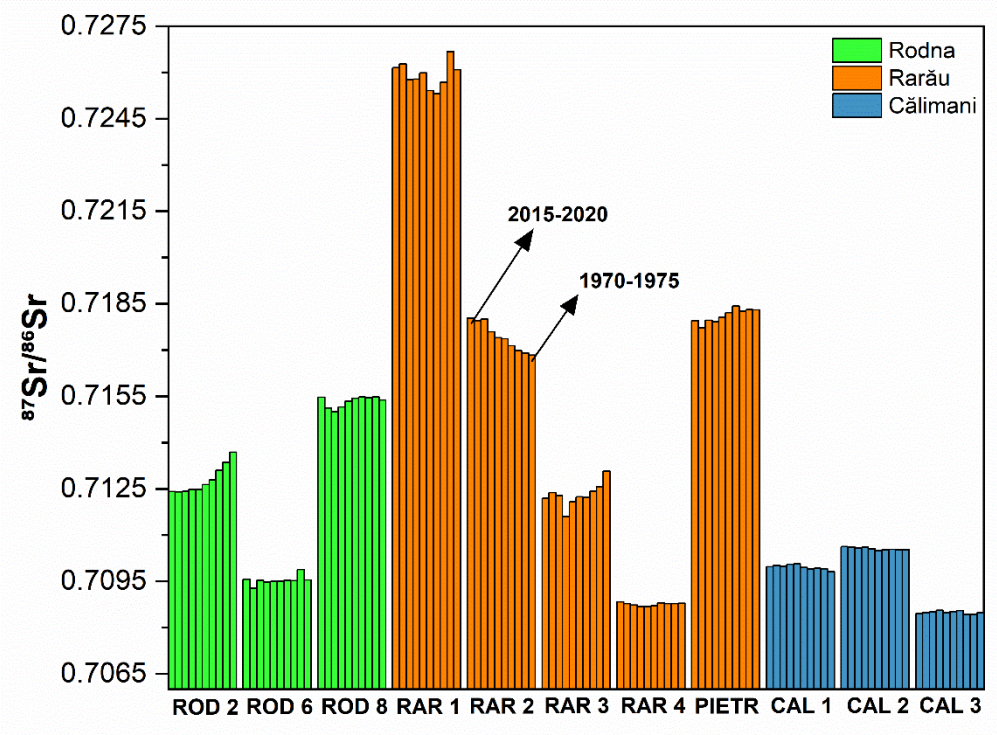

Figure 3.14: $^{87}Sr/^{86}Sr$ isotope ratio across wood samples (10 core segments per each site). Samples are numbered from 1 to 10, with segment 1 corresponding to the period 2015–2020, and segment 10 to the period 1970–1975.

Each bar on the histogram in Figure 3.14 represents Sr isotope ratio of one wood sample (one core segment), with a total of 10 bars (samples) corresponding to study site displayed on the x-axis. Based on annual rings, it is determined that each core segment corresponds to five years of tree growth, meaning that the 10 collected and analyzed samples from a single tree correspond to 50 years of a tree lifespan. By analyzing wood parts that cover a long period, it is possible to monitor possible changes in the chemical and isotopic composition that were induced by the changes in the environment like changes in the amount of precipitation, soil weathering rates, soil pH and/or CEC, etc. Since there was a decline of Rb/Sr ratio in wood cores 1–10 (2020–1970), as illustrated by Figure 3.13, it was needed to measure Sr isotope ratio in all of them. However, analyzing multiple core segments showed a high degree of within-tree $^{87}Sr/^{86}Sr$ ratio homogeneity. Previous studies also reported no significant differences among organs/tissues of the same tree (Aguzzoni et al., 2019). Moreover, while some studies demonstrated differences in the Sr isotope ratio of different species collected at the same location (Poszwa et al., 2004), there were some instances where different plant species showed similar foliar $^{87}Sr/^{86}Sr$ ratios (Choi et al., 2023). Since all studied tree samples are specimens of the same, typically deep-rooting species (Norway spruce), the plant physiology, i.e., its preferences for certain isotopes or forms of Sr over others can be neglected as a potential reason for intra-species variability in $^{87}Sr/^{86}Sr$ ratios (Burger & Lichtscheidl, 2019). Other factors need to be considered, such as the age of the plant, its growth rate, the season in which it was sampled, the fine root distribution, as well as the abundance of other species, and subsequently, belowground competition (Schmid, 2002). However, the mentioned intra-species variability might be due to different bedrock types. Not only was there variability in $^{87}Sr/^{86}Sr$ in trees from different areas, but also in different trees sampled at different sites within the same region. While the $^{87}Sr/^{86}Sr$ values within Călimani area are quite uniform, that is not the case for sampling sites in other regions: Rodna and Rarău. This variability could be attributed to differences in soil type and composition, including variations in soil carbonate content, depth, and moisture, as well as differences in topography, surrounding vegetation, and other environmental factors. Some of the sampling sites within Rarău region are located at the geological contact between two distinct rock bodies – limestones and sandstones/schists. Since soil geochemistry reflects major lithological trends, two soil samples were collected from Rarău 3, at approximately 5 m apart, on either side of a geological contact between schists and limestone. Expectedly, the Sr isotope ratio differed in these samples, both bulk and bioavailable fractions. The Sr isotope ratios were 0.70957 for the bioavailable fraction and 0.71248 for the bulk soil sample from the limestone area, while for the schist area, the ratios were 0.71082 for the bioavailable fraction and 0.72936 for the bulk soil sample. Water samples collected at this location – a spring fed from a wide marshy area and possibly on the lithological contact, and a river flowing on schist but with possible headwaters on limestone, have lower Sr isotope ratios than the analyzed soil samples. Furthermore, terrain elevation varies within studied areas (each sampling site was at a different altitude), meaning it is possible that other factors, such as differences in precipitation, temperature, erosion, and atmospheric circulation patterns also contribute to differences in Sr isotope ratio between sites at different altitudes (Hoogewerff et al., 2019; Nagavciuc et al., 2019; Snoeck et al., 2020). All these factors may facilitate variable rates of Sr dissolution from the soil and rocks, potentially leading to heterogeneity in Sr isotopic ratios even across similar bedrock compositions. Rainwater and other forms of precipitation can contain different Sr isotopes depending on the local atmospheric conditions. It bears mentioning that rainfall may be dominated by Sr originating from marine aerosols, even at inland sites situated 450 km from the nearest sea, although the effect of sea spray seems to be the highest within the first (10–20) km depending on the relief (Erban Kochergina et al., 2021; Frank, Frei, Moutafi, et al., 2021).

3.2.3 Correlation of $^{87}Sr/^{86}Sr$ Ratios in Wood and Corresponding Environmental Samples

Figure 3.15 shows the pairwise correlation of investigated proxies (wood, water, soil). There is a strong positive correlation between the Sr isotope ratio values of samples from all three matrices. However, it is important to bear in mind that only four river samples were collected. Results indicate that water (rivers $R^2 = 0.99$ and groundwaters $R^2 = 0.98$), as a source of Sr, exerts dominant control over $^{87}Sr/^{86}Sr$ ratio in trees. At the same time, they also demonstrate a close relationship between $^{87}Sr/^{86}Sr$ in bioavailable soil fraction and trees ($R^2 = 0.94$). These results are aligned with the study published by Choi et al. (2023), who elucidated the relationship between plants and soil using linear regression and obtained similar coefficient – adjusted $R^2 = 0.93$. This may be due to significantly different susceptibilities towards weathering, which impart a complex release pattern of soil-hosted Sr to the readily available, mobile Sr fractions. Biological processes make the Sr cycle within the soil-root system more complex, making soil profiles isotopically heterogeneous. Soils and plants are considered to be point samples and generally average Sr over a smaller area, but still reflect the Sr composition of ground and surface waters. Our recorded water Sr isotope signatures, ranging from 0.70820 to 0.72270, overlap with previously published data by Voerkelius et al. (2010). Their study investigated European natural mineral waters and had one sampling point in Romania, Eastern Carpathians, which corresponds to $^{87}Sr/^{86}Sr$ range of 0.70701–0.70900, but based on a spatial prediction, this whole area was assigned $^{87}Sr/^{86}Sr$ ratio values of 0.702–0.780.

In addition, Figure 3.15 displays a quite strong positive correlation between wood and bulk soil samples ($R^2 = 0.81$). Since rain is deposited on the soil surface, as opposed to releases from soil mineral weathering, the Sr isotopic ratio may form a depth gradient. Therefore, the depth of Sr uptake and root density profiles influence the $^{87}Sr/^{86}Sr$ of bioavailable Sr. Poszwa et al. (2004) explored the Sr cycle, and demonstrated that the $^{87}Sr/^{86}Sr$ ratio of bioavailable Sr generally increased in soils with depth, while also observing that the bulk topsoil $^{87}Sr/^{86}Sr$ ratio might be closer to the $^{87}Sr/^{86}Sr$ ratio of some deeper soil layers. The Sr signature of the analyzed trees is closer to that of the soil exchangeable Sr pool, which is supplied with Sr derived from both weathering of bulk soil minerals and atmospheric deposition. However, our results show that the Sr isotope ratio of the tree cores is in good agreement with the Sr ratio of the bulk soil, representing the local bedrock, which indicates that roots are reaching deeper soil horizons.

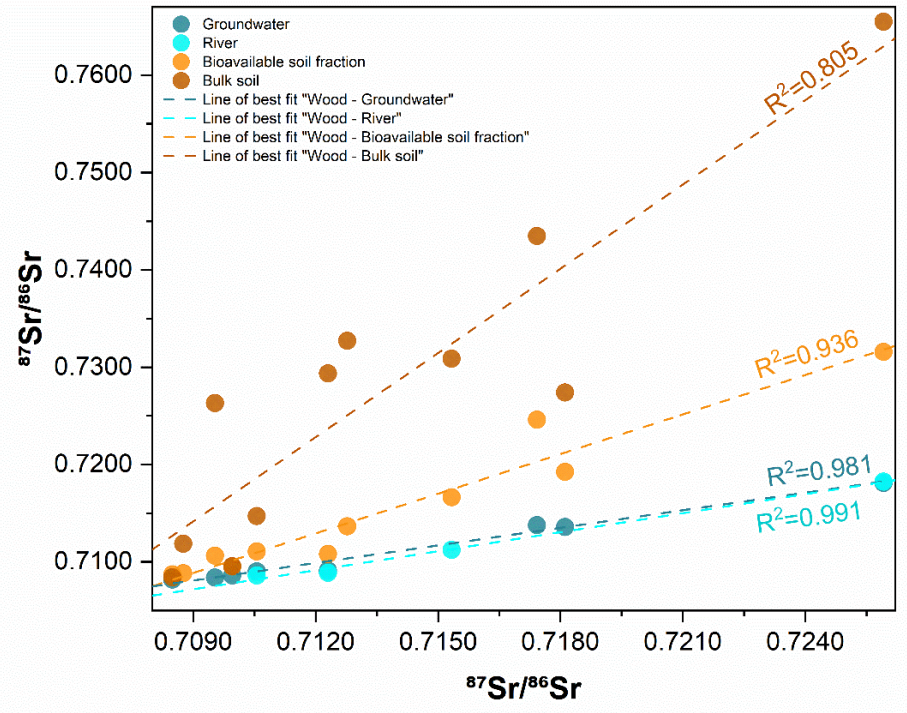

Figure 3.15: Correlation of $^{87}Sr/^{86}Sr$ ratio values of wood (x-axis) and bulk soil, bioavailable soil fraction, groundwater, and river samples (y-axis).

3.2.4 Contributions to Strontium Isotopic Composition of Norway Spruce Wood

Figure 3.16 illustrates Sr isotope ratio values of wood, river, groundwater, bioavailable fraction, and bulk soil samples from all investigated locations (a), and provides a summarized breakdown of these values by region (b). Evidently, the Sr isotopic composition of wood typically falls between the comparable Sr signatures in soil and water samples. The Sr isotope ratio of wood samples turns out to fall in the middle of these two values, as is the case for samples from locations Rarău 1 and Rarău 2, indicating that the two Sr sources most likely contributed the same amount to the Sr isotopic composition of wood. On the other hand, when the Sr isotope ratio values of bioavailable soil fraction and water samples are close to each other, or even overlap, while the Sr isotope ratio for the corresponding wood sample is relatively far from them, it is possible that other sources also had a great impact in forming the wood Sr signature. The graph shows that there are some variations between the $^{87}Sr/^{86}Sr$ ratios of groundwater and river waters, which are likely due to differences in the characteristics of lithological sources present in their catchments and aquifers (Nickolas et al., 2017). Boxplots confirm the existence of a tendency of plants to show slightly lower $^{87}Sr/^{86}Sr$ values compared to the respective bioavailable soil fractions, which probably derives from the assumption that Sr is taken up from deeper soil horizons (Figure 3.16a)).

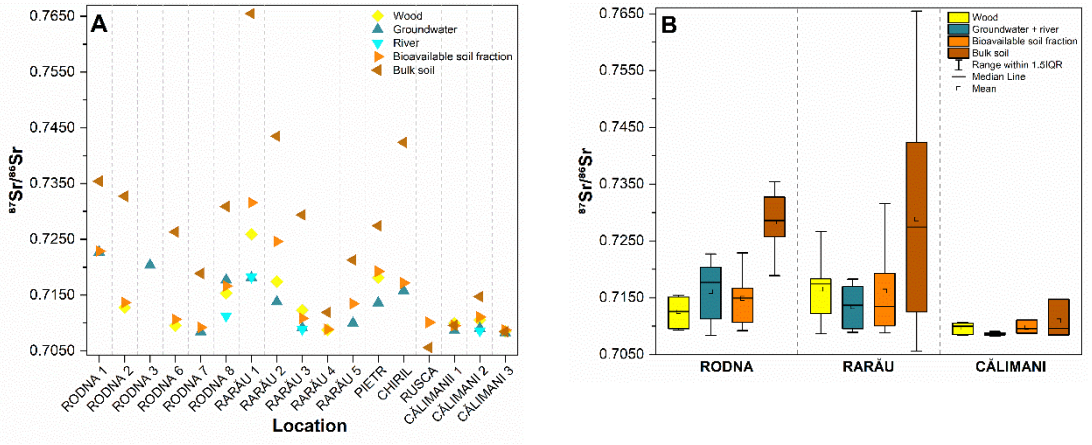

Figure 3.16: (a) Scatter plot representing the $^{87}Sr/^{86}Sr$ values for all samples across each study site, (b) Boxplots showing the distribution of $^{87}Sr/^{86}Sr$ values within each studied region, categorized by matrix.

Determining the most relevant Sr sources is important in archaeological studies, and their Sr concentrations, therefore, have a significant role (Frank et al., 2021). The diagrams plotting the $^{87}Sr/^{86}Sr$ values of investigated proxies against their respective inverse Sr concentration might be useful in revealing the source of the wood Sr signature. These diagrams suggest that environmental proxies sampled at sites across different areas share a similar contribution to the Sr isotopic composition of the wood samples. As shown in Figure 3.17a), most of the tree sites can be separated based on their Sr mass fractions and Sr isotope ratios. While Sr isotope ratio values in the cores of the trees from the same site are quite similar, that is not the case for the total Sr concentration. Figure 3.17b), c), and d) show no clear correlation between Sr concentrations and $^{87}Sr/^{86}Sr$ values of either proxy. Furthermore, there is no clear differentiation based on the geographical origin of the sample. However, it is still evident that wood, as well as water and bulk soil samples, have a very narrow range of the Sr isotope ratio values within the Călimani region, unlike the samples from the other two regions. In order to examine the mixing of different Sr sources and their influence on wood Sr isotopic signature, all samples were put together in Figure 3.18 which depicts the distribution of wood samples between soil and water samples. In addition, it is noticeable that the wood samples are “mixed” with the bioavailable soil fraction samples, indicating that it is a major contributor to the wood Sr signature. Although the correlation between the wood and water samples appears to be somewhat stronger (as shown in Figure 3.15) than that between the wood and bioavailable soil fraction, the Sr mass concentrations in water are substantially lower than in soil. This discrepancy explains why the bioavailable soil fraction is the predominant contributor to the wood’s Sr isotopic fingerprint. These findings are aligned with the results of previous studies in other regions (R. Frei et al., 2022). Correspondingly, Figure 3.18 confirms that other Sr sources, such as above-mentioned wet deposition, as well as dry deposition of local and foreign dust and potential anthropogenic Sr contamination mainly from agriculture probably play a minor role (little to no effect) in determining the wood isotope composition.

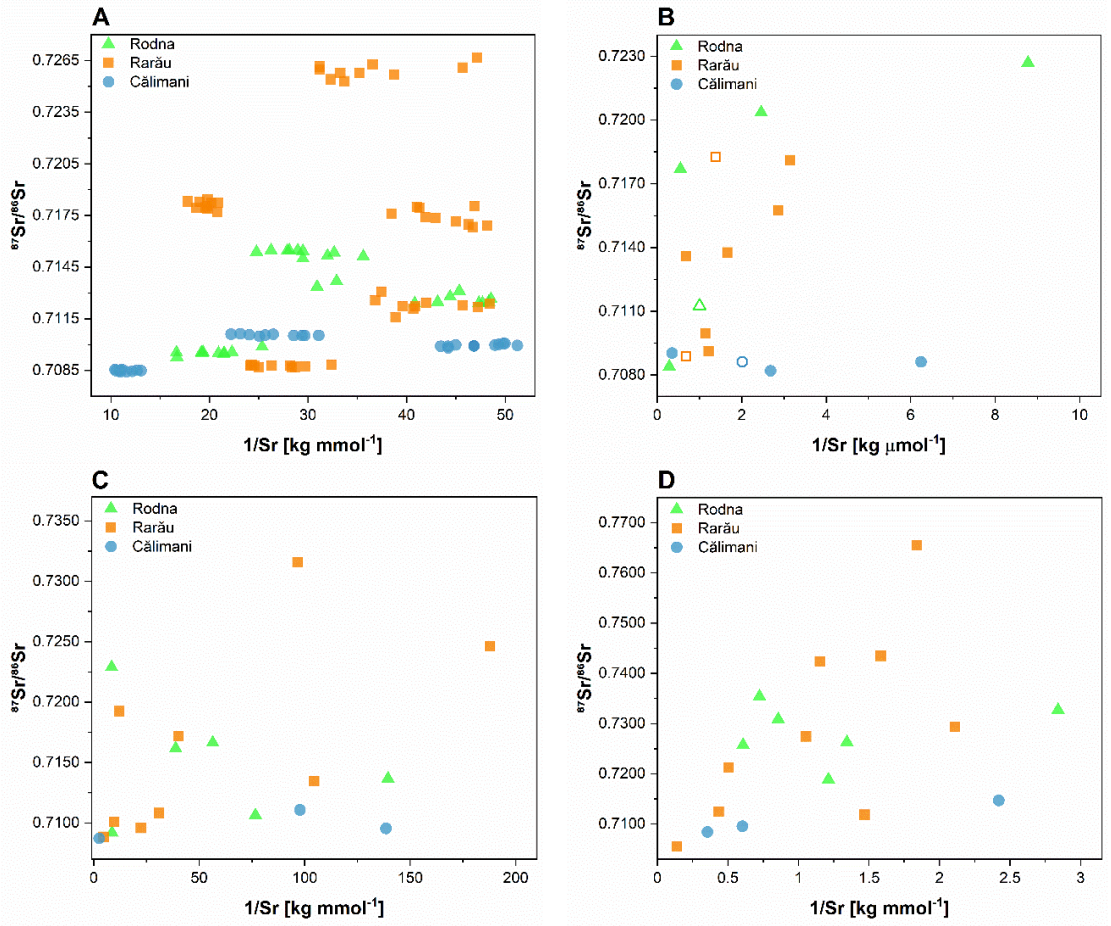

Figure 3.17: $^{87}Sr/^{86}Sr$ isotope ratio values of a) wood, b) water – groundwater (solid shapes) and river (empty shapes), c) bioavailable soil fraction, and d) bulk soil samples plotted against their respective inverse Sr concentrations.

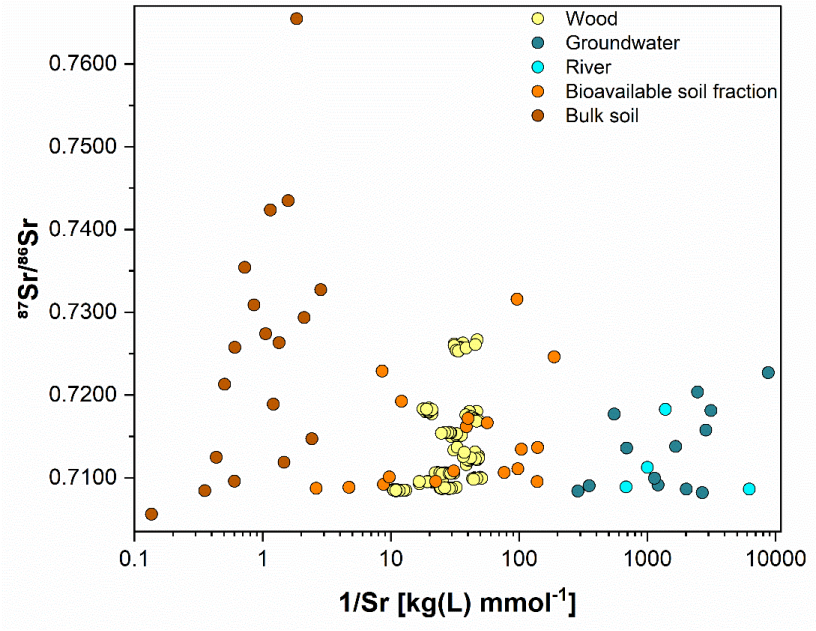

Figure 3.18: $^{87}Sr/^{86}Sr$ isotope ratio values of the samples plotted against their respective inverse Sr concentrations on a logarithmic scale. Concentrations are in mmol kg^{-1} for solids and mmol L^{-1} for water samples.

3.2.5 Principal Component Analysis: Exploratory Analysis for Geographic Differentiation in Wood Provenance Studies

We conducted a preliminary analysis to assess the feasibility of regional differentiation using Sr isotopic and multi-elemental analysis. Although the limited sample size constrains a more extensive investigation, this initial effort could serve as a foundational step toward achieving that goal. PCA was used on Sr isotopic and multi-elemental data derived from trees at 11 distinct locations across three regions to reduce the dimensionality of the data, identify patterns, and assess the potential for local differentiation based on the geochemical signatures. To ensure sample independence, necessary for effective PCA, averages rather than individual core segments were used as the data points for each study location. Before averaging, outliers in each variable were identified and removed. While this approach may not be the ideal solution, particularly given earlier discussions about the distribution of elements across different core segments, it still effectively captures comparable information for each study site. This consistency is ensured as all trees are of the same species, sampled in the same manner, and the tree rings analyzed correspond to the same period.

Given the limited sample size, it was crucial to limit the number of variables to prevent overfitting. Therefore, after conducting preliminary statistical tests and considering their theoretical relevance, only 10 variables were selected for the PCA. Since first two components explain a substantial portion of the variance (> 70 %), they were retained for visualization. Figure 3.19a) clearly illustrates that samples from Călimani and Rarău are well differentiated, whereas Rodna samples show considerable overlap, indicating less distinction. Additionally, the Călimani samples cluster closely together, aligning with the Sr isotope ratio analysis results shown in Figure 3.14, which indicate minimal variability within the Călimani region. In contrast, the biplot reveals a more scattered distribution among the Rodna and Rarău samples, suggesting greater variability within these regions.

This comparison underlines the usefulness of Sr isotopic composition as a tool for discriminating geographic origin. Figure 3.19b) depicts the relationship of each component with the original variables and the extent to which each variable contributes to the components. For example, elements such as Rb, K, and Mg are strongly associated with the Călimani samples, as demonstrated by their placement in the biplot. Additionally, variables like Cr, Fe, and the $^{87}Sr/^{86}Sr$ isotope ratio appear to influence the variance explained by both principal components. Their concentrations are key to differentiating the samples across both axes, in contrast to elements like Co and Na.

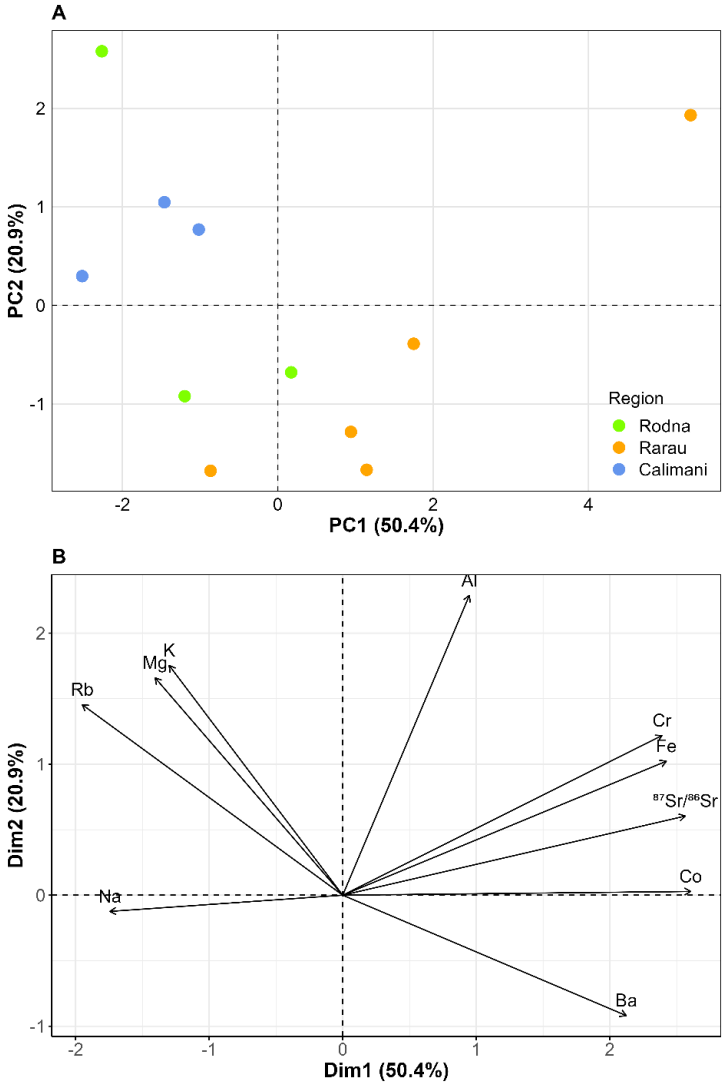

Figure 3.19: Principal component analysis (PCA) of wood samples from Rodna, Rarău, and Călimani Mountains: a) discriminant function score plot, and b) discriminant loading plot, showing correlations between initial variables and the discriminant functions.

3.2.6 Spatial Distribution of $^{87}Sr/^{86}Sr$ Ratio Values Across Romania

To investigate the spatial distribution of Sr isotope ratio values across Romania, we analyzed groundwater samples from the Eastern Carpathians (n=13) along with 187 additional groundwater samples from six other regions (Apuseni Mountains (n=11), Banat (n=18), Cluj-Neamț (n=56), NW Romania (n=10), Târnavele (n=27), and the Southern

Carpathians (n=65)). Sampling points are concentrated primarily in the mountainous areas of the country. Before moving towards building an isoscape, we first examined the general distribution of $^{87}Sr/^{86}Sr$ ratios, focusing on how they vary across different geographical regions and geological units. Figure 3.20 illustrates both the sample distribution and the lithology of Romania, with special emphasis on areas where sampling points are densely concentrated.

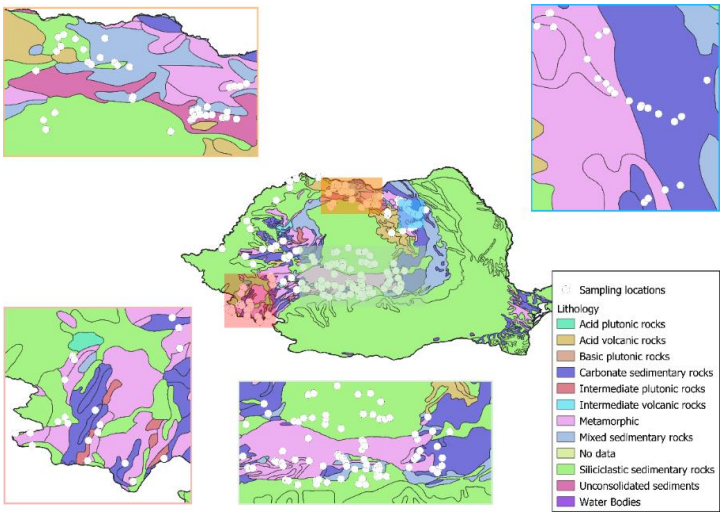

Figure 3.20: Sampling locations presetend on the lithological map of Romania.

Figure 3.21 provides an overview of Sr isotope ratio values for each lithological unit. The largest number of samples corresponds to siliciclastic sedimentary rock formations (n=66). For most lithological units, the median of the distribution is well-defined. However, for metamorphic rocks (n=54), the Sr isotope ratio values show a wide distribution, scattered along the x-axis, with no clearly discernible median. The graph also shows that samples from environments characterized by acid volcanic rocks tend to exhibit lower Sr isotope ratios compared to other lithological units.

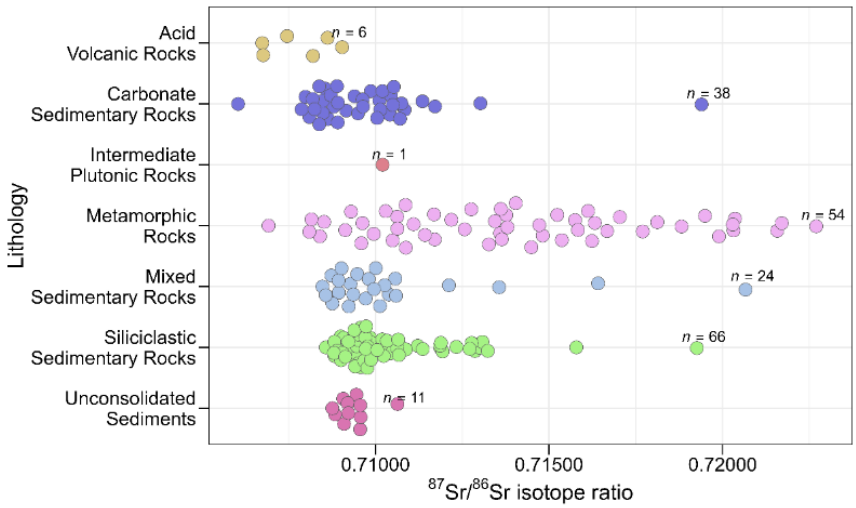

Figure 3.21: $^{87}Sr/^{86}Sr$ isotope ratio values of groundwater samples classified by lithological units.

Figure 3.22 presents the distribution of Sr isotope ratios using kernel density and rug plots. The KDE, with bandwidth determined by Scott's thumb rule, provides a continuous curve representing the probability density of Sr isotope ratios, while the rug plot indicates individual data points along the x-axis. The minimum measured Sr isotope ratio is 0.70604 (Apuseni Mts.), and the maximum is 0.72270 (Eastern Carpathians). The KDE peaks show that Sr isotope ratios are concentrated around 0.709. However, for all study regions except Cluj-Neamț and Târnavele, we observe multiple peaks. These multimodal distributions suggest a heterogeneous spread of Sr isotope ratio values across samples within a region. A wider distribution implies a broader range of $^{87}Sr/^{86}Sr$ values. Examining the rug plot, it is evident that the cluster formed between 0.708 and 0.711 represents a region with a higher number of samples. We also observe some gaps in the rug plot, particularly at very low or very high values, which could indicate regions with fewer samples or potential outliers in Sr isotope ratios that deviate from the main distribution. Compared to other regions, Cluj-Neamț and Târnavele show a much tighter distribution, meaning there is less variability in the Sr isotope ratios of the samples from these areas. The Eastern Carpathians (black line) display the broadest and flattest distribution compared to all other regions, with no sharp peaks. This suggests significant variability in Sr isotope ratios and reflects the geological diversity of the region. The broad distribution implies contributions from multiple geological sources, leading to such a wide range of Sr isotope values. This once again highlights possible large variations in Sr isotope ratios even within small areas and emphasizes the importance of the results obtained in the Norway spruce study focused on the Eastern Carpathians region.

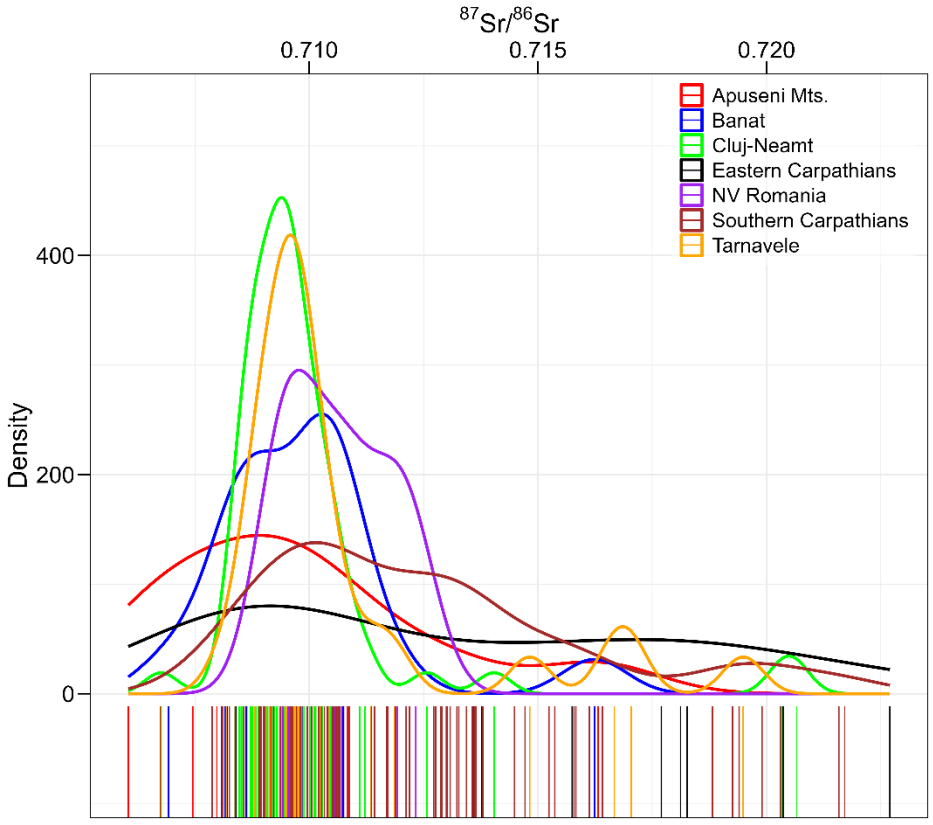

Figure 3.22: Distribution of Sr isotope ratios across study regions of Romania using Kernel density and rug plots.

Figure 3.23 confirms that the Cluj-Neamț region shows the least variability in Sr isotope ratio values compared to other regions. A Kruskal-Wallis test ($\alpha = 0.05$) was conducted to determine if there were statistically significant differences in the medians of Sr isotope ratios among the regions. The results indicated a significant difference among the regions ($p < 0.05$), prompting a post-hoc analysis using Dunn's test to pinpoint where these differences occurred. Most pairwise comparisons did not reveal significant differences, except for the Southern Carpathians, which differed significantly from the Apuseni Mts., Banat, and Cluj-Neamț regions. Although Figure 3.23 suggests that the mean Sr isotope ratio in the Eastern Carpathians differs from most other regions, the statistical test did not detect significant differences between the Eastern Carpathians and the other regions.

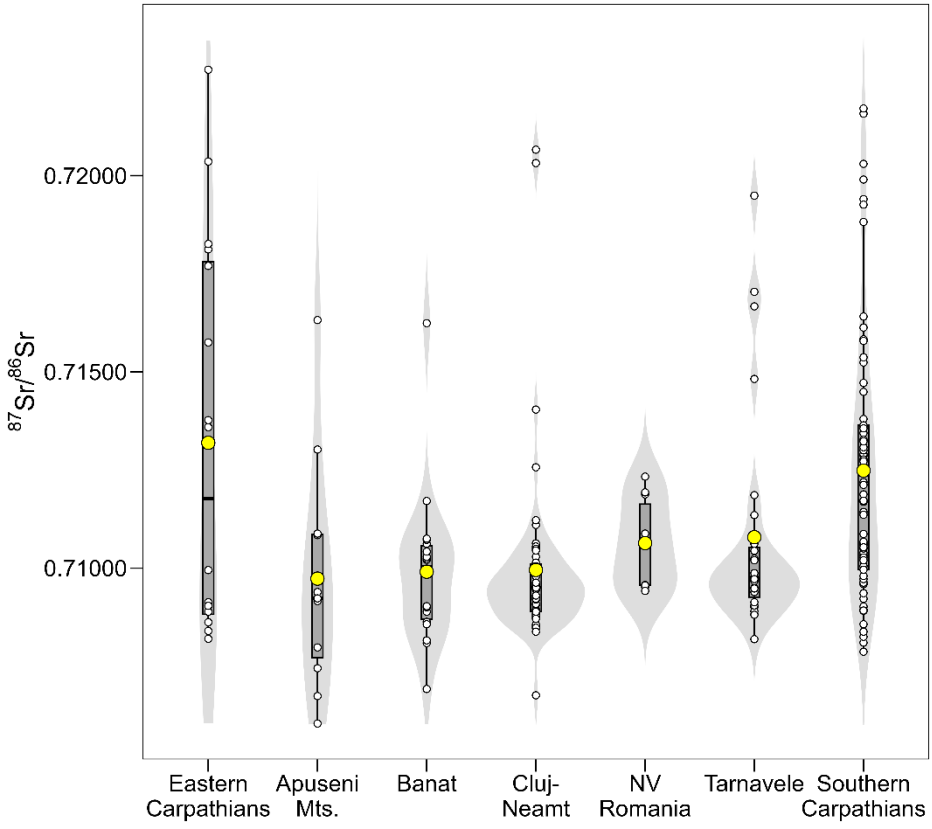

Figure 3.23: Boxplots and violin plots showing Sr isotope ratio values for each study region. Yellow dots are mean values.

In comparison to the study by Török et al. (2023), which reported $^{87}Sr/^{86}Sr$ isotope ratios ranging from 0.7038 to 0.7149 for the Apuseni Mts., and 0.7042 to 0.7158 for the Southern Carpathians, our study shows higher ranges for both regions. In our study, the Apuseni Mts. exhibited a range of $^{87}Sr/^{86}Sr$ ratios from 0.70604 to 0.71632, while the Southern Carpathians showed a broader range from 0.70787 to 0.72171.

Apart from the Apuseni Mts. and Southern Carpathians, which were studied by Török et al. (2023) and Harris et al. (2013), there is, to the best of our knowledge, no Sr isotopic data available for the rest of Romania. This makes the current study a significant contribution, as it provides a reference database that can serve as a foundation for future research. However, there are some limitations in the applicability of these results.

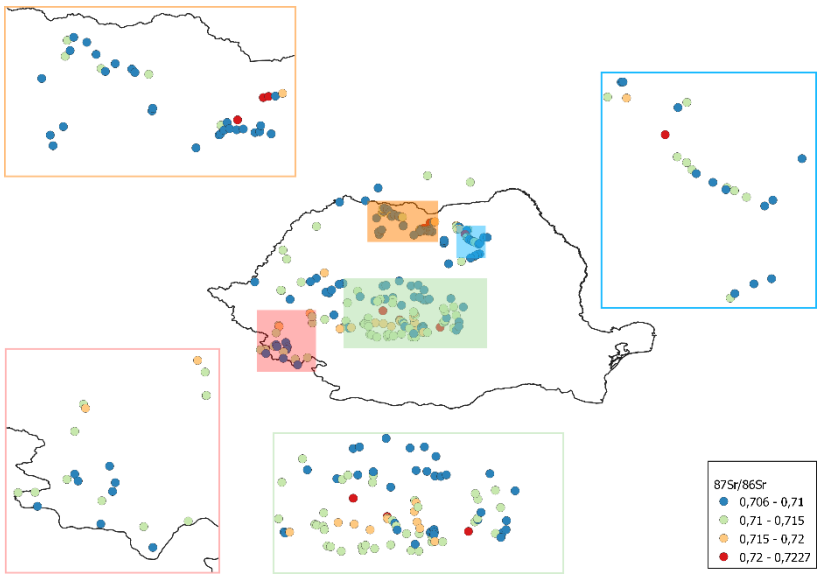

Figure 3.24: Spatial distribution of $^{87}Sr/^{86}Sr$ isotope ratios in groundwater samples from Romania.

As discussed in Paragraph 3.1.6. there are ongoing debates about whether groundwater is an appropriate proxy for bioavailable Sr isotope ratio isoscapes. Additionally, while groundwater Sr isotope ratios are not expected to exhibit large seasonal fluctuations, some variation does exist. Since our samples were collected across various seasons in 2021, using these values to construct a comprehensive isoscape might not be ideal. For this reason, the current study focused on investigating the general distribution of Sr isotope ratios across Romania rather than building an isoscape. The study covered mostly mountainous areas, but there is room for improvement in the database, particularly in the eastern parts of the country, which remain largely unsampled. As seen in Figure 3.24, no clear geographic trends in Sr isotope ratios are immediately apparent. However, it is evident that high Sr isotope ratios ($^{87}Sr/^{86}Sr > 0.72$) are rare, though they are present in all regions except Banat. The majority of the values fall within the blue and green range (0.706–0.715) indicating a relatively consistent Sr isotope signature across the studied regions.

Chapter 4

Conclusions

This dissertation merges two projects with different aims but based on the application of the same methodology: Sr isotope ratio and multi-element analysis. This approach underlines the versatility of Sr isotopic analysis. The two studies, aside from their purposes and hypotheses, differed in several ways, particularly the sources of Sr influencing the Sr isotopic composition of the materials of interest (cheese and wood). Furthermore, the studies revealed that the range of Sr isotope ratio values can vary even within small areas, complicating the application of this ratio in provenance studies. For instance, Naxos, the Greek island, showed high uniformity in Sr isotope ranges, mostly concentrated around the Sr isotope ratio of modern seawater. Conversely, the Eastern Carpathians in Romania, also a small region, exhibited a wide range of values due to high geological variability.

Regarding the proposed hypotheses, several conclusions were drawn. The study on PDO Graviera Naxos cheese represents a significant advancement in the geochemical authentication of dairy products, specifically focusing on the complex matrix of blended milk cheese such as PDO Graviera Naxos. Using Sr isotopic and multi-elemental analysis for geographic discrimination remains challenging due to several limitations. Firstly, the Sr isotopic composition of milk varies throughout the seasons, and secondly, sea salt significantly contributes to the Sr isotopic composition of cheese, complicating origin determination. Correlation studies showed strong positive correlations between milk and feed/milk and water samples from the same farms. However, since PDO Graviera Naxos is produced from blends of these milks, it was not possible to correlate the cheese directly with specific farm samples. Milk samples correlated with feed samples' Sr isotope ratios only in winter, and with water samples' Sr isotope ratios only in summer, due to the seasonal variations in the animals' diet and water intake. These variations make it challenging to determine a consistent Sr isotope ratio fingerprint for PDO Graviera Naxos cheese.

Using stable isotope mixing models, the contributions of diverse sources – milk, sea salt, and rennet – to the Sr isotopic composition of cheese were dissected. Sea salt, influenced by local environmental factors, emerged as a predominant contributor to the Sr isotopic signature of cheese. However, the close isotopic ratios between different sources and seasonal variations pose challenges in distinctly delineating their contributions. This difficulty points to the potential limitations of SIMMs when sources share similar isotopic signatures. Additionally, seasonal variations significantly impact the Sr isotopic composition in milk, suggesting that environmental factors like diet changes and sea spray may mask local isotopic signals, further complicating source attribution.

A preliminary isoscape for Naxos island was constructed, representing the first isoscape for this part of Greece. Other isoscapes focused on Europe do not provide high enough resolution to determine the range of Sr isotope ratios for the island. Despite its usefulness, some parts of the island lack sampling sites, necessitating additional sampling to enhance

the map's reliability as a reference dataset. This preliminary assessment of $^{87}Sr/^{86}Sr$ variation across Naxos is an initial step toward developing a comprehensive baseline map of the island that includes only bioavailable $^{87}Sr/^{86}Sr$ values. With more bioavailable $^{87}Sr/^{86}Sr$ data and improved spatial algorithms, more accurate geo-provenancing of isotope values for forensic and archaeological applications can be achieved.

The second research project has documented the Sr isotopic and multi-elemental signatures of Norway spruce trees in the Eastern Carpathians, Romania, specifically in the Rodna, Rarău, and Călimani Mountains. Alongside these analyses, corresponding soil, groundwater, and river samples were also examined. This research illuminates the previously uncharted terrain of bioavailable $^{87}Sr/^{86}Sr$ ratios in Romanian ecosystems, establishing a foundational basis for the development of regional isoscapes. The study demonstrates the direct transmission of unique geochemical signatures from the local environment to the wood, emphasizing the potential of Sr isotopic and multi-elemental analysis as a promising method for verifying the provenance of timber products.

In line with the set objectives, this study developed site-specific Sr isotopic and multi-elemental fingerprints for the Eastern Carpathians, Romania, providing a valuable tool for differentiating timber origins within this region. Despite the relatively small geographical area, the Sr isotope ratios exhibited a wide range, underlining their utility for local discrimination studies. By examining wood core segments corresponding to the last 50 years of growth, variations in both elemental distribution and Sr isotope ratios were observed. While certain elements, such as K and Rb, showed trends of peaking in the most recent core segments and then declining, the Sr isotope ratio exhibited negligible variability over time.

Principal component analysis of our dataset managed to differentiate trees from the Călimani and Rarău areas, primarily due to the concentrations of K, Mg, and Rb. However, we acknowledge that this approach alone is insufficient for comprehensive discrimination due to the limited number of studied sites. Our findings emphasize the need for caution in using this approach for discriminant analysis. Temporal differences observed in the elemental composition suggest that it is crucial to use comparable information for such analyses to avoid drawing inaccurate conclusions.

Amidst the pressing challenge of illegal logging in Romania, the implications of these findings extend far beyond the academic sphere, paving the way for more stringent controls on wood sourcing. This project also brings novelty by focusing on the temporal variability of Sr isotopic and elemental composition over the past 50 years (1970-2020), assessing whether the Sr isotopic and elemental fingerprint of trees could be used in provenance tracing studies. This study expands beyond the previously discussed Eastern Carpathians and is the first to include such an extensive collection of groundwater samples from various regions across Romania for Sr isotope ratio analysis, revealing values ranging from 0.70604 to 0.72270. Consequently, it provides the first spatial distribution data of Sr isotope ratios across the entire country, establishing a valuable reference database for future provenance studies. Although the results are highly informative, further refinement using advanced kriging models is needed to construct precise isoscapes, enhancing their usefulness as a reference for future research.

Future research should aim to refine the application of SIMMs by incorporating additional complementary techniques that can enhance the resolution of isotopic distinctions between sources. Investigating the influence of environmental and processing factors in greater detail will also be crucial, involving a broader range of environmental conditions and processing variables. Ultimately, the goal is to develop a more robust methodological framework that can reliably authenticate the geographical origins of complex dairy products like Graviera Naxos cheese, thereby supporting the protection of PDO products and ensuring product integrity for consumers. For the Eastern Carpathians

project, more extensive sampling is necessary to statistically differentiate timber-producing areas. Furthermore, using Laser Ablation (LA)-MC-ICP-MS for analyzing solid samples, like wood, will allow high throughput, limited sample preparation, and sufficient analytical precision. This method will help develop large datasets and enable a better understanding of the distribution of Sr isotope ratios across different tree rings and cell types. In conclusion, the combined application of Sr isotope ratio and multi-element analysis has shown promise in both the geochemical authentication of dairy products and wood provenance studies. However, continued advancements in analytical techniques and expanded sampling frameworks are essential to overcome existing limitations and enhance the reliability of these methods.

Appendix A

Supplementary Information

A.1 Obtained and Certified Values for Elements' Mass Fractions in Analyzed CRMs

Table A.1: Obtained and certified values for elements' mass fractions in IAEA 153 material.

CRM material	Value	$^{87}Sr/^{86}Sr$	Cu	Fe	Mg	Mn
IAEA 153 (Milk powder)	Obtained	0.70834 ± 0.00003	0.530 ± 0.0836	2.44 ± 0.439	1088 ± 8.49	0.194 ± 0.034
	Certified	0.708289 ± 0.000004*	0.57	2.53	1060	0.19
	95% Confidence interval	/	0.38 – 0.78	1.66 – 3.47	1000 – 1159	0.12 – 0.26
	Value	Mo	Na	Rb	Sr	Zn
	Obtained	0.275 ± 0.008	4129 ± 39.8	14.15 ± 0.525	4.05 ± 0.383	38.79 ± 0.376
	Certified	0.31	4180	14.03	4.09	39.56
	95% Confidence interval	0.09 – 0.60	3870 – 4440	12.27 – 16.20	3.49 – 4.73	37.66 – 41.23

*The $^{87}Sr/^{86}Sr$ isotope ratio value is not certified, it was reported by Gregorčič et al. (2021).

Table A.2: Obtained and certified values for elements' mass fractions in ERM – CC141 material.

CRM material	Value	$^{87}Sr/^{86}Sr$	As	Cd	Co	Cr
ERM – CC141 (Loam soil)	Obtained	0.72738 ± 0.00006	9.35 ± 0.585	0.354 ± 0.0311	8.11 ± 0.232	79.4 ± 0.176
	Certified	0.7291 ± 0.0014*	9.9 ± 1.5	0.35 ± 0.05	8.5 ± 0.50	86 ± 8
	Value	Cu	Mn	Ni	Pb	Zn
	Obtained	13.4 ± 1.33	450 ± 4.59	24.8 ± 0.405	42.7 ± 1.01	58.5 ± 2.60
	Certified	14.4 ± 1.4	464 ± 18	26.4 ± 2.4	41 ± 4	57 ± 4

*The $^{87}Sr/^{86}Sr$ isotope ratio value is not certified, it was reported by Pallavicini et al. (2018).

Table A.3: Obtained and certified values for elements' mass fractions in NIST SRM1573a material.

CRM material	Value	$^{87}Sr/^{86}Sr$	Ag	Al	As	B
NIST SRM1573a (Tomato leaves)	Obtained	0.71016 ± 0.00011	0.019 ± 0.0012	598.7 ± 29.4	0.1143 ± 0.018	32.81 ± 1.59
	Certified	0.71008 ± 0.00003*	0.017	598.4 ± 7.1	0.1126 ± 0.0024	33.13 ± 0.42
	Value	Ba	Ca	Cd	Cr	Co
	Obtained	62.2 ± 1.49	50405 ± 411	1.514 ± 0.127	1.959 ± 0.108	0.579 ± 0.0286

Certified	63	50450 ± 550	1.541 ± 0.027	1.988 ± 0.034	0.5773 ± 0.0071
Value	Cu	Fe	Mg	Mn	Mo
Obtained	4.67 ± 0.167	368.6 ± 5.26	11321 ± 220	241.2 ± 11.9	0.46 ± 0.053
Certified	4.70 ± 0.14	367.5 ± 4.3	12000	246.3 ± 7.1	0.46
Value	Ni	K	Rb	Sb	Se
Obtained	1.563 ± 0.141	26685 ± 119	14.85 ± 0.799	0.0614 ± 0.0038	0.0531 ± 0.0086
Certified	1.582 ± 0.041	26760 ± 480	14.83 ± 0.31	0.0619 ± 0.0032	0.0543 ± 0.0020
Value	Sr	Na	V	U	Zn
Obtained	83.4 ± 5.45	133.3 ± 19.6	0.814 ± 0.103	0.035 ± 0.008	31.28 ± 1.38
Certified	85	136.1 ± 3.7	0.835 ± 0.034	0.035	30.94 ± 0.55

*The $^{87}Sr/^{86}Sr$ isotope ratio value is not certified, it was reported in GeoReM database (last accessed online on 16.7.2024).

A.2 Content of Selected Elements in Samples from Naxos, Greece

Table A.4: $^{87}Sr/^{86}Sr$ isotope ratios and concentrations expressed in µg L^{-1} of selected elements with SDs in water samples from Naxos, Greece.

Sample code	$^{87}Sr/^{86}Sr$	As	Cd	Pb	Rb	Sr	Zn
water#51	0.70906 ± 0.00002	0.199 ± 3.79	<LOD	0.206 ± 1.36	4.68 ± 0.762	426.0 ± 1.69	93.3 ± 1.44
water#52	0.70918 ± 0.00002	0.280 ± 0.086	<LOD	0.0162 ± 2.31	5.13 ± 2.05	547.0 ± 1.14	9.71 ± 1.81
water#53	0.70909 ± 0.00002	0.167 ± 1.60	<LOD	<LOD	3.28 ± 2.37	366.0 ± 0.635	1.77 ± 5.66
water#54	0.71139 ± 0.00002	0.137 ± 4.92	<LOD	0.0229 ± 1.24	2.14 ± 1.86	414.0 ± 0.915	16.7 ± 1.28
water#55	0.71066 ± 0.00002	0.071 ± 6.95	<LOD	0.0171 ± 1.45	20.2 ± 0.159	2484.0 ± 0.235	6.30 ± 1.94
water#56	0.70967 ± 0.00002	0.213 ± 6.27	<LOD	0.0306 ± 5.01	1.44 ± 5.10	330.0 ± 0.671	1.68 ± 3.96
water#57	0.70950 ± 0.00002	0.259 ± 4.29	<LOD	0.0416 ± 5.22	1.00 ± 1.87	310.0 ± 0.561	2.83 ± 2.55
water#58	0.70930 ± 0.00002	0.431 ± 1.13	<LOD	0.082 ± 2.98	1.10 ± 2.61	251.0 ± 0.747	17.8 ± 1.40
water#59	0.70984 ± 0.00002	0.307 ± 1.91	<LOD	<LOD	0.432 ± 1.70	380.0 ± 1.56	0.310 ± 5.82
water#60	0.70973 ± 0.00002	0.258 ± 5.57	<LOD	<LOD	1.81 ± 2.67	360.0 ± 0.450	6.85 ± 1.48
water#61	0.70831 ± 0.00002	0.783 ± 1.88	<LOD	<LOD	3.12 ± 1.97	571.0 ± 0.236	0.559 ± 6.82
water#62	0.71021 ± 0.00002	0.200 ± 6.81	<LOD	1.17 ± 3.22	1.20 ± 1.87	211.0 ± 0.805	2.61 ± 2.73
water#63	0.71003 ± 0.00002	0.873 ± 2.67	<LOD	0.0184 ± 1.01	0.488 ± 2.22	285.0 ± 0.780	0.645 ± 0.638
water#65	0.71209 ± 0.00002	0.251 ± 4.82	<LOD	<LOD	2.02 ± 0.457	170.0 ± 0.457	0.426 ± 6.31
water#66	0.71013 ± 0.00002	0.350 ± 4.81	<LOD	<LOD	0.244 ± 2.91	103.0 ± 1.36	<LOD
water#67	0.71190 ± 0.00002	0.496 ± 4.57	<LOD	<LOD	0.548 ± 5.68	117.0 ± 0.525	0.434 ± 1.28
water#68	0.70928 ± 0.00002	0.262 ± 1.77	<LOD	<LOD	0.792 ± 2.66	111.0 ± 1.37	1.53 ± 0.612
water#69	0.70994 ± 0.00002	0.123 ± 5.07	<LOD	0.0901 ± 2.89	0.776 ± 2.39	162.0 ± 0.334	1.20 ± 2.63

*LODs for Cd, Pb, and Zn are 0.0052, 0.0039, and 0.0268, respectively.

Table A.5: $^{87}Sr/^{86}Sr$ isotope ratios and concentrations expressed in mg kg^{-1} of selected elements with SDs in bulk soil samples from Naxos, Greece.

Sample code	$^{87}Sr/^{86}Sr$	As	Cd	Pb	Rb	Sr	Zn
soil#1	0.71075 ± 0.00003	4.8 ± 0.551	<LOD	44.3 ± 2.53	128.3 ± 1.15	345.9 ± 1.54	139.9 ± 3.14
soil#3	0.71083 ± 0.00003	3.28 ± 0.526	<LOD	44.1 ± 5.96	61.9 ± 2.64	241.5 ± 1.81	150.5 ± 2.06
soil#6	0.71166 ± 0.00003	4.11 ± 0.588	<LOD	33.2 ± 0.832	111.8 ± 0.877	182.6 ± 2.58	146.1 ± 5.34
soil#7	0.71285 ± 0.00003	7.80 ± 1.24	0.0639 ± 0.0044	34.4 ± 1.34	64.3 ± 1.08	168.3 ± 1.82	104.5 ± 0.43
soil#9	0.71116 ± 0.00003	6.28 ± 0.645	0.132 ± 0.0588	58.6 ± 4.60	97.0 ± 0.756	207.8 ± 1.59	219.7 ± 7.16
soil#14	0.71110 ± 0.00003	3.77 ± 0.668	<LOD	44.8 ± 3.44	85.1 ± 2.31	234.0 ± 3.06	130.1 ± 4.49
soil#16	0.71197 ± 0.00003	8.20 ± 0.685	<LOD	28.3 ± 2.87	53.3 ± 0.240	155.4 ± 0.677	85.9 ± 2.65
soil#17	0.71069 ± 0.00003	9.32 ± 1.17	<LOD	27.1 ± 1.08	74.9 ± 1.76	189.3 ± 1.65	143.4 ± 23.4

Sample code	$^{87}Sr/^{86}Sr$	As	Cd	Pb	Rb	Sr	Zn
soil#19	0.70865 ± 0.00003	4.32 ± 0.55	0.111 ± 0.0108	14.8 ± 1.76	23.1 ± 0.346	150.6 ± 1.30	75.7 ± 4.63
soil#21	0.71207 ± 0.00003	7.36 ± 0.56	0.534 ± 0.0453	31.8 ± 2.76	48.4 ± 0.710	100.1 ± 1.65	118.2 ± 4.60
soil#26	0.71544 ± 0.00003	7.73 ± 1.75	<LOD	35.5 ± 1.33	70.8 ± 0.227	110.8 ± 2.04	130.4 ± 4.69
soil#28	0.71238 ± 0.00003	8.75 ± 0.474	<LOD	18.0 ± 0.948	60.2 ± 1.31	118.6 ± 1.53	76.0 ± 0.82
soil#32	0.72019 ± 0.00003	6.48 ± 0.208	<LOD	38.2 ± 1.34	76.4 ± 1.26	89.1 ± 0.387	59.0 ± 14.3
soil#36	0.71060 ± 0.00003	3.07 ± 0.449	<LOD	21.8 ± 0.455	35.8 ± 0.160	110.5 ± 0.856	102.1 ± 2.23
soil#37	0.72276 ± 0.00003	42.5 ± 1.74	0.142 ± 0.0092	38.2 ± 3.58	31.6 ± 0.190	77.7 ± 1.55	116.0 ± 1.16
soil#40	0.71540 ± 0.00003	13.0 ± 0.728	0.672 ± 0.0128	40.1 ± 3.91	79.5 ± 0.159	80.4 ± 1.21	106.9 ± 1.07

*LOD for Cd is 0.0383.

Table A.6: $^{87}Sr/^{86}Sr$ isotope ratios and concentrations expressed in mg kg^{-1} of selected elements with SDs in bioavailable soil fraction samples from Naxos, Greece.

Sample code	$^{87}Sr/^{86}Sr$	As	Cd	Pb	Rb	Sr	Zn
soil#1	0.70930 ± 0.00003	0.0146 ± 0.0016	0.0010 ± 0.0001	0.0037 ± 0.0003	0.714 ± 0.0043	8.24 ± 0.0906	0.132 ± 0.0053
soil#3	0.70940 ± 0.00003	0.0044 ± 0.0006	0.0010 ± 0.00004	0.0031 ± 0.0001	1.69 ± 0.0220	6.47 ± 0.0259	0.200 ± 0.0056
soil#6	0.70943 ± 0.00003	0.0333 ± 0.0002	0.0008 ± 0.00004	0.0011 ± 0.0001	2.04 ± 0.0163	3.97 ± 0.0397	0.0389 ± 0.0054
soil#7	0.70859 ± 0.00003	0.0565 ± 0.0014	0.0003 ± 0.00004	0.0004 ± 0.0001	0.385 ± 0.0038	5.75 ± 0.0287	0.0105 ± 0.0044
soil#9	0.70935 ± 0.00003	0.0345 ± 0.0007	0.0010 ± 0.0001	0.0007 ± 0.00003	1.66 ± 0.0100	5.86 ± 0.0879	0.0299 ± 0.0028
soil#14	0.70954 ± 0.00003	0.0055 ± 0.0003	0.0012 ± 0.0001	0.0015 ± 0.0001	0.845 ± 0.0059	9.63 ± 0.0770	0.144 ± 0.0073
soil#16	0.70958 ± 0.00003	0.0046 ± 0.0003	0.0005 ± 0.00002	0.0001 ± 0.0001	0.0600 ± 0.0019	1.81 ± 0.0109	<LOD
soil#17	0.71060 ± 0.00003	0.0128 ± 0.0003	0.0007 ± 0.00003	0.0006 ± 0.0001	0.0982 ± 0.0019	18.8 ± 0.150	0.0126 ± 0.0020
soil#19	0.70966 ± 0.00003	0.0319 ± 0.0004	0.0008 ± 0.00004	0.0003 ± 0.0001	0.0783 ± 0.0011	3.24 ± 0.0065	<LOD
soil#21	0.70903 ± 0.00003	0.0423 ± 0.0006	0.0044 ± 0.00003	0.0019 ± 0.00002	5.39 ± 0.0269	2.43 ± 0.0292	0.0681 ± 0.0081
soil#26	0.70983 ± 0.00003	0.0412 ± 0.0006	0.0005 ± 0.00004	0.0004 ± 0.00004	0.724 ± 0.0087	3.19 ± 0.0319	0.0318 ± 0.0014
soil#28	0.71024 ± 0.00003	0.0056 ± 0.0004	0.0002 ± 0.00001	<LOD	0.143 ± 0.0031	5.49 ± 0.0549	<LOD
soil#32	0.71150 ± 0.00003	0.0127 ± 0.0002	0.0003 ± 0.00001	0.0002 ± 0.0001	0.185 ± 0.0024	7.24 ± 0.0362	0.0048 ± 0.0009
soil#36	0.70966 ± 0.00003	0.0020 ± 0.0001	0.0011 ± 0.0001	<LOD	0.180 ± 0.0018	9.06 ± 0.0544	<LOD
soil#37	0.70986 ± 0.00003	0.0626 ± 0.0008	0.0021 ± 0.00002	0.0007 ± 0.0001	0.588 ± 0.0082	2.97 ± 0.0208	0.0116 ± 0.0024
soil#40	0.70920 ± 0.00003	0.0028 ± 0.0003	0.0022 ± 0.0002	0.0001 ± 0.0001	0.717 ± 0.0072	5.12 ± 0.0717	<LOD

*LODs for Pb and Zn are 0.0001 and 0.0045, respectively.

Table A.7: $^{87}Sr/^{86}Sr$ isotope ratios and concentrations expressed in mg kg^{-1} of selected elements with SDs in feed samples from Naxos, Greece.

Sample code	$^{87}Sr/^{86}Sr$	As	Ca	Cd	Mg	Pb	Rb	Sr	Zn
					August 2020				
feed#1	0.70947 ± 0.00003	0.0663 ± 0.0022	7334 ± 231	0.0728 ± 0.0028	3718 ± 77.8	0.0851 ± 0.0018	10.9 ± 0.0983	25.3 ± 0.482	78.7 ± 1.42

Sample code	$^{87}Sr/^{86}Sr$	As	Ca	Cd	Mg	Pb	Rb	Sr	Zn
feed#2	0.70935 ± 0.00003	0.0551 ± 0.0055	3489 ± 65.1	0.114 ± 0.0038	3582 ± 22.4	0.0649 ± 0.0033	12.8 ± 0.154	6.69 ± 0.181	49.6 ± 0.447
feed#3	0.70961 ± 0.00003	0.0739 ± 0.0035	9300 ± 337	0.0240 ± 0.0010	3579 ± 148	0.110 ± 0.0043	10.4 ± 0.156	28.4 ± 0.455	116.7 ± 1.75
feed#4	0.70898 ± 0.00003	0.0628 ± 0.0058	6324 ± 89.1	0.0341 ± 0.0018	2771 ± 36.6	0.0408 ± 0.0016	6.05 ± 0.0363	7.16 ± 0.0860	93.6 ± 3.18
feed#4_2	0.70900 ± 0.00003	0.0401 ± 0.0033	5296 ± 55.1	0.0165 ± 0.0009	2693 ± 7.87	0.0320 ± 0.0016	4.98 ± 0.0847	5.42 ± 0.141	32.6 ± 0.620
feed#5	0.70929 ± 0.00003	0.0310 ± 0.0040	811 ± 38.6	0.130 ± 0.0043	2300 ± 61.2	0.107 ± 0.0037	6.97 ± 0.139	2.53 ± 0.0279	97.8 ± 1.08
feed#6	0.70901 ± 0.00003	0.0528 ± 0.0039	4846 ± 76.5	0.138 ± 0.0044	2880 ± 17.8	0.144 ± 0.0027	10.6 ± 0.181	6.27 ± 0.0940	51.2 ± 0.870
feed#7	0.70942 ± 0.00003	0.0624 ± 0.0036	6068 ± 119	0.188 ± 0.0038	2302 ± 29.8	0.0599 ± 0.0023	7.83 ± 0.0627	17.8 ± 0.373	74.3 ± 0.966
feed#7_2	0.70943 ± 0.00003	0.0825 ± 0.0030	6836 ± 71.3	0.0280 ± 0.0007	2598 ± 31.7	0.0638 ± 0.0040	8.08 ± 0.218	22.0 ± 0.374	141.0 ± 2.68
feed#9	0.71040 ± 0.00003	0.0525 ± 0.0028	4252 ± 98.8	0.173 ± 0.0028	2738 ± 35.7	0.0495 ± 0.0020	6.83 ± 0.143	7.05 ± 0.0634	102.6 ± 1.54
feed#12	0.70964 ± 0.00003	0.0772 ± 0.0052	13840 ± 266	0.255 ± 0.0056	3157 ± 25.8	0.365 ± 0.0120	12.7 ± 0.304	14.4 ± 0.316	42.1 ± 0.841
feed#14	0.70964 ± 0.00003	0.0738 ± 0.0033	8797 ± 122	0.0310 ± 0.0021	3223 ± 39.3	0.129 ± 0.0045	8.85 ± 0.177	57.8 ± 1.56	196.6 ± 2.95
feed#15	0.71002 ± 0.00003	0.155 ± 0.0050	4581 ± 146	0.0380 ± 0.0009	2736 ± 53.5	0.651 ± 0.0280	12.1 ± 0.291	14.6 ± 0.218	119.7 ± 1.56
feed#16	0.70961 ± 0.00003	0.0528 ± 0.0058	10071 ± 74.4	0.0170 ± 0.0016	5641 ± 65.7	0.0425 ± 0.0016	7.92 ± 0.0871	10.7 ± 0.279	49.6 ± 0.843
feed#17	0.70882 ± 0.00003	0.0192 ± 0.0017	2440 ± 58.0	0.0150 ± 0.0006	2148 ± 62.6	0.0124 ± 0.0006	6.91 ± 0.228	2.63 ± 0.0527	99.5 ± 1.00
feed#17_2	0.70899 ± 0.00003	0.0183 ± 0.0017	1612 ± 19.0	0.0326 ± 0.0021	2488 ± 17.2	0.0218 ± 0.0016	6.84 ± 0.164	2.35 ± 0.0822	38.1 ± 0.838
feed#18	0.70961 ± 0.00003	0.0339 ± 0.0020	780 ± 31.8	0.0069 ± 0.0009	2498 ± 82.4	0.0461 ± 0.0025	7.42 ± 0.111	2.89 ± 0.0260	32.7 ± 0.719
feed#19	0.70905 ± 0.00003	0.0217 ± 0.0020	779 ± 43.8	0.0106 ± 0.0020	1790 ± 14.0	0.0065 ± 0.0009	5.58 ± 0.0725	2.49 ± 0.0771	19.4 ± 0.291
feed#21	0.70897 ± 0.00003	0.0145 ± 0.0028	384 ± 16.4	0.0338 ± 0.0020	1402 ± 8.37	0.0321 ± 0.0028	4.55 ± 0.0773	0.810 ± 0.0251	108.4 ± 1.19
feed#23	0.70897 ± 0.00003	0.0464 ± 0.0027	6080 ± 96.0	0.0549 ± 0.0021	2836 ± 38.2	0.0459 ± 0.0039	7.30 ± 0.146	6.68 ± 0.0334	28.4 ± 0.794
feed#24	0.70984 ± 0.00003	0.111 ± 0.0051	3578 ± 95.4	0.0081 ± 0.0009	2341 ± 41.6	0.152 ± 0.0068	9.26 ± 0.148	23.6 ± 0.424	27.3 ± 0.546
feed#25	0.70921 ± 0.00003	0.0115 ± 0.0017	290 ± 13.2	0.0079 ± 0.0005	1607 ± 13.0	0.0203 ± 0.0021	5.16 ± 0.0825	1.22 ± 0.0353	27.4 ± 0.549
feed#25_2	0.70918 ± 0.00003	<LOD	335 ± 8.48	0.0225 ± 0.0005	1492 ± 13.9	<LOD	4.11 ± 0.0616	1.67 ± 0.0450	28.7 ± 0.373
feed#26	0.70928 ± 0.00003	0.0147 ± 0.0018	942 ± 31.2	0.0376 ± 0.0015	2823 ± 54.6	0.0587 ± 0.0033	8.40 ± 0.193	2.15 ± 0.0515	120.7 ± 2.05
feed#27	0.70867 ± 0.00003	0.0625 ± 0.0084	8293 ± 81.4	0.221 ± 0.0027	2411 ± 26.3	0.0807 ± 0.0019	8.51 ± 0.128	10.4 ± 0.156	135.2 ± 3.11
feed#28	0.70929 ± 0.00003	0.0933 ± 0.0038	6574 ± 201	0.148 ± 0.0025	3744 ± 81.2	0.118 ± 0.0046	17.5 ± 0.297	12.3 ± 0.160	54.8 ± 0.602
feed#33	0.70951 ± 0.00003	0.0320 ± 0.0040	3261 ± 83.9	0.259 ± 0.0031	3475 ± 69.2	0.0917 ± 0.0038	12.5 ± 0.250	10.3 ± 0.207	62.7 ± 1.63
feed#34	0.70939 ± 0.00003	0.0537 ± 0.0059	3968 ± 77.9	0.0523 ± 0.0019	3912 ± 93.7	0.0758 ± 0.0052	19.3 ± 0.154	11.2 ± 0.371	544.7 ± 14.2
feed#35	0.70925 ± 0.00003	0.108 ± 0.0051	19563 ± 321	0.0249 ± 0.0017	5302 ± 39.9	0.168 ± 0.0077	6.38 ± 0.0511	16.3 ± 0.212	29.5 ± 0.709
feed#36	0.70942 ± 0.00003	0.0217 ± 0.0048	780 ± 23.9	0.0163 ± 0.0012	2467 ± 33.8	0.0282 ± 0.0019	7.34 ± 0.103	2.30 ± 0.108	19.4 ± 0.562
feed#37	0.70914 ± 0.00003	0.0104 ± 0.0020	356 ± 18.8	<LOD	1442 ± 18.2	0.0165 ± 0.0007	6.19 ± 0.105	0.873 ± 0.0672	17.9 ± 0.411
barley	0.70901 ± 0.00003	<LOD	420 ± 10.7	<LOD	1388 ± 34.7	0.0033 ± 0.0002	2.92 ± 0.0292	1.21 ± 0.0206	18.5 ± 0.278
corn	/	<LOD	47.5 ± 0.483	0.1217 ± 0.0038	873 ± 13.6	<LOD	3.87 ± 0.101	0.1 ± 0.0079	77.1 ± 1.85
cow breeding-1	0.70919 ± 0.00003	0.0472 ± 0.0056	13173 ± 138	0.1421 ± 0.0057	2950 ± 51.0	0.0506 ± 0.0016	12.5 ± 0.249	11.1 ± 0.267	79.8 ± 0.877

Sample code	$^{87}Sr/^{86}Sr$	As	Ca	Cd	Mg	Pb	Rb	Sr	Zn
cow breeding-1_2	0.70889 ± 0.00003	0.0525 ± 0.0039	16376 ± 227	0.1808 ± 0.0040	3549 ± 71.2	0.0942 ± 0.0026	15.3 ± 0.382	15.3 ± 0.290	107.9 ± 1.73
cow breeding plus	0.70907 ± 0.00003	0.115 ± 0.0045	14629 ± 137	0.0523 ± 0.0035	3149 ± 36.4	0.117 ± 0.0059	12.0 ± 0.192	17.8 ± 0.480	76.6 ± 1.38
bran	0.70955 ± 0.00003	0.0337 ± 0.0026	1095 ± 26.7	0.0313 ± 0.0021	4993 ± 63.3	0.0305 ± 0.0019	10.1 ± 0.404	8.53 ± 0.239	36.8 ± 0.441
cotton cake	0.70905 ± 0.00003	0.0136 ± 0.0021	1558 ± 76.0	0.0372 ± 0.0025	4201 ± 76.5	0.0249 ± 0.0010	11.3 ± 0.124	2.88 ± 0.0606	39.7 ± 1.23
cow breeding-2	0.70940 ± 0.00003	0.136 ± 0.0061	7435 ± 114.7	0.0675 ± 0.0018	3335 ± 39.6	0.454 ± 0.0177	10.4 ± 0.353	13.6 ± 0.449	93.6 ± 2.72
fine bran	0.70964 ± 0.00003	0.0322 ± 0.0061	1076 ± 19.1	0.0431 ± 0.0031	3435 ± 35.9	0.0128 ± 0.0012	8.46 ± 0.228	8.48 ± 0.254	48.0 ± 0.864
soya-1	0.71041 ± 0.00003	0.0581 ± 0.0037	3557 ± 52.4	0.0728 ± 0.0028	3204 ± 24.7	0.0314 ± 0.0013	16.5 ± 0.298	11.4 ± 0.228	78.7 ± 1.42
					January 2021				
feed#51	0.71000 ± 0.00003	0.130 ± 0.0061	5538 ± 109	0.0541 ± 0.0022	2619 ± 53.8	0.281 ± 0.0115	10.1 ± 0.272	47.6 ± 0.476	24.7 ± 0.594
feed#51_2	0.71009 ± 0.00003	0.0836 ± 0.0054	4143 ± 112	0.0342 ± 0.0024	2546 ± 33.4	0.181 ± 0.0080	8.91 ± 0.160	34.9 ± 0.349	27.8 ± 0.612
feed#52	0.70903 ± 0.00003	0.0512 ± 0.0041	6169 ± 107	0.0508 ± 0.0007	2363 ± 25.2	0.0782 ± 0.0039	6.82 ± 0.150	5.42 ± 0.217	118 ± 4.60
feed#53	0.70872 ± 0.00003	0.0689 ± 0.0027	12940 ± 149	0.0463 ± 0.0006	2860 ± 28.6	0.129 ± 0.0034	6.60 ± 0.178	11.6 ± 0.312	115 ± 4.26
feed#54	0.70921 ± 0.00003	0.0983 ± 0.0083	8637 ± 141	0.0648 ± 0.0018	2337 ± 19.6	0.471 ± 0.0136	15.5 ± 0.558	45.5 ± 1.50	30.4 ± 1.00
feed#55	0.70989 ± 0.00003	0.0357 ± 0.0024	1889 ± 44.1	0.0258 ± 0.0025	2948 ± 55.5	0.0740 ± 0.0016	9.74 ± 0.244	9.13 ± 0.338	31.5 ± 1.16
feed#56	0.70940 ± 0.00003	0.0277 ± 0.0033	1350 ± 26.0	0.0739 ± 0.0011	3108 ± 11.8	0.0301 ± 0.0008	10.4 ± 0.219	4.31 ± 0.172	40.2 ± 1.09
feed#57	0.70872 ± 0.00003	0.0501 ± 0.0042	7368 ± 19.1	0.0087 ± 0.0002	3096 ± 162	0.0688 ± 0.0030	9.95 ± 0.129	14.7 ± 0.206	96.8 ± 0.968
feed#58	0.70904 ± 0.00003	0.0747 ± 0.0075	6324 ± 93.0	0.0242 ± 0.0015	3449 ± 52.2	0.139 ± 0.0072	9.00 ± 0.108	18.2 ± 0.400	34.2 ± 0.718
feed#59	0.70981 ± 0.00003	0.107 ± 0.0045	5064 ± 81.4	0.0485 ± 0.0029	2472 ± 55.8	0.324 ± 0.0175	8.67 ± 0.208	12.1 ± 0.229	62.9 ± 0.629
feed#60	0.70979 ± 0.00003	0.0576 ± 0.0031	4339 ± 64.2	0.0303 ± 0.0013	2204 ± 42.2	0.0979 ± 0.0107	8.23 ± 0.165	17.4 ± 0.156	36.6 ± 0.549
feed#60_2	0.70983 ± 0.00003	0.0767 ± 0.0051	6515 ± 80.6	0.0384 ± 0.0010	2795 ± 58.7	0.117 ± 0.0047	9.37 ± 0.0375	21.9 ± 0.372	49.3 ± 0.592
feed#61	0.70899 ± 0.00003	0.0113 ± 0.0020	630 ± 33.6	0.0172 ± 0.0002	1781 ± 20.0	0.0091 ± 0.0007	6.27 ± 0.113	1.50 ± 0.0524	23.5 ± 0.587
feed#62	0.70892 ± 0.00003	0.0272 ± 0.0029	4879 ± 93.9	0.0548 ± 0.0024	2143 ± 38.3	0.0252 ± 0.0015	7.82 ± 0.141	5.25 ± 0.105	52.7 ± 1.37
feed#63	0.70946 ± 0.00003	0.0611 ± 0.0058	6539 ± 153	0.0968 ± 0.0025	2682 ± 36.3	0.125 ± 0.0099	7.25 ± 0.160	44.2 ± 1.28	32.0 ± 0.608
trifolium	0.70855 ± 0.00003	0.0423 ± 0.0028	9338 ± 132	0.0103 ± 0.0001	3727 ± 28.0	0.0477 ± 0.0033	19.3 ± 0.135	35.2 ± 0.352	21.7 ± 0.413
pasture P1	0.71245 ± 0.00003	1.80 ± 0.0715	9245 ± 112	0.0621 ± 0.0014	4528 ± 71.7	1.79 ± 0.0645	19.3 ± 0.657	34.8 ± 1.04	48.8 ± 2.10
pasture P2	0.71055 ± 0.00003	1.41 ± 0.0833	18986 ± 233	0.114 ± 0.0021	2090 ± 23.1	2.14 ± 0.0897	6.02 ± 0.223	20.3 ± 0.244	37.8 ± 0.491
pasture P3	0.70939 ± 0.00003	0.155 ± 0.0051	9715 ± 155	0.0465 ± 0.0018	3404 ± 46.3	0.316 ± 0.0133	1.63 ± 0.0472	9.27 ± 0.102	24.7 ± 0.594
					June 2021				
feed#51	0.70919 ± 0.00003	0.0259 ± 0.0008	877 ± 17.9	0.0287 ± 0.0010	2305 ± 36.9	0.0149 ± 0.0013	8.93 ± 0.399	2.33 ± 0.0517	23.8 ± 0.262
feed#51_2	0.70922 ± 0.00003	<LOD	1120 ± 39.1	0.0359 ± 0.0021	3391 ± 33.0	0.0091 ± 0.0005	11.1 ± 0.270	3.12 ± 0.0351	31.0 ± 0.374
51 pasture	0.70977 ± 0.00003	0.386 ± 0.0148	4526 ± 99.3	0.0388 ± 0.0026	811 ± 15.7	2.16 ± 0.111	1.33 ± 0.0354	14.1 ± 0.0894	15.6 ± 0.340
feed#52	0.70894 ± 0.00003	0.0615 ± 0.0007	4287 ± 45.9	0.0212 ± 0.0017	1973 ± 60.2	0.0764 ± 0.0035	6.78 ± 0.162	6.85 ± 0.0757	28.5 ± 0.566
feed#53	0.71295 ± 0.00003	0.0559 ± 0.0007	17840 ± 328	0.0453 ± 0.0021	4345 ± 52.1	0.0785 ± 0.0038	8.68 ± 0.257	10.6 ± 0.0706	102 ± 1.47

Sample code	$^{87}Sr/^{86}Sr$	As	Ca	Cd	Mg	Pb	Rb	Sr	Zn
feed#53	0.71180 ±	0.105 ±	16435	0.1837 ±	4769 ±	0.0702 ±	9.53 ±	9.21 ±	132 ±
_2	0.00003	0.0012	± 167	0.0040	53.9	0.0019	0.743	0.0817	7.89
feed#54	0.71078 ±	0.182 ±	5456 ±	0.0248 ±	2975 ±	0.790 ±	9.70 ±	15.6 ±	34.4 ±
	0.00003	0.0107	140	0.0023	29.0	0.0312	0.666	0.257	0.397
feed#55	0.70910 ±	0.0255 ±	597 ±	0.0146 ±	1802 ±	0.0150 ±	6.37 ±	1.30 ±	17.3 ±
	0.00003	0.0007	27.1	0.0014	58.0	0.0015	0.134	0.0120	0.245
feed#55	0.70913 ±	<LOD	667 ±	0.0243 ±	2612 ±	0.0134 ±	8.33 ±	1.78 ±	24.6 ±
_2	0.00003		14.8	0.0007	31.4	0.0015	0.204	0.0196	0.479
feed#56	0.70951 ±	0.0342 ±	1553 ±	0.0970 ±	3121 ±	0.0305 ±	12.9 ±	4.89 ±	42.3 ±
	0.00003	0.0010	50.8	0.0030	49.4	0.0021	1.00	0.141	3.43
feed#57	0.71013 ±	0.101 ±	8615 ±	0.0205 ±	3525 ±	0.144 ±	10.7 ±	12.7 ±	84.9 ±
	0.00003	0.0067	107	0.0007	51.0	0.0061	0.223	0.110	0.606
feed#57	0.70997 ±	0.0497 ±	8810 ±	0.0286 ±	3311 ±	0.164 ±	10.0 ±	13.0 ±	88.7 ±
_2	0.00003	0.0008	183	0.0028	57.4	0.0035	0.387	0.115	1.63
feed#58	0.70921 ±	0.0721 ±	6117 ±	0.0357 ±	2543 ±	0.336 ±	13.1 ±	13.4 ±	26.6 ±
	0.00003	0.0067	121	0.0024	54.4	0.0128	0.413	0.107	0.392
feed#58	0.70932 ±	0.0418 ±	6352 ±	0.0429 ±	2565 ±	0.437 ±	13.3 ±	14.8 ±	26.7 ±
_2	0.00003	0.0035	122	0.0021	39.7	0.0083	0.317	0.174	0.615
feed#59	0.71162 ±	0.0528 ±	5413 ±	0.0553 ±	2807 ±	0.143 ±	11.8 ±	9.81 ±	62.4 ±
	0.00003	0.0007	70.0	0.0023	35.3	0.0039	0.296	0.0750	2.20
feed#60	0.70901 ±	<LOD	2811 ±	0.0215 ±	2866 ±	0.0418 ±	9.17 ±	9.00 ±	23.7 ±
	0.00003		43.6	0.0010	62.6	0.0017	0.284	0.0980	0.531
feed#60	0.70909 ±	<LOD	2103 ±	0.0221 ±	2141 ±	0.0532 ±	9.18 ±	5.32 ±	19.6 ±
_2	0.00003		57.3	0.0015	25.7	0.0030	0.295	0.0394	0.272
feed#61	0.70889 ±	<LOD	1171 ±	0.0191 ±	2706 ±	0.0322 ±	7.42 ±	3.42 ±	25.8 ±
	0.00003		10.7	0.0014	55.0	0.0023	0.240	0.0292	0.551
feed#62	0.71613 ±	<LOD	756 ±	0.0097 ±	1481 ±	0.0091 ±	6.35 ±	2.35 ±	24.7 ±
	0.00003		20.4	0.0010	20.8	0.0014	0.210	0.0310	0.337
feed#63	0.71145 ±	<LOD	5255 ±	0.0328 ±	2666 ±	0.0888 ±	7.95 ±	7.49 ±	85.5 ±
	0.00003		90.4	0.0014	51.6	0.0033	0.136	0.0957	1.21

*LODs for As, Cd, and Pb are 0.0091, 0.0015, and 0.0020, respectively.

Table A.8: $^{87}Sr/^{86}Sr$ isotope ratios and concentrations expressed in mg kg^{-1} of selected elements with SDs in milk samples from Naxos, Greece.

Sample code	$^{87}Sr/^{86}Sr$	Ca	K	Mg	Rb	Sr	Zn
			August 2020				
milk#1	0.70960 ± 0.00002	9005 ± 164	13124 ± 210	964 ± 12.3	19.2 ± 0.114	2.64 ± 0.035	17.5 ± 0.095
milk#2	0.70954 ± 0.00002	9660 ± 197	11410 ± 116	924 ± 12.4	16.2 ± 0.162	2.24 ± 0.065	21.7 ± 0.276
milk#4	0.70896 ± 0.00002	8642 ± 226	12242 ± 52.2	820 ± 8.18	11.1 ± 0.094	2.07 ± 0.042	21.1 ± 0.506
milk#5	0.70929 ± 0.00002	10047 ± 280	24455 ± 361	1462 ± 34.8	26.4 ± 0.085	3.39 ± 0.014	18.2 ± 0.172
milk#6	0.70950 ± 0.00002	8946 ± 176	12863 ± 145	993 ± 14.8	17.1 ± 0.186	3.23 ± 0.069	21.5 ± 0.393
milk#6_2	0.70948 ± 0.00002	9110 ± 191	13054 ± 295	1024 ± 12.8	16.7 ± 0.091	4.47 ± 0.072	20.7 ± 0.298
milk#7	0.70918 ± 0.00002	7621 ± 121	13215 ± 229	690 ± 12.7	11.9 ± 0.133	5.61 ± 0.045	13.8 ± 0.084
milk#9	0.70956 ± 0.00002	9124 ± 162	14145 ± 158	1109 ± 26.8	20.3 ± 0.304	3.92 ± 0.031	17.9 ± 0.487
milk#14	0.70986 ± 0.00002	8758 ± 215	12101 ± 204	843 ± 12.9	12.5 ± 0.061	3.07 ± 0.018	23.1 ± 1.260
milk#15	0.70953 ± 0.00002	7760 ± 191	11277 ± 79.9	657 ± 15.4	13.3 ± 0.097	2.18 ± 0.051	27.3 ± 0.290
milk#16	0.70952 ± 0.00002	7268 ± 123	9702 ± 126	789 ± 15.3	10.5 ± 0.039	1.50 ± 0.014	18.4 ± 0.171
milk#17	0.70966 ± 0.00002	8742 ± 160	18059 ± 330	1082 ± 10.4	24.5 ± 0.231	2.59 ± 0.013	29.6 ± 0.306
milk#18	0.70985 ± 0.00002	9476 ± 218	13470 ± 181	873 ± 9.58	16.2 ± 0.097	2.03 ± 0.020	22.4 ± 0.138
milk#19	0.70922 ± 0.00002	6291 ± 248	8825 ± 248	730 ± 23.2	9.50 ± 0.071	1.89 ± 0.007	15.0 ± 0.118
milk#20	0.70816 ± 0.00002	10429 ± 117	12553 ± 101	1356 ± 20.4	23.8 ± 0.170	6.14 ± 0.046	17.3 ± 0.091
milk#21	0.70932 ± 0.00002	10776 ± 310	13793 ± 210	1501 ± 24.9	23.1 ± 0.164	3.12 ± 0.051	18.1 ± 0.088
milk#23	0.70942 ± 0.00002	8921 ± 248	13380 ± 136	918 ± 14.5	11.4 ± 0.133	1.87 ± 0.043	19.2 ± 0.218
milk#24	0.70948 ± 0.00002	9030 ± 149	4787 ± 31.4	1020 ± 9.60	6.93 ± 0.102	3.81 ± 0.043	11.1 ± 0.200
milk#25	0.70916 ± 0.00002	8874 ± 97.5	15907 ± 252	1476 ± 19.9	13.3 ± 0.070	2.51 ± 0.144	14.4 ± 0.230
milk#26	0.70926 ± 0.00002	10226 ± 136	15794 ± 120	1239 ± 23.6	16.9 ± 0.209	4.14 ± 0.043	19.1 ± 0.014
milk#27	0.70907 ± 0.00002	9157 ± 213	14741 ± 313	1174 ± 13.1	36.2 ± 0.167	3.74 ± 0.047	21.2 ± 0.045
milk#28	0.70960 ± 0.00002	9083 ± 80.5	15988 ± 298	1190 ± 14.2	43.4 ± 0.257	2.39 ± 0.059	26.0 ± 0.333
milk#31a	0.71170 ± 0.00002	11483 ± 159	5349 ± 57.4	1408 ± 22.5	5.20 ± 0.046	11.5 ± 0.196	12.0 ± 0.116
milk#31b	0.71225 ± 0.00002	10502 ± 157	14104 ± 343	1276 ± 14.6	31.3 ± 0.077	9.29 ± 0.069	19.5 ± 0.113
milk#33	0.71024 ± 0.00002	13570 ± 290	21753 ± 358	1100 ± 9.73	31.6 ± 0.136	3.15 ± 0.013	32.0 ± 0.098
milk#34	0.71042 ± 0.00002	5316 ± 205	9819 ± 112	808 ± 13.7	17.0 ± 0.194	1.31 ± 0.026	12.5 ± 0.239
milk#35	0.70987 ± 0.00002	8477 ± 189	15045 ± 198	1127 ± 26.6	22.1 ± 0.157	6.44 ± 0.028	21.6 ± 0.338

Sample code	$^{87}Sr/^{86}Sr$	Ca	K	Mg	Rb	Sr	Zn
milk#36	0.71068 ± 0.00002	9372 ± 197	14078 ± 182	1125 ± 10.1	28.3 ± 0.237	7.34 ± 0.082	23.0 ± 0.286
milk#36_2	0.71068 ± 0.00002	9220 ± 170	13622 ± 157	1084 ± 13.7	24.5 ± 0.146	6.42 ± 0.058	27.7 ± 0.372
milk#37	0.70942 ± 0.00002	8616 ± 220	3804 ± 64.4	850 ± 16.3	5.28 ± 0.128	3.32 ± 0.049	11.5 ± 0.082
milk#38	0.70881 ± 0.00002	8194 ± 192	11496 ± 126	921 ± 12.1	8.76 ± 0.156	2.32 ± 0.074	22.4 ± 0.288
milk#39	0.70781 ± 0.00002	9336 ± 146	15342 ± 205	1316 ± 23.6	21.8 ± 0.365	13.3 ± 0.223	29.9 ± 0.142
milk#42	0.70926 ± 0.00002	8820 ± 109	12464 ± 216	853 ± 11.5	14.7 ± 0.171	2.51 ± 0.083	23.7 ± 1.197
milk#43	0.70931 ± 0.00002	9337 ± 147	12126 ± 123	875 ± 28.4	15.2 ± 0.250	2.79 ± 0.036	27.9 ± 0.105
			January 2021				
milk#51 sheep	0.70922 ± 0.00002	9002 ± 122	6301 ± 126	834 ± 12.3	6.05 ± 0.103	7.56 ± 0.091	30.7 ± 0.368
milk#51 sheep_2	0.70926 ± 0.00002	8852 ± 142	6180 ± 81.8	822 ± 17.8	5.04 ± 0.091	6.13 ± 0.104	25.5 ± 0.433
milk#51 goat	0.70913 ± 0.00002	8241 ± 162	9658 ± 98.2	808 ± 8.59	14.6 ± 0.102	7.30 ± 0.117	35.4 ± 0.319
milk#52 cow	0.70885 ± 0.00002	7168 ± 135	10310 ± 166	582 ± 1.77	11.3 ± 0.079	2.85 ± 0.037	30.7 ± 0.706
milk#53 cow	0.70864 ± 0.00002	8247 ± 91.4	10276 ± 133.5	731 ± 8.53	14.2 ± 0.242	1.90 ± 0.047	32.5 ± 0.617
milk#54 sheep	0.70929 ± 0.00002	8415 ± 52.8	5229 ± 138.4	710 ± 10.1	10.2 ± 0.142	7.93 ± 0.182	35.8 ± 0.465
milk#54 goat	0.70909 ± 0.00002	7935 ± 149	10411 ± 55.0	844 ± 8.14	23.2 ± 0.232	7.27 ± 0.174	31.3 ± 0.344
milk#55 sheep	0.70952 ± 0.00002	8902 ± 88.7	5599 ± 117	725 ± 11.5	7.76 ± 0.078	4.67 ± 0.089	38.6 ± 0.463
milk#55 goat	0.70968 ± 0.00002	7834 ± 90.8	11267 ± 128	765 ± 10.4	18.9 ± 0.132	5.84 ± 0.099	33.3 ± 0.433
milk#55 goat_2	0.70958 ± 0.00002	8198 ± 110	11380 ± 167	783 ± 4.47	15.7 ± 0.329	5.40 ± 0.097	28.1 ± 0.617
milk#56 cow	0.70939 ± 0.00002	7988 ± 106	8825 ± 153	687 ± 7.98	13.6 ± 0.231	3.94 ± 0.031	35.9 ± 0.682
milk#57 cow	0.70877 ± 0.00002	7352 ± 30.9	9146 ± 115	671 ± 10.2	12.7 ± 0.598	2.18 ± 0.129	36.6 ± 1.207
milk#58 cow	0.70884 ± 0.00002	7925 ± 66.2	9848 ± 30.1	709 ± 5.21	12.5 ± 0.149	2.16 ± 0.035	38.5 ± 0.308
milk#59 cow	0.70939 ± 0.00002	7744 ± 123	9857 ± 144	662 ± 9.41	11.0 ± 0.221	2.41 ± 0.075	34.8 ± 0.696
milk#60 sheep	0.70918 ± 0.00002	8332 ± 105	5509 ± 107	745 ± 9.24	5.07 ± 0.147	2.90 ± 0.096	35.4 ± 0.815
milk#60 goat	0.70914 ± 0.00002	7457 ± 124	10761 ± 153	833 ± 11.3	10.7 ± 0.128	2.95 ± 0.056	29.6 ± 0.592
milk#61 sheep	0.70872 ± 0.00002	7763 ± 64.5	5133 ± 69.4	588 ± 11.1	3.22 ± 0.103	2.97 ± 0.095	40.4 ± 0.687
milk#62 cow	0.70879 ± 0.00002	7457 ± 126	9168 ± 144	653 ± 10.4	11.7 ± 0.540	2.41 ± 0.116	33.4 ± 1.368
milk#62 cow_2	0.70878 ± 0.00002	7586 ± 100	9347 ± 77.1	666 ± 6.01	10.7 ± 0.535	2.35 ± 0.134	30.3 ± 1.180
milk#63 cow	0.70910 ± 0.00002	7711 ± 112	9784 ± 80.0	714 ± 17.6	8.71 ± 0.087	2.40 ± 0.077	26.5 ± 0.317
milk#64 mixed	0.70916 ± 0.00002	7703 ± 77.8	9495 ± 124	689 ± 14.0	10.9 ± 0.142	2.53 ± 0.025	31.7 ± 0.665
milk#64 mixed_2	0.70913 ± 0.00002	7778 ± 90.0	9088 ± 64.4	676 ± 10.2	9.55 ± 0.582	2.37 ± 0.194	28.5 ± 1.112
milk#64 renned	0.70917 ± 0.00002	7850 ± 102	9527 ± 100	700 ± 13.7	11.2 ± 0.537	2.56 ± 0.080	32.3 ± 1.065
milk#65 mixed tq	0.70919 ± 0.00002	8107 ± 195	5997 ± 120	723 ± 12.6	8.61 ± 0.146	3.67 ± 0.084	31.2 ± 0.375
milk#65 mixed	0.70934 ± 0.00002	7671 ± 98.4	5868 ± 149	673 ± 9.79	8.74 ± 0.210	3.46 ± 0.035	29.3 ± 0.410
milk#66 cow	0.70921 ± 0.00002	7593 ± 119	9227 ± 152	685 ± 10.9	10.9 ± 0.710	2.74 ± 0.183	32.4 ± 1.779
milk#66 cow A	0.70917 ± 0.00002	7685 ± 35.6	9212 ± 54.3	691 ± 7.03	10.4 ± 0.135	2.61 ± 0.042	31.5 ± 0.158
milk#66 cow B	0.70921 ± 0.00002	7312 ± 85.7	8671 ± 75.7	655 ± 2.79	10.1 ± 0.457	2.58 ± 0.152	30.3 ± 0.968

Sample code	$^{87}Sr/^{86}Sr$	Ca	K	Mg	Rb	Sr	Zn
milk#66 cow C	0.70915 ± 0.00002	6889 ± 162	8314 ± 141	616 ± 12.9	9.16 ± 0.715	2.26 ± 0.147	26.9 ± 2.045
milk#66 cow D	0.70913 ± 0.00002	4998 ± 52.9	6151 ± 50.6	450 ± 4.48	6.59 ± 0.046	1.61 ± 0.029	19.1 ± 0.115
milk#66 cow E	0.70925 ± 0.00002	7050 ± 122	9025 ± 140	635 ± 5.84	10.4 ± 0.240	2.63 ± 0.087	28.7 ± 0.401
milk#66 cow F	0.70900 ± 0.00002	5770 ± 116	7435 ± 204	492 ± 9.64	7.42 ± 0.082	1.96 ± 0.045	23.8 ± 0.309
			June 2021				
milk #51 goat	0.70892 ± 0.00002	6920 ± 35.3	10762 ± 118	787 ± 10.9	14.9 ± 0.608	1.49 ± 0.055	19.7 ± 1.003
milk #52 cow	0.70923 ± 0.00002	7597 ± 95.4	10346 ± 74.9	632 ± 6.51	9.83 ± 0.412	2.64 ± 0.064	27.4 ± 0.399
milk #53 cow	0.70903 ± 0.00002	7787 ± 86.1	10319 ± 122	680 ± 12.3	11.3 ± 0.706	1.63 ± 0.019	26.0 ± 0.402
milk #54 sheep	0.70998 ± 0.00002	8048 ± 45.8	5369 ± 52.0	858 ± 11.1	8.13 ± 0.346	3.67 ± 0.066	15.8 ± 0.308
milk #55 sheep	0.70977 ± 0.00002	8283 ± 106	4563 ± 120	709 ± 9.60	9.78 ± 0.418	2.74 ± 0.048	22.4 ± 0.970
milk #55 sheep_2	0.70977 ± 0.00002	8958 ± 269	4926 ± 137	784 ± 11.4	9.55 ± 0.343	2.90 ± 0.063	22.7 ± 0.478
milk #55 goat	0.70986 ± 0.00002	7672 ± 86.6	13052 ± 231	892 ± 7.69	26.9 ± 1.628	3.11 ± 0.057	22.3 ± 0.578
milk #56 cow	0.70940 ± 0.00002	7702 ± 82.0	9628 ± 142	686 ± 12.3	14.1 ± 0.326	2.56 ± 0.041	26.3 ± 0.844
milk #57 cow	0.70951 ± 0.00002	7575 ± 128	9318 ± 82	677 ± 3.49	12.0 ± 0.212	2.05 ± 0.019	28.0 ± 0.556
milk #58 cow	0.70892 ± 0.00002	7551 ± 87.2	10188 ± 175	689 ± 13.3	13.5 ± 0.120	1.99 ± 0.015	25.6 ± 0.289
milk #59 cow	0.71021 ± 0.00002	7415 ± 105	10385 ± 136	640 ± 10.0	12.9 ± 0.369	1.74 ± 0.044	27.9 ± 0.778
milk #60 sheep	0.70916 ± 0.00002	7563 ± 93.0	4963 ± 70.9	825 ± 13.6	4.59 ± 0.100	2.26 ± 0.042	17.5 ± 0.169
milk #60 goat	0.70916 ± 0.00002	7681 ± 86.6	12224 ± 246	897 ± 9.56	8.49 ± 0.334	2.21 ± 0.038	14.1 ± 0.290
milk #61 sheep	0.70864 ± 0.00002	7887 ± 135	3955 ± 31.1	820 ± 7.59	4.32 ± 0.090	4.85 ± 0.028	12.4 ± 0.195
milk #61 goat	0.70896 ± 0.00002	7761 ± 95.0	11319 ± 140	803 ± 12.4	17.2 ± 0.423	3.09 ± 0.022	18.5 ± 0.288
milk #62 cow	0.71027 ± 0.00002	8365 ± 39.5	11049 ± 68.1	704 ± 7.21	11.6 ± 0.264	2.87 ± 0.046	28.7 ± 0.309
milk #62 cow_2	0.71026 ± 0.00002	8309 ± 209	10846 ± 93.1	690 ± 7.55	11.3 ± 0.327	2.77 ± 0.037	27.7 ± 0.604
milk #63 cow	0.71005 ± 0.00002	7845 ± 124	10209 ± 281	713 ± 7.60	10.2 ± 0.198	2.96 ± 0.042	19.2 ± 0.289
			July 2021				
D3 mixed milk	0.70971 ± 0.00002	7672 ± 107	10364 ± 120	666 ± 13.2	11.9 ± 0.215	2.27 ± 0.027	24.0 ± 0.531
D4 mixed milk	0.70968 ± 0.00002	7365 ± 88.3	10241 ± 148	644 ± 8.32	12.3 ± 0.597	2.05 ± 0.024	22.8 ± 0.362
D5 mixed milk	0.70942 ± 0.00002	7581 ± 121	10436 ± 173	666 ± 7.97	13.2 ± 0.402	2.47 ± 0.026	24.5 ± 0.158
D6 mixed milk	0.70968 ± 0.00002	6797 ± 79.1	9352 ± 136	617 ± 9.76	10.6 ± 0.165	2.24 ± 0.020	21.1 ± 0.418
K1 mixed milk	0.70973 ± 0.00002	7230 ± 57.0	9774 ± 43.6	633 ± 5.43	11.5 ± 0.509	2.16 ± 0.048	22.9 ± 1.059
K2 mixed milk	0.70975 ± 0.00002	7097 ± 59.9	9707 ± 105	620 ± 3.39	11.8 ± 0.942	2.15 ± 0.062	24.6 ± 0.756
K3 mixed milk	0.70973 ± 0.00002	6874 ± 125	9602 ± 154	634 ± 8.25	10.4 ± 0.308	2.21 ± 0.039	21.0 ± 0.308
K4 mixed milk	0.70938 ± 0.00002	7492 ± 105	10352 ± 249	667 ± 7.94	12.5 ± 0.312	2.57 ± 0.015	23.6 ± 0.384
K5 mixed milk	0.70966 ± 0.00002	7400 ± 120	10018 ± 192	663 ± 6.78	12.4 ± 0.337	2.12 ± 0.053	22.9 ± 0.368
K6 mixed milk	0.70940 ± 0.00002	7573 ± 54.7	10542 ± 176	673 ± 8.57	12.5 ± 0.374	2.58 ± 0.031	25.0 ± 0.383
			January 2022				

Sample code	$^{87}Sr/^{86}Sr$	Ca	K	Mg	Rb	Sr	Zn
A cow milk II	0.70920 ± 0.00002	6134 ± 66.7	7533 ± 68.6	566 ± 6.52	7.85 ± 0.071	1.53 ± 0.034	20.3 ± 0.263
A cow milk III	0.70926 ± 0.00002	6856 ± 39.7	8122 ± 87.4	698 ± 6.20	8.68 ± 0.146	1.57 ± 0.031	21.5 ± 0.337
A cow milk IV	0.70926 ± 0.00002	8877 ± 107	7188 ± 71.8	635 ± 15.2	8.34 ± 0.049	2.33 ± 0.050	29.9 ± 0.216
A cow milk V	0.70926 ± 0.00002	10503 ± 154	8314 ± 148	820 ± 10.5	8.04 ± 0.073	2.84 ± 0.015	13.3 ± 0.291
B cow milk I	0.70926 ± 0.00002	10132 ± 107	4613 ± 78.5	538 ± 8.14	5.09 ± 0.344	2.97 ± 0.199	48.9 ± 0.627
B cow milk II	0.70920 ± 0.00002	7870 ± 108	9621 ± 72.4	690 ± 11.5	10.7 ± 0.092	2.14 ± 0.036	28.4 ± 0.218
B cow milk III	0.70926 ± 0.00002	7914 ± 42.3	9396 ± 124	698 ± 14.9	10.7 ± 0.153	2.19 ± 0.048	29.8 ± 0.230
B cow milk IV	0.70927 ± 0.00002	7131 ± 165	10305 ± 80.4	745 ± 8.37	11.8 ± 0.244	2.13 ± 0.044	28.4 ± 0.471
B cheese curd V	0.70925 ± 0.00002	7562 ± 144	9444 ± 189	668 ± 14.1	10.7 ± 0.194	2.11 ± 0.084	29.2 ± 0.247

Table A.9: $^{87}Sr/^{86}Sr$ isotope ratios and concentrations expressed in mg kg^{-1} of selected elements with SDs in Graviera Naxos cheese samples.

Sample code	$^{87}Sr/^{86}Sr$	Ca	K	Mg	Rb	Sr	Zn
			August 2020				
Graviera 1	0.70943 ± 0.00003	12718 ± 261	1239 ± 27.6	545 ± 9.83	1.61 ± 0.032	4.34 ± 0.030	46.5 ± 0.630
Graviera 1_2	0.70943 ± 0.00003	13654 ± 194	1252 ± 23.1	571 ± 9.47	1.37 ± 0.107	4.77 ± 0.067	17.6 ± 0.266
Graviera 2	0.70937 ± 0.00003	12796 ± 170	1235 ± 19.2	502 ± 7.98	1.72 ± 0.032	4.49 ± 0.095	49.2 ± 1.06
Graviera 2_2	0.70945 ± 0.00003	24780 ± 404	2409 ± 66.3	989 ± 20.7	1.29 ± 0.032	4.42 ± 0.057	36.4 ± 0.228
Graviera 3	0.70940 ± 0.00003	12869 ± 186	1221 ± 23.1	513 ± 5.07	1.60 ± 0.037	4.35 ± 0.059	45.2 ± 0.444
Graviera 3_2	0.70940 ± 0.00003	12383 ± 321	1199 ± 39.3	503 ± 11.0	1.32 ± 0.019	4.19 ± 0.055	39.9 ± 0.415
			January 2021				
Graviera 4	0.70891 ± 0.00003	10661 ± 261	920 ± 19.3	433 ± 7.18	1.25 ± 0.044	4.22 ± 0.101	58.2 ± 0.349
Graviera 4_2	0.70893 ± 0.00003	10054 ± 73.0	878 ± 24.6	395 ± 3.31	1.33 ± 0.024	4.37 ± 0.092	63.0 ± 0.756
			June 2021				
Graviera 5	0.70912 ± 0.00003	11593 ± 82.6	1052 ± 15.8	441 ± 5.32	1.14 ± 0.031	3.41 ± 0.055	50.4 ± 1.33
Graviera 5_2	0.70911 ± 0.00003	10933 ± 95.9	1047 ± 4.92	417 ± 7.90	1.19 ± 0.056	3.05 ± 0.042	49.1 ± 0.635
			January 2022				
Graviera 6 Fresh	0.70936 ± 0.00003	11280 ± 215	861 ± 20.9	437 ± 7.38	0.995 ± 0.028	3.44 ± 0.045	65.6 ± 0.516
Graviera 7 Cured	0.70952 ± 0.00003	11392 ± 95.2	1104 ± 15.0	452 ± 3.88	1.35 ± 0.045	3.51 ± 0.053	68.6 ± 0.365

A.3 Content of Selected Elements in Samples from Eastern Carpathians, Romania

Table A.10: $^{87}Sr/^{86}Sr$ isotope ratios and concentrations expressed in µg L^{-1} of selected elements with SDs in water samples from Eastern Carpathians, Romania.

Sample code	$^{87}Sr/^{86}Sr$	As	Ca	Cd	Mg	Pb	Rb	Sr	Zn
ROD 1i	0.72270 ± 0.00003	0.118 ± 6.21	3.25 ± 0.0044	<LOD	0.787 ± 0.0013	<LOD	0.0700 ± 8.15	9.98 ± 1.56	8.90 ± 1.79
ROD 3i	0.72036 ± 0.00003	0.351 ± 5.62	7.99 ± 0.0045	0.010 ± 29.2	1.34 ± 0.0026	0.135 ± 4.31	0.877 ± 3.59	35.6 ± 1.85	2.67 ± 3.52
ROD 7i	0.70840 ± 0.00003	0.056 ± 14.0	45.82 ± 0.0031	<LOD	1.74 ± 0.0019	<LOD	0.326 ± 4.36	305 ± 1.28	0.732 ± 3.87
ROD 8i	0.71770 ± 0.00003	0.105 ± 13.4	31.26 ± 0.0031	0.008 ± 17.2	11.8 ± 0.0026	0.165 ± 2.43	0.630 ± 5.32	159 ± 0.871	3.57 ± 2.72
ROD 8R	0.71125 ± 0.00003	0.249 ± 4.56	23.85 ± 0.0031	0.005 ± 36.9	3.10 ± 0.0020	0.203 ± 0.721	0.509 ± 5.09	87.4 ± 0.79	1.56 ± 2.84
RAR 1i	0.71812 ± 0.00003	1.425 ± 3.55	16.89 ± 0.0019	0.050 ± 6.62	2.30 ± 0.0041	1.54 ± 1.04	1.12 ± 7.45	27.9 ± 1.16	10.5 ± 1.45
RAR 1R	0.71826 ± 0.00003	0.288 ± 2.49	20.84 ± 0.0048	0.003 ± 37.7	3.94 ± 0.0037	0.117 ± 1.79	0.510 ± 2.75	63.4 ± 0.995	0.649 ± 3.31
RAR 2i	0.71377 ± 0.00003	0.579 ± 2.30	20.64 ± 0.0039	0.008 ± 16.0	2.37 ± 0.0028	0.141 ± 5.04	0.303 ± 9.35	52.7 ± 1.48	1.43 ± 4.40
RAR 3i	0.70913 ± 0.00003	0.255 ± 8.08	73.21 ± 0.0031	0.019 ± 10.2	1.96 ± 0.0045	0.088 ± 4.41	0.224 ± 2.72	72.1 ± 1.75	2.37 ± 3.97
RAR 3R	0.70889 ± 0.00003	0.305 ± 3.72	64.38 ± 0.0021	0.010 ± 9.76	5.91 ± 0.0042	0.568 ± 3.46	0.416 ± 9.01	128 ± 2.36	2.57 ± 2.65
RAR 5	0.70995 ± 0.00003	3.930 ± 2.60	57.99 ± 0.0058	0.027 ± 7.43	7.53 ± 0.0017	0.492 ± 1.94	3.05 ± 3.20	76.9 ± 1.81	4.55 ± 3.28
PIETR	0.71359 ± 0.00003	2.203 ± 2.86	45.18 ± 0.0028	0.149 ± 1.17	12.2 ± 0.0039	6.97 ± 0.887	0.297 ± 5.81	127 ± 1.65	183 ± 0.92
CHIRIL 2i	0.71575 ± 0.00003	0.376 ± 4.01	7.79 ± 0.0045	0.007 ± 9.42	1.87 ± 0.0024	0.485 ± 1.39	0.188 ± 10.1	30.7 ± 1.20	6.19 ± 1.64
CAL 1	0.70862 ± 0.00003	0.079 ± 9.65	2.67 ± 0.0028	<LOD	0.844 ± 0.0038	0.024 ± 9.46	3.380 ± 5.09	14.0 ± 2.75	1.55 ± 3.19
CAL 2i	0.70904 ± 0.00003	4.83 ± 2.64	94.31 ± 0.0031	2.04 ± 0.777	33.8 ± 0.0023	4.29 ± 2.10	8.71 ± 1.97	249 ± 1.65	639 ± 1.47
CAL 2R	0.70862 ± 0.00003	0.484 ± 5.71	8.97 ± 0.0035	0.074 ± 4.19	2.61 ± 0.0015	0.197 ± 1.95	4.93 ± 3.42	43.5 ± 1.32	15.3 ± 0.991
CAL 3i	0.70820 ± 0.00003	0.181 ± 5.15	8.14 ± 0.0010	0.005 ± 20.0	1.71 ± 0.0037	0.150 ± 2.71	4.52 ± 3.74	32.7 ± 0.985	6.15 ± 2.47

*LODs for Cd and Pb are 0.001, and 0.008, respectively.

Table A.11: $^{87}Sr/^{86}Sr$ isotope ratios and concentrations expressed in mg kg^{-1} of selected elements with SDs in bioavailable soil fraction samples from Eastern Carpathians, Romania.

Sample code	$^{87}Sr/^{86}Sr$	As	Cd	Pb	Rb	Sr	Zn
ROD 1	0.72289 ± 0.00005	0.0069 ± 0.0001	0.0135 ± 0.0002	0.0390 ± 0.0009	0.191 ± 0.0025	10.3 ± 0.0586	0.302 ± 0.0030
ROD 2	0.71366 ± 0.00005	0.0423 ± 0.0003	0.169 ± 0.0129	6.84 ± 0.0410	0.0534 ± 0.0083	0.628 ± 0.0697	1.95 ± 0.218
ROD 6	0.71063 ± 0.00005	0.0568 ± 0.0106	0.0814 ± 0.0068	3.31 ± 0.865	0.177 ± 0.0059	1.14 ± 0.0296	2.52 ± 0.121
ROD 7	0.70919 ± 0.00005	0.0043 ± 0.0023	0.0151 ± 0.0009	0.0703 ± 0.0008	0.590 ± 0.0231	10.0 ± 0.467	0.187 ± 0.0069
ROD 8a	0.71664 ± 0.00005	0.0029 ± 0.0009	0.0074 ± 0.0003	0.0157 ± 0.0013	0.120 ± 0.0041	1.55 ± 0.0189	0.105 ± 0.0013
ROD 8b	0.71616 ± 0.00005	0.0010 ± 0.0001	0.0014 ± 0.0001	0.0046 ± 0.0011	0.267 ± 0.0069	2.25 ± 0.0019	0.0115 ± 0.0003
RAR 1	0.73157 ± 0.00005	0.0226 ± 0.0004	0.0546 ± 0.0025	1.85 ± 0.0467	0.0807 ± 0.0059	0.907 ± 0.0477	3.63 ± 0.159
RAR 2	0.72462 ± 0.00005	0.0053 ± 0.0002	0.0248 ± 0.0022	0.405 ± 0.291	0.607 ± 0.0475	0.467 ± 0.0358	1.88 ± 0.337
RAR 3 Si	0.71082 ± 0.00005	0.0048 ± 0.0002	0.0344 ± 0.0026	0.926 ± 0.0067	1.05 ± 0.0863	2.83 ± 0.178	0.886 ± 0.0702
RAR 3 Ca	0.70957 ± 0.00005	<LOD	0.0016 ± 0.0004	0.0022 ± 0.0015	0.432 ± 0.0143	3.92 ± 0.0347	0.0057 ± 0.0008
RAR 4	0.70884 ± 0.00005	0.182 ± 0.0217	0.0138 ± 0.0024	0.0302 ± 0.0085	0.162 ± 0.0043	18.6 ± 1.76	0.103 ± 0.0082
RAR 5	0.71345 ± 0.00005	<LOD	0.0001 ± 0.000	0.0002 ± 0.000	0.594 ± 0.0709	0.838 ± 0.0275	0.0093 ± 0.0000

Sample code	$^{87}Sr/^{86}Sr$	As	Cd	Pb	Rb	Sr	Zn
PIETR	0.71925 ± 0.00005	0.0155 ± 0.0002	0.119 ± 0.0010	0.136 ± 0.0048	1.18 ± 0.0084	7.24 ± 0.0067	0.388 ± 0.0000
CHIRIL	0.71717 ± 0.00005	0.0048 ± 0.0002	0.0227 ± 0.0004	0.272 ± 0.0102	0.216 ± 0.0054	2.18 ± 0.0432	1.32 ± 0.0121
RUSCA	0.71009 ± 0.00005	0.0013 ± 0.0003	0.0011 ± 0.0001	0.0005 ± 0.0005	0.0331 ± 0.0025	9.03 ± 0.0915	0.0087 ± 0.0011
CAL 1	0.70954 ± 0.00005	0.0022 ± 0.0011	0.0619 ± 0.0011	0.0528 ± 0.0002	1.96 ± 0.0447	0.632 ± 0.0152	1.42 ± 0.0488
CAL 2	0.71108 ± 0.00005	0.0050 ± 0.0004	0.0278 ± 0.0002	1.90 ± 0.0236	0.433 ± 0.0001	0.896 ± 0.0150	0.877 ± 0.0941
CAL 3	0.70873 ± 0.00005	0.0026 ± 0.0017	0.0239 ± 0.0004	0.0031 ± 0.0004	3.87 ± 0.0090	33.5 ± 0.0420	0.304 ± 0.0020

*LOD for As is 0.0008.

Table A.12: $^{87}Sr/^{86}Sr$ isotope ratios and concentrations expressed in mg kg^{-1} of selected elements with SDs in bulk soil samples from Eastern Carpathians, Romania.

Sample code	$^{87}Sr/^{86}Sr$	As	Ca	Cd	Mg	Pb	Rb	Sr	Zn
ROD 1	0.73541 ± 0.0001	16.6 ± 0.599	2379 ± 104	0.715 ± 0.0471	9494 ± 161	34.3 ± 1.55	134 ± 1.42	121 ± 1.35	94.4 ± 2.00
ROD 2	0.73272 ± 0.0001	16.3 ± 0.216	571 ± 7.65	0.687 ± 0.0346	3846 ± 63.3	84.9 ± 2.17	87.6 ± 1.87	30.85 ± 0.642	30.9 ± 0.561
ROD 6	0.72632 ± 0.0001	13.8 ± 0.357	1737 ± 73.8	0.523 ± 0.0272	4038 ± 57.3	71.1 ± 2.78	59.7 ± 0.813	65.20 ± 0.724	56.4 ± 2.23
ROD 7	0.71888 ± 0.0001	6.87 ± 0.187	2254 ± 83.6	0.456 ± 0.0145	6999 ± 170	30.4 ± 1.10	74.4 ± 0.950	72.23 ± 1.66	70.3 ± 1.68
ROD 8a	0.72576 ± 0.0001	1.38 ± 0.081	1777 ± 58.4	<LOD	3910 ± 78.5	22.1 ± 0.739	156 ± 1.14	144 ± 1.27	30.3 ± 0.707
ROD 8b	0.73088 ± 0.0001	5.96 ± 0.355	4482 ± 161	0.267 ± 0.0460	4372 ± 75.1	31.3 ± 0.903	117 ± 1.48	102 ± 1.36	52.2 ± 0.861
RAR 1	0.76548 ± 0.0001	21.0 ± 0.671	698 ± 24.1	1.10 ± 0.0870	8623 ± 196	68.6 ± 1.82	197 ± 2.35	47.63 ± 0.543	119 ± 2.09
RAR 2	0.74347 ± 0.0001	8.51 ± 0.480	1346 ± 42.3	0.389 ± 0.1397	8489 ± 186	21.2 ± 0.640	161 ± 2.52	55.34 ± 0.864	64.6 ± 2.26
RAR 3 Si	0.72936 ± 0.0001	6.85 ± 0.219	1496 ± 39.3	0.238 ± 0.0125	9144 ± 138	55.2 ± 1.34	107 ± 2.13	41.54 ± 1.60	97.8 ± 3.34
RAR 3 Ca	0.71248 ± 0.0001	8.34 ± 0.196	118828 ± 1495	0.275 ± 0.100	25300 ± 867	21.3 ± 0.461	110 ± 2.00	201 ± 2.96	65.0 ± 1.90
RAR 4	0.71188 ± 0.0001	13.0 ± 0.393	42153 ± 417	2.79 ± 0.107	3173 ± 65.0	130 ± 4.38	34.8 ± 0.835	59.66 ± 1.07	97.4 ± 2.86
RAR 5	0.72128 ± 0.0001	10.1 ± 0.428	2245 ± 59.5	0.897 ± 0.0961	3188 ± 98.2	23.8 ± 1.05	118 ± 2.19	173 ± 2.42	78.3 ± 3.27
PIETR	0.72741 ± 0.0001	77.1 ± 0.410	2355 ± 74.8	1.48 ± 0.150	14416 ± 190	56.6 ± 2.40	139 ± 0.951	83.11 ± 2.03	176 ± 5.03
CHIRIL	0.74237 ± 0.0001	13.7 ± 0.452	3319 ± 134	0.647 ± 0.0582	12060 ± 152	44.8 ± 1.49	161 ± 2.05	76.11 ± 0.857	109 ± 4.20
RUSCA	0.70559 ± 0.0001	2.84 ± 0.139	39286 ± 564	0.348 ± 0.0844	25479 ± 306	10.5 ± 0.632	35.5 ± 0.396	643 ± 6.83	153 ± 2.09
CAL 1	0.70958 ± 0.0001	5.11 ± 0.287	9754 ± 274	1.00 ± 0.0211	7198 ± 147	38.7 ± 1.92	48.1 ± 1.04	145 ± 1.12	73.9 ± 3.13
CAL 2	0.71471 ± 0.0001	20.9 ± 0.277	1228 ± 149	0.372 ± 0.0597	2170 ± 42.6	75.0 ± 2.74	25.9 ± 0.784	36.21 ± 0.886	22.4 ± 0.444
CAL 3	0.70843 ± 0.0001	4.47 ± 0.237	22960 ± 162	1.72 ± 0.151	9514 ± 140	28.2 ± 0.765	28.4 ± 0.452	247 ± 0.947	83.3 ± 3.08

*LODs for Cd is 0.157.

Table A.13: $^{87}Sr/^{86}Sr$ isotope ratios and concentrations expressed in mg kg^{-1} of selected elements with SDs in wood samples (core segments) from Eastern Carpathians, Romania.

Sample code	$^{87}Sr/^{86}Sr$	Ca	Cd	K	Mg	Pb	Rb	Sr	Zn
ROD 2_1	0.71241 ± 0.00002	713 ± 12.9	0.0323 ± 0.0027	695 ± 5.81	106 ± 4.05	0.311 ± 0.0093	2.15 ± 0.0454	1.84 ± 0.118	9.27 ± 0.165

Sample code	$^{87}Sr/^{86}Sr$	Ca	Cd	K	Mg	Pb	Rb	Sr	Zn
ROD 2_2	0.71240 ± 0.00002	575 ± 3.20	0.0274 ± 0.0022	545 ± 4.30	87.3 ± 4.06	0.297 ± 0.0069	1.76 ± 0.0719	2.15 ± 0.0270	8.40 ± 0.220
ROD 2_3	0.71241 ± 0.00002	564 ± 16.7	0.0247 ± 0.0002	493 ± 5.09	92.2 ± 5.12	0.387 ± 0.0053	1.58 ± 0.0282	1.85 ± 0.0781	10.9 ± 0.167
ROD 2_4	0.71248 ± 0.00002	549 ± 10.6	0.0286 ± 0.0006	515 ± 5.44	93.1 ± 1.12	0.380 ± 0.0082	1.69 ± 0.0502	1.81 ± 0.0742	11.1 ± 0.559
ROD 2_5	0.71248 ± 0.00002	518 ± 13.2	0.0240 ± 0.0002	572 ± 4.79	110 ± 1.87	0.491 ± 0.0174	1.83 ± 0.0698	2.03 ± 0.0372	11.9 ± 0.252
ROD 2_6	0.71264 ± 0.00002	436 ± 2.15	0.0341 ± 0.0001	527 ± 8.27	106 ± 3.98	0.595 ± 0.0052	1.61 ± 0.0635	1.80 ± 0.0465	12.5 ± 0.368
ROD 2_7	0.71278 ± 0.00002	506 ± 18.4	0.0479 ± 0.0005	521 ± 4.45	117 ± 7.71	0.567 ± 0.0141	1.53 ± 0.0298	1.97 ± 0.0378	16.1 ± 0.140
ROD 2_8	0.71310 ± 0.00002	495 ± 7.63	0.0596 ± 0.0017	462 ± 5.92	129 ± 5.48	0.377 ± 0.0158	1.37 ± 0.0110	1.93 ± 0.0704	12.9 ± 0.0638
ROD 2_9	0.71336 ± 0.00002	649 ± 14.6	0.146 ± 0.0003	523 ± 8.42	169 ± 10.42	0.403 ± 0.0121	1.50 ± 0.0298	2.83 ± 0.176	23.6 ± 0.733
ROD 2_10	0.71368 ± 0.00002	809 ± 11.5	0.119 ± 0.0018	560 ± 7.54	156 ± 10.69	0.438 ± 0.0137	1.53 ± 0.133	2.66 ± 0.131	15.2 ± 0.255
ROD 6_1	0.70957 ± 0.00002	628 ± 10.3	0.0429 ± 0.0009	727 ± 14.6	95.3 ± 2.21	0.269 ± 0.0085	1.48 ± 0.0355	3.93 ± 0.0923	9.24 ± 0.0740
ROD 6_2	0.70927 ± 0.00002	746 ± 3.25	0.0544 ± 0.0021	529 ± 4.95	69.4 ± 3.05	0.566 ± 0.0053	0.698 ± 0.0351	5.24 ± 0.234	7.43 ± 0.108
ROD 6_3	0.70954 ± 0.00002	743 ± 39.4	0.0555 ± 0.0005	424 ± 9.44	75.2 ± 1.07	0.709 ± 0.0298	1.04 ± 0.0434	4.57 ± 0.226	8.71 ± 0.192
ROD 6_4	0.70947 ± 0.00002	686 ± 8.38	0.0554 ± 0.0027	392 ± 0.771	67.0 ± 2.06	0.704 ± 0.0204	0.820 ± 0.0137	4.09 ± 0.202	9.30 ± 0.119
ROD 6_5	0.70950 ± 0.00002	716 ± 13.0	0.0592 ± 0.0027	444 ± 3.00	70.3 ± 1.31	0.813 ± 0.0154	0.938 ± 0.0508	4.19 ± 0.102	8.38 ± 0.133
ROD 6_6	0.70950 ± 0.00002	711 ± 10.7	0.0887 ± 0.0008	409 ± 2.10	88.5 ± 4.10	0.714 ± 0.0066	0.826 ± 0.0044	4.08 ± 0.0098	16.3 ± 0.0942
ROD 6_7	0.70954 ± 0.00002	784 ± 48.6	0.0952 ± 0.0058	326 ± 2.50	97.2 ± 3.19	0.303 ± 0.0061	0.635 ± 0.0033	4.52 ± 0.131	9.07 ± 0.113
ROD 6_8	0.70952 ± 0.00002	899 ± 5.05	0.0889 ± 0.0024	260 ± 2.26	92.2 ± 3.93	0.225 ± 0.0084	0.440 ± 0.0269	4.55 ± 0.246	6.83 ± 0.124
ROD 6_9	0.70988 ± 0.00002	707 ± 16.0	0.160 ± 0.0083	183 ± 1.14	71.2 ± 2.18	0.316 ± 0.0163	0.508 ± 0.0013	3.46 ± 0.108	9.68 ± 0.277
ROD 6_10	0.70954 ± 0.00002	840 ± 10.0	0.0885 ± 0.0033	261 ± 2.10	93.3 ± 3.29	0.113 ± 0.0060	0.270 ± 0.0170	5.26 ± 0.182	10.6 ± 0.227
ROD 8_1	0.71547 ± 0.00002	729 ± 6.23	0.0425 ± 0.0019	709 ± 5.69	111 ± 3.80	0.161 ± 0.0032	1.78 ± 0.106	3.12 ± 0.114	10.4 ± 0.274
ROD 8_2	0.71512 ± 0.00002	633 ± 2.60	0.0249 ± 0.0012	331 ± 6.33	61.6 ± 3.01	0.199 ± 0.0048	0.888 ± 0.0473	2.46 ± 0.0362	7.25 ± 0.237
ROD 8_3	0.71500 ± 0.00002	807 ± 3.14	0.0408 ± 0.0023	564 ± 7.30	65.2 ± 0.15	0.286 ± 0.0015	1.22 ± 0.0217	2.97 ± 0.0260	8.15 ± 0.135
ROD 8_4	0.71515 ± 0.00002	651 ± 12.5	0.0178 ± 0.0006	370 ± 6.21	70.2 ± 1.24	0.202 ± 0.0137	0.872 ± 0.0430	2.74 ± 0.119	6.60 ± 0.101
ROD 8_5	0.71534 ± 0.00002	694 ± 13.4	0.0531 ± 0.0009	289 ± 4.33	73.1 ± 1.74	0.296 ± 0.0051	0.619 ± 0.0070	2.68 ± 0.0811	8.91 ± 0.316
ROD 8_6	0.71543 ± 0.00002	660 ± 10.6	0.0486 ± 0.0024	283 ± 2.90	78.5 ± 1.20	0.295 ± 0.0113	0.698 ± 0.0399	2.97 ± 0.115	6.90 ± 0.373
ROD 8_7	0.71547 ± 0.00002	700 ± 12.5	0.0278 ± 0.0004	282 ± 4.37	101 ± 0.989	0.407 ± 0.0055	0.663 ± 0.0337	3.03 ± 0.0888	8.25 ± 0.0440
ROD 8_8	0.71545 ± 0.00002	816 ± 7.06	0.0612 ± 0.0020	279 ± 3.94	119 ± 3.91	0.254 ± 0.0035	0.614 ± 0.0054	3.14 ± 0.0509	9.00 ± 0.153
ROD 8_9	0.71547 ± 0.00002	828 ± 35.0	0.0536 ± 0.0014	272 ± 5.43	132 ± 6.89	0.290 ± 0.0117	0.601 ± 0.0274	3.34 ± 0.180	8.49 ± 0.254
ROD 8_10	0.71538 ± 0.00002	904 ± 13.3	0.0478 ± 0.0026	257 ± 2.17	137 ± 6.73	0.329 ± 0.0124	0.537 ± 0.0278	3.54 ± 0.126	9.26 ± 0.273
RAR 1_1	0.72615 ± 0.00002	522 ± 5.29	0.0241 ± 0.0001	457 ± 7.43	70.8 ± 3.51	0.379 ± 0.0145	0.918 ± 0.0309	2.81 ± 0.0389	7.97 ± 0.159
RAR 1_2	0.72628 ± 0.00002	646 ± 11.1	0.0385 ± 0.0040	343 ± 5.66	53.9 ± 2.34	0.540 ± 0.0023	0.568 ± 0.0029	2.40 ± 0.0145	4.10 ± 0.189
RAR 1_3	0.72576 ± 0.00002	678 ± 29.0	0.0175 ± 0.0005	387 ± 4.12	62.6 ± 2.92	0.726 ± 0.0376	0.705 ± 0.0059	2.49 ± 0.0255	4.80 ± 0.193
RAR 1_4	0.72578 ± 0.00002	724 ± 1.94	0.0415 ± 0.0003	422 ± 4.52	73.2 ± 4.03	0.592 ± 0.0274	0.747 ± 0.0064	2.63 ± 0.0400	6.72 ± 0.186

Sample code	$^{87}Sr/^{86}Sr$	Ca	Cd	K	Mg	Pb	Rb	Sr	Zn
RAR 1_5	0.72598 ± 0.00002	769 ± 61.2	0.0457 ± 0.0006	404 ± 6.16	70.1 ± 0.248	0.892 ± 0.0104	0.664 ± 0.0120	2.81 ± 0.108	7.52 ± 0.172
RAR 1_6	0.72541 ± 0.00002	744 ± 20.2	0.0431 ± 0.0013	284 ± 3.15	69.7 ± 3.00	0.933 ± 0.0132	0.446 ± 0.0180	2.72 ± 0.0461	7.71 ± 0.202
RAR 1_7	0.72530 ± 0.00002	799 ± 19.5	0.0456 ± 0.0005	225 ± 5.12	67.2 ± 2.26	0.868 ± 0.0207	0.325 ± 0.0167	2.60 ± 0.0331	7.95 ± 0.142
RAR 1_8	0.72567 ± 0.00002	662 ± 27.6	0.0519 ± 0.0018	213 ± 4.52	70.1 ± 2.07	0.735 ± 0.0155	0.291 ± 0.0092	2.26 ± 0.0294	9.28 ± 0.149
RAR 1_9	0.72667 ± 0.00002	724 ± 29.8	0.0691 ± 0.0031	180 ± 1.74	72.0 ± 3.92	0.667 ± 0.0119	0.281 ± 0.0086	1.86 ± 0.0586	7.42 ± 0.301
RAR 1_10	0.72609 ± 0.00002	629 ± 26.9	0.0812 ± 0.0031	182 ± 1.35	68.2 ± 1.83	0.538 ± 0.0140	0.323 ± 0.0073	1.92 ± 0.0654	8.61 ± 0.307
RAR 2_1	0.71804 ± 0.00002	437 ± 4.50	0.351 ± 0.0145	413 ± 2.85	80.3 ± 3.40	0.267 ± 0.0053	1.01 ± 0.0292	1.87 ± 0.0450	8.90 ± 0.132
RAR 2_2	0.71795 ± 0.00002	530 ± 21.9	0.0626 ± 0.0028	325 ± 4.51	68.8 ± 4.18	0.338 ± 0.0043	0.793 ± 0.0106	2.12 ± 0.0623	8.66 ± 0.316
RAR 2_3	0.71800 ± 0.00002	625 ± 24.7	0.0431 ± 0.0018	346 ± 2.33	69.1 ± 1.95	0.410 ± 0.0045	0.775 ± 0.0195	2.13 ± 0.0513	14.1 ± 0.184
RAR 2_4	0.71759 ± 0.00002	586 ± 1.29	0.0569 ± 0.0019	368 ± 7.04	71.3 ± 2.19	0.315 ± 0.0089	0.815 ± 0.0183	2.28 ± 0.111	9.89 ± 0.522
RAR 2_5	0.71740 ± 0.00002	640 ± 29.9	0.0718 ± 0.0009	342 ± 0.566	72.5 ± 2.61	0.296 ± 0.0085	0.794 ± 0.0139	2.09 ± 0.0085	9.97 ± 0.260
RAR 2_6	0.71736 ± 0.00002	618 ± 28.1	0.0761 ± 0.0031	326 ± 5.10	73.5 ± 2.37	0.266 ± 0.0017	0.731 ± 0.0144	2.04 ± 0.0776	9.08 ± 0.256
RAR 2_7	0.71714 ± 0.00002	608 ± 64.5	0.0742 ± 0.0009	295 ± 4.05	91.7 ± 1.84	0.287 ± 0.0064	0.604 ± 0.0206	1.95 ± 0.0434	9.00 ± 0.126
RAR 2_8	0.71698 ± 0.00002	536 ± 46.5	0.0809 ± 0.0028	281 ± 0.604	86.3 ± 2.44	0.322 ± 0.0028	0.544 ± 0.0207	1.89 ± 0.0468	9.26 ± 0.286
RAR 2_9	0.71690 ± 0.00002	635 ± 48.4	0.112 ± 0.0006	278 ± 2.6	94.8 ± 2.32	0.221 ± 0.0086	0.466 ± 0.0222	1.82 ± 0.0528	9.22 ± 0.206
RAR 2_10	0.71683 ± 0.00002	564 ± 8.21	0.0961 ± 0.0014	299 ± 1.47	99.8 ± 2.35	0.202 ± 0.0064	0.492 ± 0.0191	1.88 ± 0.0271	9.63 ± 0.180
RAR 3_1	0.71219 ± 0.00002	675 ± 61.4	0.102 ± 0.0040	492 ± 3.69	102 ± 4.84	0.125 ± 0.0041	0.374 ± 0.0088	1.86 ± 0.0490	6.70 ± 0.129
RAR 3_2	0.71238 ± 0.00002	690 ± 19.8	0.0838 ± 0.0011	344 ± 6.64	74.2 ± 4.66	0.131 ± 0.0038	0.231 ± 0.0145	1.81 ± 0.0363	4.92 ± 0.272
RAR 3_3	0.71228 ± 0.00002	684 ± 39.5	0.0917 ± 0.0026	336 ± 6.72	79.4 ± 1.68	0.165 ± 0.0079	0.245 ± 0.0020	1.92 ± 0.0492	5.94 ± 0.234
RAR 3_4	0.71159 ± 0.00002	666 ± 33.6	0.108 ± 0.0007	336 ± 10.7	70.9 ± 4.04	0.194 ± 0.0093	0.277 ± 0.0157	2.25 ± 0.0424	5.64 ± 0.117
RAR 3_5	0.71208 ± 0.00002	819 ± 8.70	0.132 ± 0.0028	357 ± 2.92	82.9 ± 5.46	0.238 ± 0.0016	0.280 ± 0.0080	2.16 ± 0.0618	7.08 ± 0.0954
RAR 3_6	0.71224 ± 0.00002	771 ± 28.5	0.155 ± 0.0062	334 ± 4.57	77.3 ± 0.798	0.173 ± 0.0088	0.263 ± 0.0145	2.14 ± 0.0455	7.19 ± 0.308
RAR 3_7	0.71221 ± 0.00002	884 ± 57.0	0.167 ± 0.0013	299 ± 6.42	87.9 ± 2.26	0.232 ± 0.0074	0.232 ± 0.0024	2.21 ± 0.0510	6.82 ± 0.215
RAR 3_8	0.71241 ± 0.00002	738 ± 50.6	0.171 ± 0.0029	256 ± 3.97	77.6 ± 3.47	0.192 ± 0.0034	0.200 ± 0.0030	2.09 ± 0.0663	7.05 ± 0.0791
RAR 3_9	0.71257 ± 0.00002	897 ± 28.8	0.187 ± 0.0021	285 ± 2.73	92.4 ± 1.51	0.181 ± 0.0043	0.196 ± 0.0107	2.38 ± 0.177	14.2 ± 0.208
RAR 3_10	0.71307 ± 0.00002	1065 ± 35.8	0.180 ± 0.0024	307 ± 3.76	89.4 ± 0.683	0.093 ± 0.0005	0.135 ± 0.0015	2.34 ± 0.0592	6.49 ± 0.465
RAR 4_1	0.70883 ± 0.00002	701 ± 32.3	0.0104 ± 0.0013	426 ± 9.04	61.3 ± 3.77	0.026 ± 0.0017	1.10 ± 0.0382	2.71 ± 0.0940	6.23 ± 0.289
RAR 4_2	0.70877 ± 0.00002	728 ± 83.0	0.0263 ± 0.0124	274 ± 3.72	51.0 ± 0.975	0.043 ± 0.0015	0.826 ± 0.1008	3.11 ± 0.160	6.28 ± 0.507
RAR 4_3	0.70873 ± 0.00002	678 ± 15.2	0.0127 ± 0.0009	265 ± 5.28	54.6 ± 0.816	0.053 ± 0.0027	0.763 ± 0.0366	2.95 ± 0.0678	5.38 ± 0.136
RAR 4_4	0.70868 ± 0.00002	755 ± 48.0	0.0160 ± 0.0016	255 ± 3.60	55.8 ± 2.34	0.065 ± 0.0039	0.753 ± 0.0272	3.51 ± 0.1479	8.23 ± 0.432
RAR 4_5	0.70868 ± 0.00002	687 ± 48.9	0.0179 ± 0.0004	249 ± 5.92	49.3 ± 1.42	0.065 ± 0.0033	0.739 ± 0.0088	3.09 ± 0.0084	5.73 ± 0.0687
RAR 4_6	0.70871 ± 0.00002	751 ± 23.2	0.0267 ± 0.0010	281 ± 4.61	52.3 ± 2.04	0.082 ± 0.0046	0.664 ± 0.0196	3.06 ± 0.129	7.54 ± 0.186
RAR 4_7	0.70880 ± 0.00002	799 ± 21.5	0.0371 ± 0.0011	272 ± 6.78	57.7 ± 0.173	0.097 ± 0.0018	0.730 ± 0.0290	3.61 ± 0.0970	9.42 ± 0.261

Sample code	$^{87}Sr/^{86}Sr$	Ca	Cd	K	Mg	Pb	Rb	Sr	Zn
RAR 4_8	0.70878 ± 0.00002	845 ± 34.1	0.0387 ± 0.0008	319 ± 5.70	57.0 ± 4.35	0.091 ± 0.0003	0.748 ± 0.0439	3.63 ± 0.0861	8.98 ± 0.334
RAR 4_9	0.70878 ± 0.00002	906 ± 42.6	0.0499 ± 0.0029	320 ± 5.06	85.3 ± 3.97	0.070 ± 0.0006	0.754 ± 0.0277	3.57 ± 0.121	9.33 ± 0.323
RAR 4_10	0.70879 ± 0.00002	785 ± 21.0	0.0520 ± 0.0045	326 ± 2.27	73.0 ± 4.29	0.104 ± 0.0014	0.824 ± 0.0252	3.33 ± 0.0613	13.7 ± 0.647
PIETR 1	0.71795 ± 0.00002	672 ± 48.9	0.0695 ± 0.0027	488 ± 1.88	69.7 ± 1.56	0.086 ± 0.0035	0.828 ± 0.0171	4.69 ± 0.0653	5.39 ± 0.196
PIETR 2	0.71771 ± 0.00002	612 ± 48.2	0.0524 ± 0.0011	395 ± 1.56	58.5 ± 3.99	0.119 ± 0.0020	0.670 ± 0.0060	4.21 ± 0.0152	4.57 ± 0.0394
PIETR 3	0.71796 ± 0.00002	654 ± 38.9	0.0400 ± 0.0016	386 ± 5.41	64.0 ± 1.40	0.114 ± 0.0025	0.645 ± 0.0205	4.47 ± 0.142	5.63 ± 0.227
PIETR 4	0.71792 ± 0.00002	614 ± 40.0	0.0739 ± 0.0016	318 ± 5.08	66.6 ± 2.85	0.114 ± 0.0048	0.532 ± 0.0424	4.42 ± 0.0871	6.20 ± 0.139
PIETR 5	0.71806 ± 0.00002	533 ± 21.2	0.0490 ± 0.0023	335 ± 0.111	56.4 ± 1.29	0.137 ± 0.0031	0.616 ± 0.0961	4.44 ± 0.485	7.78 ± 1.033
PIETR 6	0.71821 ± 0.00002	583 ± 35.1	0.0540 ± 0.0007	295 ± 5.03	69.9 ± 3.34	0.094 ± 0.0029	0.528 ± 0.0031	4.34 ± 0.0962	6.00 ± 0.108
PIETR 7	0.71842 ± 0.00002	616 ± 17.9	0.0374 ± 0.0016	264 ± 1.61	62.7 ± 1.64	0.112 ± 0.0027	0.430 ± 0.0119	4.42 ± 0.0350	4.78 ± 0.110
PIETR 8	0.71825 ± 0.00002	639 ± 28.2	0.0486 ± 0.0013	235 ± 4.34	64.9 ± 2.79	0.110 ± 0.0039	0.426 ± 0.0182	4.19 ± 0.0151	4.63 ± 0.153
PIETR 9	0.71831 ± 0.00002	619 ± 37.0	0.0887 ± 0.0047	247 ± 1.92	80.2 ± 2.93	0.151 ± 0.0054	0.408 ± 0.0278	4.92 ± 0.0210	5.81 ± 0.227
PIETR 10	0.71830 ± 0.00002	589 ± 0.877	0.0643 ± 0.0011	215 ± 4.83	71.8 ± 2.03	0.057 ± 0.0050	0.363 ± 0.0121	4.62 ± 0.146	4.00 ± 0.0546
CAL 1_1	0.70997 ± 0.00002	638 ± 15.9	0.0327 ± 0.0016	621 ± 9.21	91.9 ± 2.29	0.170 ± 0.0063	4.49 ± 0.151	1.79 ± 0.112	8.93 ± 0.200
CAL 1_2	0.71001 ± 0.00002	542 ± 36.6	0.0586 ± 0.0026	428 ± 3.02	76.2 ± 4.51	0.242 ± 0.0052	3.01 ± 0.0931	1.78 ± 0.0503	9.10 ± 0.121
CAL 1_3	0.70998 ± 0.00002	648 ± 29.1	0.0505 ± 0.0021	380 ± 7.31	75.6 ± 4.14	0.226 ± 0.0010	2.49 ± 0.0741	1.95 ± 0.0742	7.95 ± 0.0592
CAL 1_4	0.71005 ± 0.00002	487 ± 10.9	0.0470 ± 0.0022	325 ± 1.57	71.8 ± 5.34	0.291 ± 0.0047	2.16 ± 0.121	1.76 ± 0.0353	8.73 ± 0.263
CAL 1_5	0.71007 ± 0.00002	586 ± 34.5	0.0458 ± 0.0012	359 ± 3.23	87.4 ± 4.72	0.416 ± 0.0068	2.35 ± 0.0512	1.75 ± 0.0567	8.67 ± 0.257
CAL 1_6	0.70995 ± 0.00002	599 ± 10.2	0.0573 ± 0.0033	341 ± 1.85	91.0 ± 5.25	0.335 ± 0.0084	2.11 ± 0.0973	1.71 ± 0.0840	8.87 ± 0.271
CAL 1_7	0.70990 ± 0.00002	590 ± 12.5	0.0631 ± 0.0011	373 ± 3.85	97.8 ± 3.86	0.247 ± 0.0044	2.39 ± 0.0411	1.98 ± 0.0726	9.71 ± 0.344
CAL 1_8	0.70992 ± 0.00002	531 ± 27.3	0.0699 ± 0.0015	354 ± 4.31	99.0 ± 5.17	0.217 ± 0.0071	2.28 ± 0.0243	1.87 ± 0.0306	9.20 ± 0.353
CAL 1_9	0.70990 ± 0.00002	638 ± 11.8	0.102 ± 0.0024	335 ± 3.12	101 ± 5.09	0.168 ± 0.0034	2.14 ± 0.122	2.02 ± 0.0908	10.6 ± 0.278
CAL 1_10	0.70981 ± 0.00002	616 ± 61.9	0.1113 ± 0.0048	342 ± 4.82	94.4 ± 2.09	0.179 ± 0.0042	2.02 ± 0.0992	1.98 ± 0.0480	12.5 ± 0.257
CAL 2_1	0.71063 ± 0.00002	1383 ± 73.7	<LOD	399 ± 9.06	195 ± 9.94	0.146 ± 0.0068	2.05 ± 0.112	3.79 ± 0.0794	9.22 ± 0.147
CAL 2_2	0.71061 ± 0.00002	866 ± 15.5	<LOD	308 ± 7.89	101 ± 1.42	0.161 ± 0.0068	1.38 ± 0.0668	3.95 ± 0.198	9.83 ± 0.350
CAL 2_3	0.71057 ± 0.00002	741 ± 24.4	<LOD	305 ± 3.80	89.5 ± 4.82	0.143 ± 0.0049	1.32 ± 0.0528	3.64 ± 0.166	8.16 ± 0.114
CAL 2_4	0.71060 ± 0.00002	654 ± 8.06	<LOD	293 ± 5.52	81.4 ± 3.32	0.315 ± 0.0099	1.22 ± 0.0787	3.31 ± 0.184	8.95 ± 0.100
CAL 2_5	0.71055 ± 0.00002	809 ± 3.65	0.0135 ± 0.0006	301 ± 3.11	114 ± 1.48	0.188 ± 0.0091	1.20 ± 0.0198	3.42 ± 0.114	11.0 ± 0.254
CAL 2_6	0.71049 ± 0.00002	667 ± 13.9	0.0119 ± 0.0005	277 ± 3.25	117 ± 6.52	0.197 ± 0.0100	1.07 ± 0.0569	3.50 ± 0.138	10.3 ± 0.185
CAL 2_7	0.71053 ± 0.00002	713 ± 15.9	0.0183 ± 0.0008	283 ± 6.03	110 ± 3.66	0.167 ± 0.0041	1.16 ± 0.0869	3.07 ± 0.140	9.94 ± 0.361
CAL 2_8	0.71053 ± 0.00002	608 ± 9.35	0.0169 ± 0.0009	257 ± 2.73	95.1 ± 0.936	0.164 ± 0.0044	0.981 ± 0.0165	2.82 ± 0.160	9.86 ± 0.268
CAL 2_9	0.71052 ± 0.00002	643 ± 6.85	0.0121 ± 0.0005	263 ± 2.15	102 ± 3.84	0.191 ± 0.0029	0.971 ± 0.0318	2.95 ± 0.117	9.87 ± 0.151
CAL 2_10	0.71052 ± 0.00002	679 ± 22.4	0.0193 ± 0.0009	242 ± 6.13	98.1 ± 0.652	0.206 ± 0.0018	0.851 ± 0.0270	2.98 ± 0.156	9.54 ± 0.298

Sample code	$^{87}Sr/^{86}Sr$	Ca	Cd	K	Mg	Pb	Rb	Sr	Zn
CAL 3_1	0.70845 ± 0.00002	690 ± 21.7	0.0318 ± 0.0005	732 ± 2.46	95.9 ± 4.03	0.630 ± 0.0080	2.82 ± 0.0537	7.20 ± 0.247	14.7 ± 0.121
CAL 3_2	0.70849 ± 0.00002	804 ± 24.0	0.0249 ± 0.0006	603 ± 6.11	86.8 ± 1.20	0.733 ± 0.0093	2.46 ± 0.0476	6.71 ± 0.155	17.3 ± 0.331
CAL 3_3	0.70851 ± 0.00002	686 ± 17.4	0.0297 ± 0.0007	499 ± 4.93	86.8 ± 2.92	0.556 ± 0.0178	1.87 ± 0.0252	6.93 ± 0.269	11.5 ± 0.176
CAL 3_4	0.70856 ± 0.00002	771 ± 4.34	0.0239 ± 0.0009	487 ± 1.99	88.7 ± 5.27	0.645 ± 0.0198	1.70 ± 0.0172	8.41 ± 0.178	15.0 ± 0.247
CAL 3_5	0.70849 ± 0.00002	840 ± 1.96	0.0257 ± 0.0015	372 ± 6.42	76.5 ± 2.70	0.472 ± 0.0247	1.27 ± 0.0287	8.32 ± 0.0776	10.9 ± 0.279
CAL 3_6	0.70851 ± 0.00002	849 ± 15.1	0.0227 ± 0.0026	309 ± 3.49	69.4 ± 1.97	0.462 ± 0.0079	1.04 ± 0.0682	7.97 ± 0.177	10.9 ± 0.429
CAL 3_7	0.70855 ± 0.00002	803 ± 19.8	0.0329 ± 0.0002	295 ± 6.40	75.3 ± 1.13	0.427 ± 0.0109	0.964 ± 0.0503	7.89 ± 0.336	11.2 ± 0.340
CAL 3_8	0.70843 ± 0.00002	772 ± 14.3	0.0377 ± 0.0007	285 ± 5.99	83.8 ± 6.97	0.328 ± 0.0018	0.917 ± 0.0111	7.57 ± 0.131	11.3 ± 0.111
CAL 3_9	0.70842 ± 0.00002	748 ± 12.9	0.0338 ± 0.0007	279 ± 4.88	79.6 ± 2.99	0.353 ± 0.0079	0.929 ± 0.0141	7.99 ± 0.278	11.8 ± 0.0780
CAL 3_10	0.70849 ± 0.00002	730 ± 2.88	0.0454 ± 0.0016	320 ± 6.70	80.9 ± 3.76	0.478 ± 0.0043	0.937 ± 0.0125	8.03 ± 0.252	14.0 ± 0.160

*LOD for Cd is 0.003.

References

Abbyad, P., Tromp, J., Lamb, J., & Salin, E. (2001). Optimization of the technique of standard additions for inductively coupled plasma mass spectrometry. *Journal of Analytical Atomic Spectrometry*, *16*(5), 464–469. https://doi.org/10.1039/B100672J

Åberg, G., Jacks, G., & Joseph Hamilton, P. (1989). Weathering rates and 87Sr/86Sr ratios: An isotopic approach. *Journal of Hydrology*, *109*(1–2), 65–78. https://doi.org/10.1016/0022-1694(89)90007-3

Adams, S., Grün, R., McGahan, D., Zhao, J. X., Feng, Y., Nguyen, A., Willmes, M., Quaresimin, M., Lobsey, B., Collard, M., & Westaway, M. C. (2019). A strontium isoscape of north-east Australia for human provenance and repatriation. *Geoarchaeology*, *34*(3), 231–251. https://doi.org/10.1002/GEA.21728

Aggarwal, J. K., Mezger, K., Pernicka, E., & Meixner, A. (2004). The effect of instrumental mass bias on δ11B measurements: A comparison between thermal ionisation mass spectrometry and multiple-collector ICP-MS. *International Journal of Mass Spectrometry*, *232*(3), 259–263. https://doi.org/10.1016/j.ijms.2004.01.016

Aguzzoni, A., Bassi, M., Robatscher, P., Scandellari, F., Tirler, W., & Tagliavini, M. (2019). Intra- And intertree variability of the 87Sr/86Sr ratio in apple orchards and its correlation with the soil 87Sr/86Sr ratio. *Journal of Agricultural and Food Chemistry*, *67*(20), 5728–5735. https://doi.org/10.1021/ACS.JAFC.9B01082/ASSET/IMAGES/LARGE/JF-2019-01082E_0006.JPEG

Aguzzoni, A., Bassi, M., Robatscher, P., Tagliavini, M., Tirler, W., & Scandellari, F. (2018). Plant Sr Isotope Ratios As Affected by the Sr Isotope Ratio of the Soil and of the External Sr Inputs. *Journal of Agricultural and Food Chemistry*, *66*(40), 10513–10521. https://doi.org/10.1021/acs.jafc.8b02604

Albarède, F., Telouk, P., Blichert-Toft, J., Boyet, M., Agranier, A., Nelson, B., Albarède, F., Telouk, P., Blichert-Toft, J., Boyet, M., Agranier, A., & Nelson, B. (2004). Precise and accurate isotopic measurements using multiple-collector ICPMS. *GeCoA*, *68*(12), 2725–2744. https://doi.org/10.1016/J.GCA.2003.11.024

Alonzi, E., Pacheco-Forés, S. I., Gordon, G. W., Kuijt, I., & Knudson, K. J. (2020). New understandings of the sea spray effect and its impact on bioavailable radiogenic strontium isotope ratios in coastal environments. *Journal of Archaeological Science: Reports*, *33*, 102462. https://doi.org/10.1016/J.JASREP.2020.102462

Amais, R. S., Moreau, P. S., Francischini, D. S., Magnusson, R., Locosselli, G. M., Godoy-Veiga, M., Ceccantini, G., Ortega Rodriguez, D. R., Tomazello-Filho, M., & Arruda, M. A. Z. (2021). Trace elements distribution in tropical tree rings through high-

resolution imaging using LA-ICP-MS analysis. *Journal of Trace Elements in Medicine and Biology*, *68*, 126872. https://doi.org/10.1016/J.JTEMB.2021.126872

Andrews, M. G., Jacobson, A. D., Lehn, G. O., Horton, T. W., & Craw, D. (2016). Radiogenic and stable Sr isotope ratios (87Sr/86Sr, δ88/86Sr) as tracers of riverine cation sources and biogeochemical cycling in the Milford Sound region of Fiordland, New Zealand. *Geochimica et Cosmochimica Acta*, *173*, 284–303. https://doi.org/10.1016/J.GCA.2015.10.005

Andriessen, P. A. M., Boelrijk, N. A. I. M., Hebeda, E. H., Priem, H. N. A., Verdurnen, E. A. T., & Verschure, R. H. (1979). Dating the events of metamorphism and granitic magmatism in the Alpine orogen of Naxos (Cyclades, Greece). *Contributions to Mineralogy and Petrology*, *69*(3), 215–225. https://doi.org/10.1007/BF00372323/METRICS

Angino, E. E., Billings, G. K., & Andersen, N. (1966). Observed variations in the strontium concentration of sea water. *Chemical Geology*, *1*(C), 145–153. https://doi.org/10.1016/0009-2541(66)90013-1

Apostol, E. N., & Budeanu, M. (2019). Adaptability of Narrow-Crowned Norway Spruce Ideotype (Picea abies (L.) Karst. pendula Form) in 25 Years Half-Sib Comparative Trials in the Eastern Carpathians. *Forests 2019, Vol. 10, Page 395*, *10*(5), 395. https://doi.org/10.3390/F10050395

Baffi, C., & Trincherini, P. R. (2016). Food traceability using the 87Sr/86Sr isotopic ratio mass spectrometry. *European Food Research and Technology 2016 242:9*, *242*(9), 1411–1439. https://doi.org/10.1007/S00217-016-2712-2

Balcaen, L., Schrijver, I. De, Moens, L., Vanhaecke, F., Balcaen, L., Schrijver, I. De, Moens, L., & Vanhaecke, F. (2005). Determination of the 87Sr/86Sr isotope ratio in USGS silicate reference materials by multi-collector ICP-mass spectrometry. *IJMSp*, *242*(2–3), 251–255. https://doi.org/10.1016/J.IJMS.2004.10.025

Barbaste, M., Barbaste, M., Robinson, K., Guilfoyle, S., Medina, B., & Lobinski, R. (2002). Precise determination of the strontium isotope ratios in wine by inductively coupled plasma sector field multicollector mass spectrometry (ICP-SF-MC-MS). *Journal of Analytical Atomic Spectrometry*, *17*(2), 135–137. https://doi.org/10.1039/B109559P

Bataille, C. P., & Bowen, G. J. (2012). Mapping 87Sr/ 86Sr variations in bedrock and water for large scale provenance studies. *Chemical Geology*, *304–305*, 39–52. https://doi.org/10.1016/j.chemgeo.2012.01.028

Bataille, C. P., Crowley, B. E., Wooller, M. J., & Bowen, G. J. (2020). Advances in global bioavailable strontium isoscapes. *Palaeogeography, Palaeoclimatology, Palaeoecology*, *555*, 109849. https://doi.org/10.1016/J.PALAEO.2020.109849

Becker, J. S. (2005). Recent developments in isotope analysis by advanced mass spectrometric techniques. *Journal of Analytical Atomic Spectrometry*, *20*(11), 1173–1184. https://doi.org/10.1039/B508895J

Beeckman, H., Jolivet-Blanc, C., Boeschoten, L., Braga, J. W. B., Cabezas, J. A., Chaix, G., Crameri, S., Degen, B., Deklerck, V., Dormontt, E., Espinoza, E., Gasson, P., Haag, V., Helmling, S., Horacek, M., Koch, G., Lancaster, C., Lens, F., Lowe, A., … Zuidema, P. (2020). Overview of current practices in data analysis for wood identification: a guide for the different timber tracking methods. *In: Schmitz, N., Ed.*

GTTN, Global Timber Tracking Network: GTTN Secretariat: European Forest Institute and Thunen Institute. 143 p. https://doi.org/10.13140/RG.2.2.21518.79689

Bernabei, M., & Bontadi, J. (2011). Determining the resonance wood provenance of stringed instruments from the Cherubini Conservatory Collection in Florence, Italy. *Journal of Cultural Heritage*, *12*(2), 196–204. https://doi.org/10.1016/J.CULHER.2010.12.001

Blake, G. M., & Fogelman, I. (2006). Strontium ranelate: a novel treatment for postmenopausal osteoporosis: a review of safety and efficacy. *Clinical Interventions in Aging*, *1*(4), 367. https://doi.org/10.2147/CIIA.2006.1.4.367

Blum, J. D., Erel, Y., & Brown, K. (1993). 87Sr/86Sr ratios of sierra nevada stream waters: Implications for relative mineral weathering rates. *Geochimica et Cosmochimica Acta*, *57*(21–22), 5019–5025. https://doi.org/10.1016/S0016-7037(05)80014-6

Boeschoten, L. E., Sass-Klaassen, U., Vlam, M., Comans, R. N. J., Koopmans, G. F., Meyer-Sand, B. R. V., Tassiamba, S. N., Tchamba, M. T., Zanguim, H. T., Zemtsa, P. T., & Zuidema, P. A. (2022). Clay and soil organic matter drive wood multi-elemental composition of a tropical tree species: Implications for timber tracing. *Science of the Total Environment*, *849*. https://doi.org/10.1016/j.scitotenv.2022.157877

Boeschoten, L. E., Vlam, M., Sass-Klaassen, U., Rocha Venâncio Meyer-Sand, B., Adzkia, U., Bouka, G. D. U., Ciliane-Madikou, J. C. U., Engone Obiang, N. L., Guieshon-Engongoro, M., Loumeto, J. J., Mbika, D. M. M. F., Moundounga, C. G., Ndangani, R. M. D., Bourobou, D. N., Rahman, M. M., Siregar, I. Z., Tassiamba, S. N., Tchamba, M. T., Toumba-Paka, B. B. L., … Zuidema, P. A. (2023). A new method for the timber tracing toolbox: applying multi-element analysis to determine wood origin. *Environmental Research Letters*, *18*(5), 054001. https://doi.org/10.1088/1748-9326/ACC81B

Bontempo, L., Barbero, A., Bertoldi, D., Camin, F., Larcher, R., Perini, M., Sepulcri, A., Zicarelli, L., & Piasentier, E. (2019). Isotopic and elemental profiles of Mediterranean buffalo milk and cheese and authentication of Mozzarella di Bufala Campana PDO: An initial exploratory study. *Food Chemistry*, *285*, 316–323. https://doi.org/10.1016/J.FOODCHEM.2019.01.160

Bontempo, L., Larcher, R., Camin, F., Hölzl, S., Rossmann, A., Horn, P., & Nicolini, G. (2011). Elemental and isotopic characterisation of typical Italian alpine cheeses. *International Dairy Journal*, *21*(6), 441–446. https://doi.org/10.1016/j.idairyj.2011.01.009

Bontempo, L., Lombardi, G., Paoletti, R., Ziller, L., & Camin, F. (2012). H, C, N and O stable isotope characteristics of alpine forage, milk and cheese. *International Dairy Journal*, *23*(2), 99–104. https://doi.org/10.1016/j.idairyj.2011.10.005

Bora, F. D., Donici, A., Rusu, T., Bunea, A., Popescu, D., & Bunea, C. I. (2018). Elemental profile and 207Pb/206Pb, 208Pb/206Pb, 204Pb/206Pb, 87Sr/86Sr isotope ratio as fingerprints for geographical traceability of Romanian wines. *Notulae Botanicae Horti Agrobotanici Cluj-Napoca*, *46*(1), 223–239. https://doi.org/10.15835/nbha46110853

Boral, S., Peucker-Ehrenbrink, B., Hemingway, J. D., Sen, I. S., Galy, V., & Fiske, G. J. (2021). Controls on short-term dissolved 87Sr/86Sr variations in large rivers: Evidence

from the Ganga–Brahmaputra. *Earth and Planetary Science Letters*, *566*, 116958. https://doi.org/10.1016/J.EPSL.2021.116958

Bozoudi, D., Pavlidou, S., Kotzamanidis, C., Georgakopoulos, P., Torriani, S., Kondyli, E., Claps, S., Belibasaki, S., & Litopoulou-Tzanetaki, E. (2016). "Graviera Naxou and Graviera Kritis Greek PDO cheeses: Discrimination based on microbiological and physicochemical criteria and volatile organic compounds profile." *Small Ruminant Research*, *136*, 161–172. https://doi.org/10.1016/J.SMALLRUMRES.2016.01.022

Brass, G. W. (1975). The effect of weathering on the distribution of strontium isotopes in weathering profiles. *Geochimica et Cosmochimica Acta*, *39*(12), 1647–1653. https://doi.org/10.1016/0016-7037(75)90086-1

Bratu, I. A., Dinca, L. C., Enescu, C. M., & Stanciu, M. (2022). The Role of Social Media in Public Forest Management Policies during COVID-19: Implications for Stakeholder Engagement. *Sustainability 2022, Vol. 14, Page 3778*, *14*(7), 3778. https://doi.org/10.3390/SU14073778

Brichau, S. (2004). *Constraining the tectonic evolution of extensional fault systems in the Cyclades (Greece) using low-temperature thermochronology.* https://theses.hal.science/tel-00006814

Bullen, T., White, A., Blum, A., Harden, J., & Schulz, M. (1997). Chemical weathering of a soil chronosequence on granitoid alluvium: II. Mineralogic and isotopic constraints on the behavior of strontium. *Geochimica et Cosmochimica Acta*, *61*(2), 291–306. https://doi.org/10.1016/S0016-7037(96)00344-4

Burger, A., & Lichtscheidl, I. (2019). Strontium in the environment: Review about reactions of plants towards stable and radioactive strontium isotopes. *Science of The Total Environment*, *653*, 1458–1512. https://doi.org/10.1016/J.SCITOTENV.2018.10.312

Čabalová, I., Bélik, M., Kučerová, V., & Jurczyková, T. (2021). Chemical and Morphological Composition of Norway Spruce Wood (Picea abies, L.) in the Dependence of Its Storage. *Polymers*, *13*(10). https://doi.org/10.3390/POLYM13101619

Cao, S., Neubauer, F., Bernroider, M., & Liu, J. (2013). The lateral boundary of a metamorphic core complex: The Moutsounas shear zone on Naxos, Cyclades, Greece. *Journal of Structural Geology*, *54*, 103–128. https://doi.org/10.1016/J.JSG.2013.07.002

Capo, R. C., Stewart, B. W., & Chadwick, O. A. (1998). Strontium isotopes as tracers of ecosystem processes: theory and methods. *Geoderma*, *82*, 197–225.

Cardot, V., Le Roux, Y., & Jurjanz, S. (2008). Drinking Behavior of Lactating Dairy Cows and Prediction of Their Water Intake. *Journal of Dairy Science*, *91*(6), 2257–2264. https://doi.org/10.3168/JDS.2007-0204

Cavazzini, G. (2009). Rayleigh's distillation law and linear hypothesis of isotope fractionation in thermal ionization mass spectrometry. *International Journal of Mass Spectrometry*, *288*(1–3), 84–91. https://doi.org/10.1016/j.ijms.2009.09.002

Cavazzini, G., Roccato, D., & Fasson, A. (2022). The determination of the isotopic composition of strontium. *International Journal of Mass Spectrometry*, *471*. https://doi.org/10.1016/j.ijms.2021.116757

Cellier, R., Bérail, S., Barre, J., Epova, E., Ronzani, A. L., Van Leeuwen, C., Milcent, S., Ors, P., & Donard, O. F. X. (2021). Specificity and Origin of the Stability of the Sr Isotopic Ratio in Champagne Wines. *Molecules*, *26*(16). https://doi.org/10.3390/MOLECULES26165104

Chadwick, O. A., Derry, L. A., Bern, C. R., & Vitousek, P. M. (2009). Changing sources of strontium to soils and ecosystems across the Hawaiian Islands. *Chemical Geology*, *267*(1–2), 64–76. https://doi.org/10.1016/J.CHEMGEO.2009.01.009

Choi, H. Bin, Lee, K. S., Park, S., Jeong, E. K., Gautam, M. K., & Shin, W. J. (2023). National-scale distribution of strontium isotope ratios in environmental samples from South Korea and its implications for provenance studies. *Chemosphere*, *317*, 137895. https://doi.org/10.1016/J.CHEMOSPHERE.2023.137895

Colin, C., Turpin, L., Blamart, D., Frank, N., Kissel, C., & Duchamp, S. (2006). Evolution of weathering patterns in the Indo-Burman Ranges over the last 280 kyr: Effects of sediment provenance on 87Sr/86Sr ratios tracer. *Geochemistry, Geophysics, Geosystems*, *7*(3), 3007. https://doi.org/10.1029/2005GC000962

Commission Regulation (EC) No 1107/96 of 12 June 1996 on the Registration of Geographical Indications and Designations of Origin under the Procedure laid down in Article 17 of Council Regulation (EEC) No 2081/92, Official Journal of the European Communities (1996).

Commission Regulation (EU) 2023/915 on Maximum Levels for Certain Contaminants in Food and Repealing Regulation (EC) No 1881/2006, Official Journal of the European Union (2023). https://eur-lex.europa.eu/legal-content/EN/TXT/?uri=CELEX:32023R0915

Council Directive 98/83/EC of 3 November 1998 on the Quality of Water Intended for Human Consumption, Official Journal of the European Communities (1998). https://eur-lex.europa.eu/legal-content/EN/TXT/?uri=OJ:L:1998:330:TOC

Council Regulation (EC) No 510/2006 on the Protection of Geographical Indications and Designations of Origin for Agricultural Products and Foodstuffs, Official Journal of the European Union (2006).

Crittenden, R. G., Andrew, A. S., Lefournour, M., Young, M. D., Middleton, H., & Stockmann, R. (2007). Determining the geographic origin of milk in Australasia using multi-element stable isotope ratio analysis. *International Dairy Journal*, *17*, 421–428. https://doi.org/10.1016/j.idairyj.2006.05.012

D'Andrea, R., Corona, C., Poszwa, A., Belingard, C., Domínguez-Delmás, M., Stoffel, M., Crivellaro, A., Crouzevialle, R., Cerbelaud, F., Costa, G., & Paradis-Grenouillet, S. (2023). Combining conventional tree-ring measurements with wood anatomy and strontium isotope analyses enables dendroprovenancing at the local scale. *Science of The Total Environment*, *858*, 159887. https://doi.org/10.1016/J.SCITOTENV.2022.159887

Danezis, G. P., Tsagkaris, A. S., Brusic, V., & Georgiou, C. A. (2016). Food authentication: state of the art and prospects. *Current Opinion in Food Science*, *10*, 22–31. https://doi.org/10.1016/J.COFS.2016.07.003

Danezis, G. P., Tsagkaris, A. S., Camin, F., Brusic, V., & Georgiou, C. A. (2016). Food authentication: Techniques, trends & emerging approaches. *TrAC Trends in Analytical Chemistry*, *85*, 123–132. https://doi.org/10.1016/J.TRAC.2016.02.026

Danezis, G., Theodorou, C., Massouras, T., Zoidis, E., Hadjigeorgiou, I., & Georgiou, C. A. (2019). Greek Graviera Cheese Assessment through Elemental Metabolomics—Implications for Authentication, Safety and Nutrition. *Molecules 2019, Vol. 24, Page 670*, *24*(4), 670. https://doi.org/10.3390/MOLECULES24040670

Dauphas, N., & Schauble, E. A. (2016). Mass Fractionation Laws, Mass-Independent Effects, and Isotopic Anomalies. *Annual Review of Earth and Planetary Sciences*, *44*(Volume 44, 2016), 709–783. https://doi.org/10.1146/ANNUREV-EARTH-060115-012157/1

Deklerck, V. (2023). Timber origin verification using mass spectrometry: Challenges, opportunities, and way forward. *Forensic Science International: Animals and Environments*, *3*, 100057. https://doi.org/10.1016/J.FSIAE.2022.100057

De Muynck, D., Huelga-Suarez, G., Van Heghe, L., Degryse, P., & Vanhaecke, F. (2009). Systematic evaluation of a strontium-specific extraction chromatographic resin for obtaining a purified Sr fraction with quantitative recovery from complex and Ca-rich matrices. *Journal of Analytical Atomic Spectrometry*, *24*(11), 1498–1510. https://doi.org/10.1039/b908645e

De Souza, G. F., Reynolds, B. C., Kiczka, M., & Bourdon, B. (2010). Evidence for mass-dependent isotopic fractionation of strontium in a glaciated granitic watershed. *Geochimica et Cosmochimica Acta*, *74*(9), 2596–2614. https://doi.org/https://doi.org/10.1016/j.gca.2010.02.012

Dimara, E., & Skuras, D. (2005). Consumer demand for informative labeling of quality food and drink products: a European Union case study. *Journal of Consumer Marketing*, *22*(2), 90–100. https://www.academia.edu/13260061/Consumer_demand_for_informative_labeling_of_quality_food_and_drink_products_a_European_Union_case_study

Dimitrakopoulou, M. E., & Vantarakis, A. (2023). Does Traceability Lead to Food Authentication? A Systematic Review from A European Perspective. *Food Reviews International*, *39*(1), 537–559. https://doi.org/10.1080/87559129.2021.1923028

Directive 2002/32/EC of the European Parliament and of the Council of 7 May 2002 on Undesirable Substances in Animal Feed, Official Journal of the European Communities (2002). https://eur-lex.europa.eu/legal-content/EN/TXT/?uri=CELEX:32002L0032

Dogaru, L. (2024). Timber Tracking Information System, a Necessity in Forest Protection and Sustainability. SUMAL Information System, an Initiative in Romania. *Lecture Notes in Networks and Systems*, *928 LNNS*, 63–71. https://doi.org/10.1007/978-3-031-54671-6_5

Drivelos, S. A., & Georgiou, C. A. (2012). Multi-element and multi-isotope-ratio analysis to determine the geographical origin of foods in the European Union. *TrAC Trends in Analytical Chemistry*, *40*, 38–51. https://doi.org/10.1016/J.TRAC.2012.08.003

Edmond, J. M. (1992). Himalayan tectonics, weathering processes, and the strontium isotope record in marine limestones. *Science*, *258*(5088), 1594–1597. https://doi.org/10.1126/SCIENCE.258.5088.1594

Emery, M. V., Stark, R. J., Murchie, T. J., Elford, S., Schwarcz, H. P., & Prowse, T. L. (2018). Mapping the origins of Imperial Roman workers (1st–4th century CE) at Vagnari, Southern Italy, using 87Sr/86Sr and δ18O variability. *American Journal of Physical Anthropology*, *166*(4), 837–850. https://doi.org/10.1002/AJPA.23473

English, N. B., Betancourt, J. L., Dean, J. S., Quade, J., & Sabloff, J. A. (2001). Strontium isotopes reveal distant sources of architectural timber in Chaco Canyon, New Mexico. *Earth, Atmospheric, and Planetary Sciences*. https://www.pnas.org

Epova, E. N., Bérail, S., Zuliani, T., Malherbe, J., Sarthou, L., Valiente, M., & Donard, O. F. X. (2018). 87Sr/86Sr isotope ratio and multielemental signatures as indicators of origin of European cured hams: The role of salt. *Food Chemistry*, *246*, 313–322. https://doi.org/10.1016/J.FOODCHEM.2017.10.143

Erban Kochergina, Y. V., Novak, M., Erban, V., & Stepanova, M. (2021). 87Sr/86Sr isotope ratios in trees as an archaeological tracer: Limitations of linking plant-biomass and bedrock Sr isotope signatures. *Journal of Archaeological Science*, *133*, 105438. https://doi.org/10.1016/J.JAS.2021.105438

Ericson, J. E. (1985). Strontium isotope characterization in the study of prehistoric human ecology. *Journal of Human Evolution*, *14*(5), 503–514. https://doi.org/10.1016/S0047-2484(85)80029-4

Erzsébet, T., & Weiszburg, T. (2010). Acta mineralogica-petrographica : field guide series. *Acta Universitatis Szegediensis*, *9*. https://www.academia.edu/100945065/Acta_mineralogica_petrographica_field_guide_series_volume_9

Faure, G., & Powell, J. L. (1972). Strontium Isotope Geology. *Strontium Isotope Geology*. https://doi.org/10.1007/978-3-642-65367-4

Fietzke, J., & Eisenhauer, A. (2006). Determination of temperature-dependent stable strontium isotope (88Sr/86Sr) fractionation via bracketing standard MC-ICP-MS. *Geochemistry, Geophysics, Geosystems*, *7*(8). https://doi.org/10.1029/2006GC001243

FOREST EUROPE. (2020). *State of Europe's Forests 2020*. www.foresteurope.org

Fortunato, G., Mumic, K., Wunderli, S., Pillonel, L., Bosset, J. O., & Gremaud, G. (2004). Application of strontium isotope abundance ratios measured by MC-ICP-MS for food authentication. *Journal of Analytical Atomic Spectrometry*, *19*(2), 227–234. https://doi.org/10.1039/B307068A

Frank, A. B., Frei, R., Moutafi, I., Voutsaki, S., Orgeolet, R., Kristiansen, K., & Frei, K. M. (2021). The geographic distribution of bioavailable strontium isotopes in Greece – A base for provenance studies in archaeology. *Science of The Total Environment*, *791*, 148156. https://doi.org/10.1016/J.SCITOTENV.2021.148156

Frank, A. B., Frei, R., Triantaphyllou, M., Vassilakis, E., Kristiansen, K., & Frei, K. M. (2021). Isotopic range of bioavailable strontium on the Peloponnese peninsula, Greece: A multi-proxy approach. *Science of The Total Environment*, *774*, 145181. https://doi.org/10.1016/J.SCITOTENV.2021.145181

Frei, K. M., & Frei, R. (2011). The geographic distribution of strontium isotopes in Danish surface waters – A base for provenance studies in archaeology, hydrology and agriculture. *Applied Geochemistry*, *26*(3), 326–340. https://doi.org/10.1016/J.APGEOCHEM.2010.12.006

Frei, R., Frank, A. B., & Frei, K. M. (2022). The proper choice of proxies for relevant strontium isotope baselines used for provenance and mobility studies in glaciated terranes – Important messages from Denmark. *Science of The Total Environment*, *821*, 153394. https://doi.org/10.1016/J.SCITOTENV.2022.153394

Gapare, W. J., Ivković, M., Dutkowski, G. W., Spencer, D. J., Buxton, P., & Wu, H. X. (2012). Genetic parameters and provenance variation of Pinus radiata D. Don. "Eldridge collection" in Australia 1: Growth and form traits. *Tree Genetics and Genomes*, *8*(2), 391–407. https://doi.org/10.1007/S11295-011-0449-4

Geană, E. I., Sandru, C., Stanciu, V., & Ionete, R. E. (2017). Elemental Profile and 87Sr/86Sr Isotope Ratio as Fingerprints for Geographical Traceability of Wines: an Approach on Romanian Wines. *Food Analytical Methods*, *10*(1), 63–73. https://doi.org/10.1007/s12161-016-0550-2

Georgia, P.-P., Kotopouli, C. N., & Piper, D. J. W. (1995). Granitoid rocks of Naxos, Greece: regional geology and petrology. *Ltd. Received*, *32*, 153–171. https://doi.org/10.1002/(SICI)1099-1034(199706)32:2

Gerritzen, C. T., Goderis, S., James, H. F., & Snoeck, C. (2024). Optimizing Zr-doped MC-ICP-MS sample-standard bracketing to simultaneously determine 87Sr/86Sr and δ88Sr for high sample-throughput. *Spectrochimica Acta Part B: Atomic Spectroscopy*, *217*, 106955. https://doi.org/10.1016/J.SAB.2024.106955

Giannakas, K., & Yiannaka, A. (2023). Food Fraud: Causes, Consequences, and Deterrence Strategies. *Https://Doi.Org/10.1146/Annurev-Resource-101422-013027*, *15*, 85–104. https://doi.org/10.1146/ANNUREV-RESOURCE-101422-013027

Gori, Y., Wehrens, R., La Porta, N., & Camin, F. (2015). Oxygen and Hydrogen Stable Isotope Ratios of Bulk Needles Reveal the Geographic Origin of Norway Spruce in the European Alps. *PLOS ONE*, *10*(3), e0118941. https://doi.org/10.1371/JOURNAL.PONE.0118941

Gosz, J. R., Brookins, D. G., & Moore, D. I. (1983). Using Strontium Isotope Ratios to Estimate Inputs to Ecosystems. *BioScience*, *33*(1), 23–30. https://doi.org/10.2307/1309240

Gosz, J. R., & Moore, D. I. (1989). Strontium isotope studies of atmospheric inputs to forested watersheds in New Mexico. *Biogeochemistry*, *8*(2), 115–134. https://doi.org/10.1007/BF00001316/METRICS

Govan, E., Jackson, A. L., Inger, R., Bearhop, S., & Parnell, A. C. (2023). *simmr: A package for fitting Stable Isotope Mixing Models in R*. https://doi.org/10.18637/jss.v000.i00

Greber, N. D., & Van Zuilenc, K. (2022). Multi-collector Inductively Coupled Plasma Mass Spectrometry: New Developments and Basic Concepts for High-precision Measurements of Massdependent Isotope Signatures. *Chimia*, *76*(1), 18–25. https://doi.org/10.2533/chimia.2022.18

Gregorčič, S. H., Ogrinc, N., Frew, R., Nečemer, M., Strojnik, L., & Zuliani, T. (2021). The provenance of slovenian milk using87sr/86sr isotope ratios. *Foods*, *10*(8), 1729. https://doi.org/10.3390/FOODS10081729/S1

Griboff, J., Baroni, M. V, Horacek, M., Wunderlin, D. A., & Monferran, M. V. (2019). Multielemental + isotopic fingerprint enables linking soil, water, forage and milk composition, assessing the geographical origin of Argentinean milk. *Food Chemistry*, *283*, 549–548. https://doi.org/10.1016/j.foodchem.2019.01.067

Gryschko, R., Kuhnle, R., Terytze, K., Breuer, J., & Stahr, K. (2005). Soil extraction of readily soluble heavy metals and as with 1 M NH4NO3-solution. Evaluation of DIN 19730. *Journal of Soils and Sediments*, *5*(2), 101–106. https://doi.org/10.1065/JSS2004.10.119/METRICS

Gupta, D. K., & Walther, C. (2017). Behaviour of strontium in plants and the environment. *Behaviour of Strontium in Plants and the Environment*, 1–170. https://doi.org/10.1007/978-3-319-66574-0/COVER

Hajj, F., Poszwa, A., Bouchez, J., & Guérold, F. (2017). Radiogenic and "stable" strontium isotopes in provenance studies: A review and first results on archaeological wood from shipwrecks. *Journal of Archaeological Science*, *86*, 24–49. https://doi.org/10.1016/J.JAS.2017.09.005

Halicz, L., Segal, I., Fruchter, N., Stein, M., & Lazar, B. (2008). Strontium stable isotopes fractionate in the soil environments? *Earth and Planetary Science Letters*, *272*(1), 406–411. https://doi.org/https://doi.org/10.1016/j.epsl.2008.05.005

Hietz, P., Horsky, M., Prohaska, T., Lang, I., & Grabner, M. (2015). High-resolution densitometry and elemental analysis of tropical wood. *Trees - Structure and Function*, *29*(2), 487–497. https://doi.org/10.1007/s00468-014-1126-7

Hill, R. C., Williams, G. D. Z., Wang, Z., Hu, J., El-Hasan, T., Duckworth, O. W., Schnug, E., Bol, R., Singh, A., & Vengosh, A. (2024). Tracing the Environmental Effects of Mineral Fertilizer Application with Trace Elements and Strontium Isotope Variations. *Environmental Science & Technology Letters*, *11*(6), 604–610. https://doi.org/10.1021/acs.estlett.4c00170

Hill, S. J. (2006). *Inductively coupled plasma spectrometry and its applications*. 427.

Holland, Grenville., & Bandura, Dmitry. (2005). *Plasma source mass spectrometry : current trends and future developments*. 356.

Holt, E., Evans, J. A., & Madgwick, R. (2021). Strontium (87Sr/86Sr) mapping: A critical review of methods and approaches. *Earth-Science Reviews*, *216*, 103593. https://doi.org/10.1016/J.EARSCIREV.2021.103593

Hoogewerff, J. A., Reimann, C., Ueckermann, H., Frei, R., Frei, K. M., van Aswegen, T., Stirling, C., Reid, M., Clayton, A., Ladenberger, A., Albanese, S., Andersson, M., Baritz, R., Batista, M., Bel-lan, A., Birke, M., Cicchella, D., Demetriades, A., De Vivo, B., … Zomeni, Z. (2019). Bioavailable 87 Sr/ 86 Sr in European soils: A baseline for provenancing studies The GEMAS Project Team. *Science of the Total Environment*, *672*, 1033–1044. https://doi.org/10.1016/j.scitotenv.2019.03.387

Horacek, M., Jakusch, M., & Krehan, H. (2009). Control of origin of larch wood: discrimination between European (Austrian) and Siberian origin by stable isotope

analysis. *Rapid Communications in Mass Spectrometry : RCM*, *23*(23), 3688–3692. https://doi.org/10.1002/RCM.4309

Horacek, M., Lage, M., & Vakhlu, J. (2023). Exploring the Potential of 87Sr/86Sr Isotope Ratio with Strontium and Rubidium Levels to Assess the Geographic Origin of Saffron. *Foods*, *12*(15), 2830. https://doi.org/10.3390/foods12152830

Irrgeher, J., Vogl, J., Santner, J., & Prohaska, T. (2015). Measurement strategies. In *New Developments in Mass Spectrometry: Sector Field Mass Spectrometry for Elemental and Isotopic Analaysis* (Vols. 2015-January, Issue 3, pp. 126–151). Royal Society of Chemistry. https://doi.org/10.1039/9781849735407-00126

Jakubowski, N., Horsky, M., Roos, P. H., Vanhaecke, F., & Prohaska, T. (2014). Inductively Coupled Plasma Mass Spectrometry. In *Sector Field Mass Spectrometry for Elemental and Isotopic Analysis* (pp. 208–318). The Royal Society of Chemistry. https://doi.org/10.1039/9781849735407-00208

James, H. F., Adams, S., Willmes, M., Mathison, K., Ulrichsen, A., Wood, R., Valera, A. C., Frieman, C. J., & Grün, R. (2022). A large-scale environmental strontium isotope baseline map of Portugal for archaeological and paleoecological provenance studies. *Journal of Archaeological Science*, *142*, 105595. https://doi.org/10.1016/J.JAS.2022.105595

Jianbang, G., Cerutti, P. O., Masiero, M., Pettenella, D., Andrighetto, N., & Dawson, T. (2016). *Chapter 3: Quantifying Illegal Logging and Related Timber Trade* (D. Kleinschmit, S. Mansourian, C. Wildburger, & A. Purret, Eds.; Volume 35). International Union of Forest Research Organizations (IUFRO). https://www.researchgate.net/publication/311493784_Quantifying_Illegal_Logging_and_Related_Timber_Trade

Joint Ministerial Decision 313071/18.01.94 - Προϋποθέσεις, Όροι Και Διαδικασία Καθιέρωσης Ονομασιών Προελεύσεως Γεωργικών Προϊόντων, Β' 23 (1994).

Joyce, M. (2017). Nuclear engineering: A conceptual introduction to nuclear power. *Nuclear Engineering: A Conceptual Introduction to Nuclear Power*, 1–419. https://doi.org/10.1016/C2015-0-05557-5

Käßner, A., Kalapurakkal, H. T., Huber, B., & Tichomirowa, M. (2023). A New Water-Based 87Sr/86Sr Isoscape Map of Central and NE Germany, with Special Emphasis on Mountainous Regions. *Aquatic Geochemistry*, *29*(2), 95–125. https://doi.org/10.1007/S10498-023-09412-5/FIGURES/8

Kelly, S., Heaton, K., & Hoogewerff, J. (2005). Tracing the geographical origin of food: The application of multi-element and multi-isotope analysis. *Trends in Food Science & Technology*, *16*(12), 555–567. https://doi.org/10.1016/J.TIFS.2005.08.008

Kennedy, M. J., Hedin, L. O., & Derry, L. A. (2002). Decoupling of unpolluted temperate forests from rock nutrient sources revealed by natural (87)Sr/(86)Sr and (84)Sr tracer addition. *Proceedings of the National Academy of Sciences of the United States of America*, *99*(15), 9639–9644. https://doi.org/10.1073/PNAS.152045499

Kern, Z., & Popa, I. (2008). Changes of Frost Damage and Treeline Advance for Swiss Stone Pine in the Calimani Mts. (Eastern Carpathians, Romania). In *Acta Silv. Lign. Hung* (Vol. 4). http://visibleearth.nasa.gov

Khan, I. T., Nadeem, M., Imran, M., Ayaz, M., Ajmal, M., Ellahi, M. Y., & Khalique, A. (2017). Antioxidant capacity and fatty acids characterization of heat treated cow and buffalo milk. *Lipids in Health and Disease*, *16*(1). https://doi.org/10.1186/S12944-017-0553-Z

Kizos, T., & Vakoufaris, H. (2011). ALTERNATIVE AGRI-FOOD GEOGRAPHIES? GEOGRAPHIC INDICATIONS IN GREECE. *Tijdschrift Voor Economische En Sociale Geografie*, *102*(2), 220–235. https://doi.org/10.1111/J.1467-9663.2010.00612.X

Klaver, M., & Coath, C. D. (2019). Obtaining Accurate Isotopic Compositions with the Double Spike Technique: Practical Considerations. *Geostandards and Geoanalytical Research*, *43*(1), 5–22. https://doi.org/10.1111/GGR.12248

Knudson, K. J., Williams, H. M., Buikstra, J. E., Tomczak, P. D., Gordon, G. W., & Anbar, A. D. (2010). Introducing δ88/86Sr analysis in archaeology: A demonstration of the utility of strontium isotope fractionation in paleodietary studies. *Journal of Archaeological Science*, *37*(9), 2352–2364. https://doi.org/10.1016/J.JAS.2010.04.009

Koch, P. L., Heisinger, J., Moss, C., Carlson, R. W., Fogel, M. L., & Behrensmeyer, A. K. (1995). Isotopic tracking of change in diet and habitat use in african elephants. *Science (New York, N.Y.)*, *267*(5202), 1340–1343. https://doi.org/10.1126/SCIENCE.267.5202.1340

Krabbenhöft, A., Eisenhauer, A., Böhm, F., Vollstaedt, H., Fietzke, J., Liebetrau, V., Augustin, N., Peucker-Ehrenbrink, B., Müller, M. N., Horn, C., Hansen, B. T., Nolte, N., & Wallmann, K. (2010). Constraining the marine strontium budget with natural strontium isotope fractionations (87Sr/86Sr∗, δ88/86Sr) of carbonates, hydrothermal solutions and river waters. *Geochimica et Cosmochimica Acta*, *74*(14), 4097–4109. https://doi.org/https://doi.org/10.1016/j.gca.2010.04.009

Kwasi Bannor, R., Arthur, K. K., Oppong, D., & Oppong-Kyeremeh, H. (2023). A comprehensive systematic review and bibliometric analysis of food fraud from a global perspective. *Journal of Agriculture and Food Research*, *14*, 100686. https://doi.org/10.1016/J.JAFR.2023.100686

Ladegaard-Pedersen, P., Achilleos, M., Dörflinger, G., Frei, R., Kristiansen, K., & Frei, K. M. (2020). A strontium isotope baseline of Cyprus. Assessing the use of soil leachates, plants, groundwater and surface water as proxies for the local range of bioavailable strontium isotope composition. *Science of The Total Environment*, *708*, 134714. https://doi.org/10.1016/J.SCITOTENV.2019.134714

Land, M., Ingri, J., Andersson, P. S., & rn È hlander, B. O. (2000). Ba/Sr, Ca/Sr and 87 Sr/ 86 Sr ratios in soil water and groundwater: implications for relative contributions to stream water discharge. *Applied Geochemistry*, *15*, 311–325.

Lengfelder, F., Grupe, G., Stallauer, A., Huth, R., & Söllner, F. (2019). Modelling strontium isotopes in past biospheres – Assessment of bioavailable 87Sr/86Sr ratios in local archaeological vertebrates based on environmental signatures. *Science of The Total Environment*, *648*, 236–252. https://doi.org/10.1016/J.SCITOTENV.2018.08.014

Leonidopolou, D., Evelpidou, N., Vasilopoulos, A., & Stournaras, G. (2008). Geomorphologic factors affecting intrinsic vulnerability in fissured media. Application

on Falatados – Livada area, SE Tinos island (Cyclades – Greece). *Conference: 8th International Hydrogeological Congress of Greece*. https://www.researchgate.net/publication/339272023_Geomorphologic_factors_affecting_intrinsic_vulnerability_in_fissured_media_Application_on_Falatados_-_Livada_area_SE_Tinos_island_Cyclades_-_Greece

Levy, G., Brechet, C., & Becker, M. (1996). Element analysis of tree rings in pedunculate oak heartwood: an indicator of historical trends in the soil chemistry, related to atmospheric deposition. *Annales Des Sciences Forestières*, *53*(2–3), 685–696. https://doi.org/10.1051/FOREST:19960246

Locosselli, G. M., Chacón-Madrid, K., Zezzi Arruda, M. A., Pereira de Camargo, E., Lopes Moreira, T. C., Saldiva de André, C. D., Afonso de André, P., Singer, J. M., Nascimento Saldiva, P. H., & Buckeridge, M. S. (2018). Tree rings reveal the reduction of Cd, Cu, Ni and Pb pollution in the central region of São Paulo, Brazil. *Environmental Pollution*, *242*, 320–328. https://doi.org/10.1016/J.ENVPOL.2018.06.098

Low, M. C., Schmitz, N., Boeschoten, L. E., Cabezas, J. A., Cramm, M., Haag, V., Koch, G., Meyer-Sand, B. R. V., Paredes-Villanueva, K., Price, E., Thornhill, A. H., Brusselen, J. Van, Zuidema, P. A., Deklerck, V., Dormontt, E. E., Shapcott, A., & Lowe, A. J. (2022). Tracing the world's timber: the status of scientific verification technologies for species and origin identification. *IAWA Journal*, *44*(1), 63–84. https://doi.org/10.1163/22941932-BJA10097

Lugli, F., Cipriani, A., Bruno, L., Ronchetti, F., Cavazzuti, C., & Benazzi, S. (2022). A strontium isoscape of Italy for provenance studies. *Chemical Geology*, *587*, 120624. https://doi.org/10.1016/J.CHEMGEO.2021.120624

Lum, T. S., & Sze-Yin Leung, K. (2016). Strategies to overcome spectral interference in ICP-MS detection. In *Journal of Analytical Atomic Spectrometry* (Vol. 31, Issue 5, pp. 1078–1088). Royal Society of Chemistry. https://doi.org/10.1039/c5ja00497g

Ma, J. L., Wei, G. J., Liu, Y., Ren, Z. Y., Xu, Y. G., & Yang, Y. H. (2013). Precise measurement of stable (δ88/86Sr) and radiogenic (87Sr/86Sr) strontium isotope ratios in geological standard reference materials using MC-ICP-MS. *Chinese Science Bulletin*, *58*(25), 3111–3118. https://doi.org/10.1007/S11434-013-5803-5/METRICS

Martínez-Salvador, L. E., Reyes-Jaime, A., Martínez-Salvador, L. E., & Reyes-Jaime, A. (2021). Sustainability in Protected Designations of Origin (PDO) in the European Union: An approach from a Systematic Literature Review. *Siembra* , *8*(2), e3288. https://doi.org/10.29166/SIEMBRA.V8I2.3288

Martín, J. A., Esteban, L. G., de Palacios, P., & Fernández, F. G. (2010). Variation in wood anatomical traits of Pinus sylvestris L. between Spanish regions of provenance. *Trees - Structure and Function*, *24*(6), 1017–1028. https://doi.org/10.1007/S00468-010-0471-4/TABLES/4

Marx, D., Rahimnejad Yazdi, A., Papini, M., & Towler, M. (2020). A review of the latest insights into the mechanism of action of strontium in bone. *Bone Reports*, *12*, 100273. https://doi.org/10.1016/J.BONR.2020.100273

Maurer, A. F., Galer, S. J. G., Knipper, C., Beierlein, L., Nunn, E. V., Peters, D., Tütken, T., Alt, K. W., & Schöne, B. R. (2012). Bioavailable 87Sr/86Sr in different

environmental samples — Effects of anthropogenic contamination and implications for isoscapes in past migration studies. *Science of The Total Environment*, *433*, 216–229. https://doi.org/10.1016/J.SCITOTENV.2012.06.046

Meerts, P. (2002). Mineral nutrient concentrations in sapwood and heartwood: a literature review. *Annals of Forest Science*, *59*(7), 713–722. https://doi.org/10.1051/FOREST:2002059

Miller, E. K., Blum, J. D., & Friedland, A. J. (1993). Determination of soil exchangeable-cation loss and weathering rates using Sr isotopes. *Nature 1993 362:6419*, *362*(6419), 438–441. https://doi.org/10.1038/362438a0

Montgomery, H., Haughey, S. A., & Elliott, C. T. (2020). Recent food safety and fraud issues within the dairy supply chain (2015–2019). *Global Food Security*, *26*, 100447. https://doi.org/10.1016/J.GFS.2020.100447

Montgomery, J., Evans, J. A., & Cooper, R. E. (2007). Resolving archaeological populations with Sr-isotope mixing models. *Applied Geochemistry*, *22*(7), 1502–1514. https://doi.org/10.1016/J.APGEOCHEM.2007.02.009

Mortier, T., Truszkowski, J., Norman, M., Boner, M., Buliga, B., Chater, C., Jennings, H., Saunders, J., Sibley, R., Antonelli, A., Waegeman, W., & Deklerck, V. (2024). A framework for tracing timber following the Ukraine invasion. *Nature Plants* , *10*(3), 390–401. https://doi.org/10.1038/s41477-024-01648-5

Munteanu, M., & Tatu, M. (2003). The East-Carpathian Crystalline-Mesozoic Zone (Romania): Paleozoic Amalgamation of Gondwana- and East European Craton-derived Terranes. *Gondwana Research*, *6*(2), 185–196. https://doi.org/10.1016/S1342-937X(05)70969-2

Nadia Marechal, C., Telouk, P., Albaredé, F., & Albaredé, A. (1999). Precise analysis of copper and zinc isotopic compositions by plasma-source mass spectrometry. In *Chemical Geology* (Vol. 156).

Nafplioti, A. (2011). Tracing population mobility in the Aegean using isotope geochemistry: a first map of local biologically available 87 Sr/ 86 Sr signatures. *Journal of Archaeological Science*, *38*, 1560–1570. https://doi.org/10.1016/j.jas.2011.02.021

Nagavciuc, V., Ionita, M., Perșoiu, A., Popa, I., Loader, N. J., & McCarroll, D. (2019). Stable oxygen isotopes in Romanian oak tree rings record summer droughts and associated large-scale circulation patterns over Europe. *Climate Dynamics*, *52*(11), 6557–6568. https://doi.org/10.1007/S00382-018-4530-7/FIGURES/7

Nečemer, M., Potočnik, D., & Ogrinc, N. (2016). Discrimination between Slovenian cow, goat and sheep milk and cheese according to geographical origin using a combination of elemental content and stable isotope data. *Journal of Food Composition and Analysis*, *52*, 16–23. https://doi.org/10.1016/j.jfca.2016.07.002

Nickolas, L. B., Segura, C., & Brooks, J. R. (2017). The influence of lithology on surface water sources. *Hydrological Processes*, *31*(10), 1913. https://doi.org/10.1002/HYP.11156

Nie, N. X., Dauphas, N., Hopp, T., Hu, J. Y., Zhang, Z. J., Yokochi, R., Ireland, T. J., & Tissot, F. L. H. (2021). Chromatography purification of Rb for accurate isotopic analysis by MC-ICPMS: A comparison between AMP-PAN, cation-exchange, and Sr

resins. *Journal of Analytical Atomic Spectrometry*, *36*(12), 2588–2602. https://doi.org/10.1039/d1ja00268f

Nier, A. O. (1938). The Isotopic Constitution of Strontium, Barium, Bismuth, Thallium and Mercury. *Physical Review*, *54*(4), 275–278. https://doi.org/10.1103/PhysRev.54.275

Nikezić, M., Chantzi, P., Irrgeher, J., & Zuliani, T. (2024). Evaluating Source Complexity in Blended Milk Cheese: Integrated Strontium Isotope and Multi-Elemental Approach to PDO Graviera Naxos. *Foods*, *13*(16). https://doi.org/10.3390/foods13162540

Nikezić, M., Perşoiu, A., Feher, R., Popa, I., & Zuliani, T. (2024). Geochemical fingerprinting of Norway spruce from the Eastern Carpathians: Sr isotopic and multi-elemental signatures. *Science of The Total Environment*, 176244. https://doi.org/10.1016/j.scitotenv.2024.176244

Novak, M., Holmden, C., Andronikov, A. V., Erban Kochergina, Y. V., Kirchner, J. W., Paces, T., Kachlik, V., Veselovsky, F., Hruška, J., Laufek, F., Koubova, M., Stepanova, M., Prechova, E., Sebek, O., Curik, J., Tesar, M., Fottova, D., Andronikova, I. E., & Komarek, A. (2024). Mg, Ca and Sr isotope dynamics in a small forested catchment underlain by paragneiss: The role of geogenic, atmospheric, and biogenic sources of base cations. *Geoderma*, *442*, 116768. https://doi.org/10.1016/J.GEODERMA.2023.116768

Odum, H. T. (1951). The stability of the world strontium cycle. *Science*, *114*(2964), 407–411. https://doi.org/10.1126/SCIENCE.114.2964.407/ASSET/1D38A12B-2796-4B4A-BB0B-ACDF00321222/ASSETS/SCIENCE.114.2964.407.FP.PNG

Oeser, R. A., & von Blanckenburg, F. (2020). Strontium isotopes trace biological activity in the Critical Zone along a climate and vegetation gradient. *Chemical Geology*, *558*, 119861. https://doi.org/10.1016/J.CHEMGEO.2020.119861

Oprea, D., & Buta, G. (2014). Research on morphological caracteristics of endokarst in Rarau Massif. Premises for local palaeoclimatic records. *GEOREVIEW: Scientific Annals of Stefan Cel Mare University of Suceava. Geography Series*, *24*(2), 122–127. http://georeview.ro/ojs/index.php/revista/article/view/233

Otero, N., Soler, A., & Canals, À. (2004). Fertilizer Characterization: Isotopic Data (N, S, O, C, and Sr). *Environmental Science & Technology*, *38*(12), 3254–3262. https://doi.org/10.1021/es0348187

Pallavicini, N., Engström, E., Baxter, D. C., Ohlander, B., Ingri, J., Hawley, S., Hirst, C., Rodushkina, K., & Rodushkin, I. (2018). Ranges of B, Cd, Cr, Cu, Fe, Pb, Sr, Tl, and Zn Concentrations and Isotope Ratios in Environmental Matrices from an Urban Area. *Journal of Spectroscopy*, *2018*(1), 7408767. https://doi.org/10.1155/2018/7408767

Papanastassiou, D. A., & Wasserburg, G. J. (1968). Initial strontium isotopic abundances and the resolution of small time differences in the formation of planetary objects. *Earth and Planetary Science Letters*, *5*(C), 361–376. https://doi.org/10.1016/S0012-821X(68)80066-4

Paredes-Villanueva, K., Boom, A., Ottenburghs, J., Van Der Sleen, P., Manzanedo, R. D., Bongers, F., & Zuidema, P. A. (2022). Isotopic Characterization of Cedrela to Verify

Species and Regional Provenance of Bolivian Timber. *Tree-Ring Research*, *78*(2), 73–89. https://doi.org/10.3959/2021-17

Partsinevelou, A. S., Lozios, S., & Stournaras, G. (2011). Fracture pattern description and analysis of the hard rock hydrogeological environment in Naxos Island, Hellas. *Advances in the Research of Aquatic Environment*, 45–52. https://doi.org/10.1007/978-3-642-24076-8_6

Pearce, C. R., Parkinson, I. J., Gaillardet, J., Charlier, B. L. A., Mokadem, F., & Burton, K. W. (2015). Reassessing the stable (δ88/86Sr) and radiogenic (87Sr/86Sr) strontium isotopic composition of marine inputs. *Geochimica et Cosmochimica Acta*, *157*, 125–146. https://doi.org/10.1016/J.GCA.2015.02.029

Pierson-Wickmann, A.-C., Aquilina, L., Weyer, C., Molénat, J., & Lischeid, G. (2009). Acidification processes and soil leaching influenced by agricultural practices revealed by strontium isotopic ratios. *Geochimica et Cosmochimica Acta*, *73*(16), 4688–4704. https://doi.org/https://doi.org/10.1016/j.gca.2009.05.051

Pillonel, L., Badertscher, R., Froidevaux, P., Haberhauer, G., Hölzl, S., Horn, P., Jakob, A., Pfammatter, E., Piantini, U., Rossmann, A., Tabacchi, R., & Bosset, J. O. (2003). Stable isotope ratios, major, trace and radioactive elements in emmental cheeses of different origins. *LWT*, *36*(6), 615–623. https://doi.org/10.1016/S0023-6438(03)00081-1

Pinta, É., Pacheco-Forés, S. I., Wallace, E. P., & Knudson, K. J. (2021). Provenancing wood used in the Norse Greenlandic settlements: A biogeochemical study using hydrogen, oxygen, and strontium isotopes. *Journal of Archaeological Science*, *131*, 105407. https://doi.org/10.1016/J.JAS.2021.105407

Plimer, I. R., & Elliott, S. M. (1979). The use of Rb/Sr ratios as a guide to mineralization. *Journal of Geochemical Exploration*, *12*(C), 21–34. https://doi.org/10.1016/0375-6742(79)90060-8

Pors Nielsen, S. (2004). The biological role of strontium. *Bone*, *35*(3), 583–588. https://doi.org/10.1016/J.BONE.2004.04.026

Poszwa, A., Ferry, B., Dambrine, E., Pollier, B., Wickman, T., Loubet, M., & Bishop, K. (2004). Variations of bioavailable Sr concentration and 87Sr/ 86Sr ratio in boreal forest ecosystems: Role of biocycling, mineral weathering and depth of root uptake. *Biogeochemistry*, *67*(1), 1–20. https://doi.org/10.1023/B:BIOG.0000015162.12857.3E

Potočnik, D., Nečemer, M., Perišić, I., Jagodic, M., Mazej, D., Camin, F., Eftimov, T., Strojnik, L., & Ogrinc, N. (2020). Geographical verification of Slovenian milk using stable isotope ratio, multi-element and multivariate modelling approaches. *Food Chemistry*, *326*. https://doi.org/10.1016/j.foodchem.2020.126958

Prevedorou, E. A., Buikstra, J. E., Knudson, K. J., Stojanowski, C. M., Fox, S. C., & Rutter, J. B. (2015). *The role of kin relations and residential mobility during the transition from final Neolithic to Early Bronze Age in Attica, Greece.*

Price, D. G. (1995). Weathering and weathering processes. *Quarterly Journal of Engineering Geology*, *28*(3), 243–252. https://doi.org/10.1144/GSL.QJEGH.1995.028.P3.03

Quemet, A., Maillard, C., & Ruas, A. (2015). Determination of zirconium isotope composition and concentration for nuclear sample analysis using Thermal Ionization

Mass Spectrometry. *International Journal of Mass Spectrometry*, *392*. https://doi.org/10.1016/j.ijms.2015.08.023ï

Regulation (EU) No 995/2010 of the European Parliament and of the Council of 20 October 2010 down the Obligations of Operators Who Place Timber and Timber Products on the Market, Official Journal of the European Union (2010).

Reynolds, A. C., Betancourt, J. L., Quade, J., Patchett, P. J., Dean, J. S., & Stein, J. (2005). 87Sr/86Sr sourcing of ponderosa pine used in Anasazi great house construction at Chaco Canyon, New Mexico. *Journal of Archaeological Science*, *32*(7), 1061–1075. https://doi.org/10.1016/J.JAS.2005.01.016

Rich, S., Manning, S. W., Degryse, P., Vanhaecke, F., & Van Lerberghe, K. (2016). Provenancing East Mediterranean cedar wood with the 87Sr/86Sr strontium isotope ratio. *Archaeological and Anthropological Sciences*, *8*(3), 467–476. https://doi.org/10.1007/S12520-015-0242-7/FIGURES/6

Rossmann, A., Haberhauer, G., Pichlmayer, F., Hölzl, S., Horn, P., & Voerkelius, S. (2000). The potential of multielement stable isotope analysis for regional origin assignment of butter. *Eur Food Res Technol*, *211*, 32–40.

Rudge, J. F., Reynolds, B. C., & Bourdon, B. (2009). The double spike toolbox. *Chemical Geology*, *265*(3–4), 420–431. https://doi.org/10.1016/j.chemgeo.2009.05.010

Russell, W. A., Papanastassiou, D. A., & Tombrello, T. A. (1978). Ca isotope fractionation on the Earth and other solar system materials. *Geochimica et Cosmochimica Acta*, *42*(8), 1075–1090. https://doi.org/https://doi.org/10.1016/0016-7037(78)90105-9

Sandulescu, M., & Dimitrescu, R. (2004). Field Trip Guide Book-B12 Geological Structure of the Romanian Carpathians. *32nd International Geological Congress*, *1*, PR01-B15.

Sattouf, M., Kratz, S., Diemer, K., Rienitz, O., Fleckenstein, J., Schiel, D., Schnug, E., Sattouf, M., Kratz, S., Diemer, K., Rienitz, O., Fleckenstein, J., Schiel, D., & Schnug, E. (2007). Identifying the origin of rock phosphates and phosphorus fertilizers through high-precision measurement of the strontium isotopes 87Sr and 86Sr. *Landbauforschung Völkenrode*, *57*(1), 1–11.

Schieber, A. (2018). Introduction to Food Authentication. *Modern Techniques for Food Authentication*, 1–21. https://doi.org/10.1016/B978-0-12-814264-6.00001-3

Schmid, I. (2002). The influence of soil type and interspecific competition on the fine root system of Norway spruce and European beech. *Basic and Applied Ecology*, *3*(4), 339–346. https://doi.org/10.1078/1439-1791-00116

Shalev, N., Segal, I., Lazar, B., Gavrieli, I., Fietzke, J., Eisenhauer, A., & Halicz, L. (2013). Precise determination of δ 88/86 Sr in natural samples by double-spike MC-ICP-MS and its TIMS verification. *Journal of Analytical Atomic Spectrometry*, *28*(6), 940–944. https://doi.org/10.1039/C3JA50039J

Sillen, A., & Kavanagh, M. (1982). Strontium and paleodietary research: A review. *American Journal of Physical Anthropology*, *25*(3 S), 67–90. https://doi.org/10.1002/AJPA.1330250505

Snoeck, C., Ryan, S., Pouncett, J., Pellegrini, M., Claeys, P., Wainwright, A. N., Mattielli, N., Lee-Thorp, J. A., & Schulting, R. J. (2020). Towards a biologically available strontium isotope baseline for Ireland. *Science of the Total Environment*, *712*. https://doi.org/10.1016/J.SCITOTENV.2019.136248

Spooner, E. T. C. (1976). The strontium isotopic composition of seawater, and seawater-oceanic crust interaction. *Earth and Planetary Science Letters*, *31*(1), 167–174. https://doi.org/10.1016/0012-821X(76)90108-4

Steiger, R. H., & Jäger, E. (1977). Subcommission on geochronology: Convention on the use of decay constants in geo- and cosmochronology. *Earth and Planetary Science Letters*, *36*(3), 359–362. https://doi.org/10.1016/0012-821X(77)90060-7

Stevenson, E. I., Aciego, S. M., Chutcharavan, P., Parkinson, I. J., Burton, K. W., Blakowski, M. A., & Arendt, C. A. (2016). Insights into combined radiogenic and stable strontium isotopes as tracers for weathering processes in subglacial environments. *Chemical Geology*, *429*, 33–43. https://doi.org/10.1016/J.CHEMGEO.2016.03.008

Swoboda, S., Brunner, M., Boulyga, S. F., Galler, P., Horacek, M., & Prohaska, T. (2008). Identification of Marchfeld asparagus using Sr isotope ratio measurements by MC-ICP-MS. *Analytical and Bioanalytical Chemistry*, *390*(2), 487–494. https://doi.org/10.1007/S00216-007-1582-7/FIGURES/3

Tchaikovsky, A., Zitek, A., Irrgeher, J., Opper, C., Scheiber, R., Moder, K., Congiu, L., & Prohaska, T. (2019). Chemometric tools for determining site-specific elemental and strontium isotopic fingerprints in raw and salted sturgeon caviar. *European Food Research and Technology*, *245*(11), 2515–2528. https://doi.org/10.1007/S00217-019-03363-4/FIGURES/5

Techer, I., Medini, S., Janin, M., & Arregui, M. (2017). Impact of agricultural practice on the Sr isotopic composition of food products: Application to discriminate the geographic origin of olives and olive oil. *Applied Geochemistry*, *82*, 1–14. https://doi.org/10.1016/J.APGEOCHEM.2017.05.010

Teixeira, J. L. da P., Baptista, D. P., Orlando, E. A., Gigante, M. L., & Pallone, J. A. L. (2022). Effect of processing on the bioaccessibility of essential minerals in goat and cow milk and dairy products assessed by different static in vitro digestion models. *Food Chemistry*, *374*, 131739. https://doi.org/10.1016/J.FOODCHEM.2021.131739

Theocharatos, G. (1978). *The climate of Cyclades*. Universitry of Athens.

Thomas, R. (2023). *A practical guide to ICP-MS and other atomic spectroscopy techniques : a tutorial for beginners*. CRC Press.

Tjoelker, M. G., Boratyński, A., & Bugała, W. (2007). Biology and Ecology of Norway Spruce. In *Biology and Ecology of Norway Spruce*. Springer Netherlands. https://doi.org/10.1007/978-1-4020-4841-8

Toncala, A., Trautmann, B., Velte, M., Kropf, E., McGlynn, G., Peters, J., & Harbeck, M. (2020). On the premises of mixing models to define local bioavailable 87Sr/86Sr ranges in archaeological contexts. *Science of The Total Environment*, *745*, 140902. https://doi.org/10.1016/J.SCITOTENV.2020.140902

Török, A. I., Moldovan, A., Tănăselia, C., Kovacs, E., Mirea, I. C., Moldovan, O. T., & Levei, E. A. (2023). Sr Isotope, Major, and Trace Element Signatures in Karst Groundwaters. *Water (Switzerland)*, *15*(7). https://doi.org/10.3390/w15071431

Urakawa, R., Ohta, T., Shin, K. C., Sase, H., Shibata, H., Chikamasa, T., & Nakano, T. (2023). Effects of geological conditions and atmospheric deposition on soil biogeochemical properties in Japanese forested ecosystems revealed by Sr isotope

analysis. *Biogeochemistry*, *162*(1), 57–77. https://doi.org/10.1007/S10533-022-00991-Z/FIGURES/6

Van Breemen, O., Hutchinson, J., & Bowden, P. (1975). Age and origin of the Nigerian mesozoic granites: A Rb-Sr isotopic study. *Contributions to Mineralogy and Petrology*, *50*(3), 157–172. https://doi.org/10.1007/BF00371037

Vance, D., & Thirlwall, M. (2002). An assessment of mass discrimination in MC-ICPMS using Nd isotopes. *Chemical Geology*, *185*, 227–240. www.elsevier.com/locate/chemgeo

Vanhaecke, Frank., & Degryse, Patrick. (2012). *Isotopic analysis : fundamentals and applications using ICP-MS*. 529.

Vatavali, K., Kosma, I., Louppis, A., Gatzias, I., Badeka, A. V., & Kontominas, M. G. (2020). Characterisation and differentiation of geographical origin of Graviera cheeses produced in Greece based on physico-chemical, chromatographic and spectroscopic analyses, in combination with chemometrics. *International Dairy Journal*, *110*, 104799. https://doi.org/10.1016/J.IDAIRYJ.2020.104799

Veizer, J. (1989). Strontium Isotopes in Seawater through Time. *Annual Review of Earth and Planetary Sciences*, *17*(Volume 17, 1989), 141–167. https://doi.org/https://doi.org/10.1146/annurev.ea.17.050189.001041

Velbel, M. A. (1988). *Weathering and Soil-Forming Processes*. 93–102. https://doi.org/10.1007/978-1-4612-3732-7_6

Visser, R. M. (2021). Dendrochronological provenance patterns. Network analysis of tree-ring material reveals spatial and economic relations of roman timber in the continental north-western provinces. *Journal of Computer Applications in Archaeology*, *4*(1), 230–253. https://doi.org/10.5334/JCAA.79

Vitousek, P. M., Kennedy, M. J., Derry, L. A., & Chadwick, O. A. (1999). Weathering versus atmospheric sources of strontium in ecosystems on young volcanic soils. *Oecologia*, *121*(2), 255–259. https://doi.org/10.1007/S004420050927/METRICS

Vlam, M., de Groot, G. A., Boom, A., Copini, P., Laros, I., Veldhuijzen, K., Zakamdi, D., & Zuidema, P. A. (2018). Developing forensic tools for an African timber: Regional origin is revealed by genetic characteristics, but not by isotopic signature. *Biological Conservation*, *220*, 262–271. https://doi.org/10.1016/J.BIOCON.2018.01.031

Voerkelius, S., Lorenz, G. D., Rummel, S., Quétel, C. R., Heiss, G., Baxter, M., Brach-Papa, C., Deters-Itzelsberger, P., Hoelzl, S., Hoogewerff, J., Ponzevera, E., Van Bocxstaele, M., & Ueckermann, H. (2010). Strontium isotopic signatures of natural mineral waters, the reference to a simple geological map and its potential for authentication of food. *Food Chemistry*, *118*(4), 933–940. https://doi.org/10.1016/J.FOODCHEM.2009.04.125

Waight, T., Baker, J., & Willigers, B. (2002). Rb isotope dilution analyses by MC-ICPMS using Zr to correct for mass fractionation: towards improved Rb–Sr geochronology? *Chemical Geology*, *186*(1–2), 99–116. https://doi.org/10.1016/S0009-2541(01)00420-X

Watkinson, C. J., Rees, G. O., Gwenael, M. C., Gasson, P., Hofem, S., Michely, L., & Boner, M. (2022). Stable Isotope Ratio Analysis for the Comparison of Timber From

Two Forest Concessions in Gabon. *Frontiers in Forests and Global Change*, *4*, 650257. https://doi.org/10.3389/FFGC.2021.650257/BIBTEX

West, J. B., Bowen, G. J., Dawson, T. E., & Tu, K. P. (2010). Isoscapes: Understanding movement, pattern, and process on earth through isotope mapping. *Isoscapes: Understanding Movement, Pattern, and Process on Earth Through Isotope Mapping*, 1–487. https://doi.org/10.1007/978-90-481-3354-3/COVER

Willmes, M., Bataille, C. P., James, H. F., Moffat, I., McMorrow, L., Kinsley, L., Armstrong, R. A., Eggins, S., & Grün, R. (2018). Mapping of bioavailable strontium isotope ratios in France for archaeological provenance studies. *Applied Geochemistry*, *90*, 75–86. https://doi.org/10.1016/J.APGEOCHEM.2017.12.025

World Health Organization. (2022). *Fourth edition incorporating the first and second addenda Guidelines for drinking-water quality*.

Xu, H., Liu, B., & Wu, F. (2010). Spatial and temporal variations of Rb/Sr ratios of the bulk surface sediments in Lake Qinghai. *Geochemical Transactions*, *11*(1), 1–8. https://doi.org/10.1186/1467-4866-11-3/FIGURES/5

Yang, J. H., Wu, F. Y., Chung, S. L., Wilde, S. A., & Chu, M. F. (2004). Multiple sources for the origin of granites: Geochemical and Nd/Sr isotopic evidence from the Gudaoling granite and its mafic enclaves, northeast China. *Geochimica et Cosmochimica Acta*, *68*(21), 4469–4483. https://doi.org/10.1016/j.gca.2004.04.015

Yang, L. (2009). Accurate and precise determination of isotopic ratios by MC-ICP-MS: A review. *Mass Spectrometry Reviews*, *28*(6), 990–1011. https://doi.org/10.1002/MAS.20251

Yang, L., Peter, C., Panne, U., & Sturgeon, R. E. (2008). Use of Zr for mass bias correction in strontium isotope ratio determinations using MC-ICP-MS. *Journal of Analytical Atomic Spectrometry*, *23*(9), 1269–1274. https://doi.org/10.1039/B803143F

Zheng, F.-L. (2006). Effect of Vegetation Changes on Soil Erosion on the Loess Plat eau*l. In *Pedosphere* (Vol. 16, Issue 4).

Zuliani, T., Kanduč, T., Novak, R., & Vreča, P. (2020). Characterization of bottled waters by multielemental analysis, stable and radiogenic isotopes. *Water (Switzerland)*, *12*(9). https://doi.org/10.3390/w12092454

Bibliography

Publications Related to the Thesis

Journal Articles

Nikezić, M., Perşoiu, A., Feher, R., Popa, I., Zuliani, T. (2024). Geochemical fingerprinting of Norway spruce from the Eastern Carpathians: Sr isotopic and multi-elemental signatures. *Science of The Total Environment, 21*(2), 176244. doi: 10.1016/j.scitotenv.2024.176244

Nikezić, M., Chantzi, P., Irrgeher, J., Zuliani, T. (2024). Evaluating source complexity in blended milk cheese: Integrated Sr isotope and multi-elemental approach to PDO Graviera Naxos. *Foods*, *13*(16), 2540. doi: 10.3390/foods13162540

Conference Papers

Nikezić, M., Chantzi, P., Giannenas, I., Zuliani, T. (2021). The use of multi-elemental and Sr isotopic composition for tracing the geographical origin of milk and cheese samples. In *Proceedings of the 27th Annual Meeting of the Slovenian Chemical Society.* Ljubljana, Slovenia: Slovenian Chemical Society.

Nikezić, M., Chantzi, P., Giannenas, I., Zuliani, T. (2022). Application of multi-elemental and Sr isotope analyses in provenance of dairy production in Naxos, Greece. In *Proceedings of the 14th Jožef Stefan International Postgraduate School Students's Conference.* Ljubljana, Slovenia: Jožef Stefan International Postgraduate School

Nikezić, M., Žerdoner, T., Furdek, M., Ivanić, M., Fiket, Ž., Mešić, A., Zgrablić, Ž., Zuliani, T. (2022). Determinations of $^{87}Sr/^{86}Sr$ ratio in truffles from Istria, Croatia. In *Proceedings of the 28th Annual Meeting of the Slovenian Chemical Society.* Ljubljana, Slovenia: Slovenian Chemical Society.

Žerdoner, T., Nikezić, M., Hauptman, Ž., Gračanin, N., Dolenec, M., Rogan Šmuc, N., Benedik, Lj., Zuliani, T. (2022). Precise determination of isotope ratios of non-traditional elements in solid environmental samples. In *Proceedings of the 28th Annual Meeting of the Slovenian Chemical Society.* Ljubljana, Slovenia: Slovenian Chemical Society.

Nikezić, M., Perşoiu, A., Feher, R., Popa, I., Zuliani, T. (2023). Sr isotope ratio as marker of wood provenance. In *Proceedings of the European Winter Conference on Plasma Spectrochemistry.* Ljubljana, Slovenia: National Institute of Chemistry.

Nikezić, M., Chantzi, P., Giannenas, I., Zuliani, T. (2023). Linking multi-elemental and Sr isotopic data of milk, cheese, water, soil, and forage. In *Proceedings of the ISO-FOOD Symposium From Food Source to Health.* Ljubljana, Slovenia: Jožef Stefan Institute.

Nikezić, M., Zuliani, T. (2023). Exploring the potential of Sr isotopic ratios as indicators of provenance. In *Proceedings of the 29th Annual Meeting of the Slovenian Chemical Society.* Ljubljana, Slovenia: Slovenian Chemical Society.

Other Publications

Zuliani, T., Jagodic Hudobivnik, M., Begu, E., Mazej, D., Nikezić, M., Horvat, M. (2022). Report on the comparison of analytical procedures routinely used at O-2 for trace element concentration determination in biological material Trout muscle. *IJS delovno poročilo, 13725, confidental.*

Biography

The author of this thesis was born on 25/11/1996 in Bar, Montenegro, and is currently residing in Ljubljana, Slovenia. She is a dedicated scientist whose academic journey started with the pursuit of a Bachelor's and Master's degree in Food Technology and Safety from the University of Donja Gorica in Podgorica, Montenegro. She completed Bachelor's degree in 2018 and earned a Master's degree in 2020. For her master's thesis, Majda conducted an in-depth analysis of the health risks associated with the content of toxic metals and polycyclic aromatic hydrocarbons in food, focusing on the Pljevlja municipality.

During her master studies, Majda has conducted a traineeship as a brewery technologist trainee at Beer Academy, the first craft brewery in Montenegro. Here, she gained insights into the craft beer production process, quality control, and brewery sanitation. Majda's professional experience includes serving as an Analytical Chemist at the Institute for Public Health of Montenegro in Podgorica. In this role, she conducted sample preparation and determined major, trace, and potentially toxic elements concentrations in water and food samples. Her expertise extends to gas chromatography, where she focused on analysing pesticides, PAHs, fatty acids in food, and trihalomethanes in water samples.

Presently, she is enrolled in doctoral studies programme Ecotechnologies at Jožef Stefan International Postgraduate School and conducts her research in the Laboratory for Trace Elements Speciation, within the Department of Environmental Sciences, Jožef Stefan Institute. Her doctoral research centers around the measurement of the Sr isotope ratio for applications in tracing the provenance of wood and food samples. Majda is actively involved in sample preparation, multi-elemental analysis of environmental samples by ICP-MS, as well as Sr isotope ratio analysis by MC-ICP-MC.

Beyond her academic and professional pursuits, Majda actively participates in scientific conferences and seminars, presenting her research at various international events. Her journey in academia and research showcases a commitment to advancing knowledge in environmental and food sciences, and she looks forward to contributing further to these fields in the future.